



**US Army Corps
of Engineers®**
Engineer Research and
Development Center



Ice Management Operations at Albeni Falls Dam

Jeremy Giovando, Chandler Engel, Joseph Rocks,
Steven F. Daly, Devin O'Connor, and Daniel Hamill

October 2019



The U.S. Army Engineer Research and Development Center (ERDC) solves the nation's toughest engineering and environmental challenges. ERDC develops innovative solutions in civil and military engineering, geospatial sciences, water resources, and environmental sciences for the Army, the Department of Defense, civilian agencies, and our nation's public good. Find out more at www.erdcenter.usace.army.mil.

To search for other technical reports published by ERDC, visit the ERDC online library at <http://acwc.sdp.sirsi.net/client/default>.

Ice Management Operations at Albeni Falls Dam

Jeremy Giovando, Chandler Engel, Joe Rocks,
Steven F. Daly, Devin O'Connor, and Daniel Hamill

*U.S. Army Engineer Research and Development Center (ERDC)
Cold Regions Research and Engineering Laboratory (CRREL)
72 Lyme Road
Hanover, NH 03755-1290*

Final Report

Approved for public release; distribution is unlimited.

Prepared for U.S. Army Corps of Engineers, Seattle District
4735 E Marginal Way S Bldg 1202
Seattle, WA 98134

Under Funding Account Code G3149647, AMSCO Code 000200,
"Albeni Falls Water Management"

Abstract

Albeni Falls Dam is located on the Pend Oreille River in northern Idaho and is part of the federal reservoir system on the Columbia River, which provides flood risk reduction and hydropower generation. The Albeni Falls Dam Water Control Manual currently defines wintertime operations for Lake Pend Oreille and the Pend Oreille River. However, this analysis finds that the current wintertime operating criteria are likely ineffective in preventing damages to shoreline structures. Additionally, discharge ramping rates are not significant factors in determining the accumulation of ice on the Pend Oreille River.

This study recommends discontinuing the current wintertime operating criteria specified in the Albeni Falls Dam Water Control Manual and that water managers use hydraulic and water temperature models to assess and monitor the ice formation for both the lake and river. This will provide increased operational flexibility and rely on real-time assessment of ice and weather conditions.

DISCLAIMER: The contents of this report are not to be used for advertising, publication, or promotional purposes. Citation of trade names does not constitute an official endorsement or approval of the use of such commercial products. All product names and trademarks cited are the property of their respective owners. The findings of this report are not to be construed as an official Department of the Army position unless so designated by other authorized documents.

DESTROY THIS REPORT WHEN NO LONGER NEEDED. DO NOT RETURN IT TO THE ORIGINATOR.

Contents

Abstract	ii
Figures and Tables.....	v
Preface.....	ix
Acronyms and Abbreviations.....	x
Unit Conversion Factors	xii
Executive Summary.....	xiii
1 Introduction.....	1
1.1 Background	1
1.1.1 Albeni Falls Dam.....	2
1.1.2 Box Canyon Dam	3
1.1.3 Wintertime operation.....	4
1.2 Objectives.....	8
1.3 Approach	8
2 Pend Oreille River Watershed.....	9
2.1 Data sources	10
2.2 Hydrology.....	12
2.2.1 Lake Pend Oreille.....	12
2.2.2 Pend Oreille River	14
2.3 Climate	16
2.4 Ice-thickness model.....	19
3 Pend Oreille River Hydraulics	22
3.1 Development of a wintertime hydraulic model	22
3.1.1 Existing hydraulic model geometry.....	22
3.1.2 Geometry modifications for winter flows.....	26
3.1.3 Model performance for wintertime flows	27
3.1.4 Flow conditions.....	28
4 Ice Formation in the Pend Oreille River.....	32
4.1 Shoreline camera ice observations	32
4.2 Ice hydraulics	34
4.2.1 Identifying ice-covered periods.....	35
4.2.2 Ice-growth effect on hydraulics.....	38
4.2.3 Spatially varying complete ice cover	40
4.2.4 Flow velocities with ice cover.....	43
4.2.5 Border ice.....	48
4.3 Ice jams	51
4.4 HEC-RAS water-temperature modeling.....	54
4.4.1 Methods and data	55
4.4.2 Water temperature	55
4.4.3 Meteorological data.....	57

4.4.4 Results 57

4.4.5 Model performance 57

4.4.6 Model sensitivity to input parameters 58

4.4.7 Model results discussion..... 62

5 Ice Formation in Lake Pend Oreille65

5.1 Shoreline camera ice observations 65

5.2 Water-temperature observations 70

5.3 Summary of Lake Pend Oreille ice conditions..... 71

6 Ice Forces on Shoreline Structures73

6.1 Wintertime conditions on Lake Pend Oreille 73

6.2 FWPO SOP criteria..... 73

6.2.1 Introduction..... 73

6.2.2 Potential ice damage on Lake Pend Oreille 73

6.2.3 The layout geometry of docks and piles of a marina..... 74

6.2.4 Pullout resistance of the piles..... 75

6.2.5 Ice thickness and ice adhesion to the piles 75

6.2.6 Rate and magnitude of changes in the water surface elevation 75

6.2.7 Simulating the interaction of the ice cover and piles..... 76

6.2.8 Forming hinge cracks through active management of the Lake Pend Oreille
water level 77

6.2.9 Uplift forces..... 79

6.3 FWPO BMP criteria..... 82

6.3.1 Introduction..... 82

6.3.2 Potential ice damage on Pend Oreille River..... 82

6.3.3 River stage change and uplift force 82

7 Improvements to Aid Wintertime Operations.....85

7.1 Forecasting ice formation..... 85

7.2 Recommendations for improving existing camera performance 85

7.2.1 Riley Camp 86

7.2.2 Kalispel..... 86

7.2.3 Bible Camp..... 86

7.2.4 Sandpoint..... 86

7.3 Automating shoreline-ice-camera ice detection..... 86

7.3.1 Ground truth data 87

7.3.2 Model training and results 87

7.3.3 Discussion..... 89

8 Summary.....90

9 AFD Ice Monitoring.....92

9.1 Lake Pend Oreille 92

9.2 Albeni Falls Dam and Pend Oreille River 93

9.3 Future analysis..... 94

References96

Figures and Tables

Figures

1	Albeni Falls Dam (USACE 2019)	2
2	POPUD mechanical removal of ice in BCD forebay.....	5
3	Pend Oreille River watershed (Easthouse 2012)	9
4	The study area including Lake Pend Oreille and the Pend Oreille River between Albeni Falls Dam and Box Canyon Dam	10
5	Monthly average Clark Fork River inflow (USGS 12391950) and Pend Oreille River outflow to Lake Pend Oreille (USGS 12395500)	13
6	Lake Pend Oreille summary hydrograph (USACE 2017).....	14
7	Lake Pend Oreille daily average lake elevation 1996–2017 based on the USGS 12392500 stage record.....	14
8	Average, maximum, and minimum daily outflow from AFD for each day of the year based on the USACE AFD daily record	15
9	Daily average maximum and minimum air temperatures	16
10	Daily average maximum, minimum, and average relative humidity.....	17
11	Daily average percent cloud cover.....	17
12	Average monthly precipitation for Sandpoint, Idaho, based on the Sandpoint Experimental Station.....	18
13	Annual wind rose for Sandpoint, Idaho, airport.....	18
14	AFDD water years 1981 to 2018.....	19
15	Modeled maximum surface-ice thickness from WYs 2003 through 2017	20
16	Average maximum ice thickness by month.....	21
17	Pend Oreille River HEC-RAS model, Albeni Falls Dam to Box Canyon Dam	23
18	Comparison of modeled and observed tailwater elevation at AFD from 2003 to 2018.....	24
19	Difference between modeled and observed tailwater at AFD as a function of discharge	25
20	Difference between modeled and observed tailwater at AFD as a function of time of year.....	25
21	Histogram of hourly discharges for winter months (December, January, and February) 2003–2018.....	26
22	Midchannel islands between RS 86.88496 and RS 85.35497	27
23	Open-water surface (WS) profiles for flows ranging from 5000 to 45,000 cfs.....	29
24	Open-water surface profiles showing the effect the BCD forebay at an elevation of 2034.0 ft has on upstream stage for flows of 15 and 40 kcfs. <i>Dashed lines</i> show the stages without the effects of BCD for the same flows.....	30
25	Open-water channel velocities for 15 kcfs under natural flow conditions and flow controlled by BCD forebay elevation at 2034.0 ft	30
26	Comparison of AFD tailwater rating curves.....	31
27	Albeni Falls Dam tailwater rating curves compared to observed stage and flow data.....	31

28	Overview of imagery data collected along the Pend Oreille River.....	32
29	Ice cover on the Pend Oreille River for winter 2014–2015.....	33
30	Ice cover on the Pend Oreille River for winter 2015–2016.....	33
31	Ice cover on the Pend Oreille River for winter 2016–2017	34
32	Comparison of open-water model stage and observed AFD tailwater stage during an ice-affected event.....	36
33	AFD tailwater stage-deviation time series in <i>red bars</i> . <i>Yellow bars</i> show stage deviations at the Cusick gage (near RS 68.5) for WYs 2016 and 2017	38
34	Expected open-water velocities from flows of 5, 15, 25, 35, and 45 kcfs.....	39
35	Comparison of open-water and ice-affected river stages. Ice cover from BCD to AFD, ice thickness 1 ft, flows 15k and 40k cfs	41
36	Comparison of open-water and ice-affected river stages. Ice cover from BCD to Cusick (RS 68.54497), ice thickness 1 ft, flows 15 and 40 kcfs	42
37	Effects of ice-cover extent (from BCD to upstream points) and flow rate on AFD tailwater elevation.....	43
38	Difference between water velocities under open-water and complete-ice-cover conditions (15 kcfs and 1 ft of ice) with BCD control. Difference calculated as ice-covered conditions minus open-water conditions	45
39	Effect of ice thickness on river stage, relative to open-water conditions (15 kcfs)	46
40	Water-surface profile (WS) for border-ice simulation in HEC-RAS at 15 kcfs. Border-ice growth of 200 ft from the right and left shore	48
41	Water surface (WS) profile for border-ice simulation in HEC-RAS at 15 kcfs. Border-ice growth of 600 ft from the right and left shores	49
42	Effect of increasing border-ice growth on the AFD tailwater stage for 15 kcfs. The percent of reach covered is the ratio of ice-cover surface area to total river surface area	50
43	Effect of border-ice growth on the AFD rating curve. Individual <i>lines</i> represent 25%, 50%, 75%, and 100% reach coverage. <i>Dots</i> represent maximum stage deviations from 2003 to 2017	50
44	Ice jam during average winter flows of 15 kcfs	52
45	Ice jam during high winter flows of 40 kcfs with prebreakup ice cover shown for reference.....	52
46	Ice jam during high winter flow of 40 kcfs compared with open-water flow of 75 kcfs	53
47	Stages at Cusick (RS 68.5). From <i>bottom</i> : 40 kcfs open water, 40 kcfs 1 ft ice cover, 40 kcfs ice jam, and 75 kcfs open water. No ice cover is present in the 40 kcfs ice jam case because the body of the jam is downstream of this cross section. All stages remain within the banks.....	54
48	Observed water temperatures at AFD and BCD forebays for December, January, and February, WYs 2012–2017	56
49	Observed temperature history at BCD for WYs 2012–2017	56
50	Nonexceedance probability of observed and modeled water temperatures at BCD forebay for December, January, and February, WYs 2012–2017	58
51	WY 2017 temperature-model results at Box Canyon Dam, Simulations 1–6.....	60

52	WY 2017 temperature-model results at Box Canyon Dam, Simulations 1, 3, and 5. Simulation 1 is based on all observed input data. Simulation 3 is based on observed AFD water temperature and average climatological data. Simulation 5 is based on observed AFD water temperature and air temperature and on average climatological data	61
53	Comparison of Simulation 1 results and observations for beginning and ending ice event dates	62
54	Modeled river temperatures for December, January, and February in WYs 2012–2017. Images are overlaid with ice conditions observed with shoreline ice cameras located at Kalispel (WYs 2015–2017) and Bible Camp (WYs 2015–2016).....	64
55	Direction of view for each shoreline ice camera located at Sandpoint.....	66
56	Typical views from Sandpoint shoreline ice cameras	66
57	Overview of imagery data collected at Sandpoint.....	67
58	Ice coverage recorded by Sandpoint shoreline ice cameras during WY 2015.....	68
59	Ice coverage recorded by Sandpoint shoreline ice cameras during WY 2016.....	69
60	Ice coverage recorded by Sandpoint shoreline ice cameras during WY 2017	69
61	Recorded Lake Pend Oreille water temperature for winter 2014–2015	70
62	Shallow areas of Lake Pend Oreille indicating likely ice-covered areas (highlighted in <i>white</i>)	71
63	Landsat image of Lake Pend Oreille acquired on 14 January 2017 showing ice cover.....	72
64	Maximum tensile stress in the ice cover as a function of the stage rise	79
65	Uplift force on each pile for different pile spacings for Case 1.....	80
66	Uplift force on each pile for different pile spacings for Case 2.....	80
67	Steel pile resistance to pullout with various factors of safety (FOS).....	81
68	Wooden Pile Resistance to pullout.....	81
69	Maximum tensile stress in the ice cover as a function of the stage rise for river cases.....	83
70	Example of manual annotations and CRF predictions. Panel A shows the input image. Panel B shows the weakly supervised user annotations. Panel C shows the results of the CRF-derived label image used to create training and testing tile libraries	87
71	Confusion matrix showing the results of applying the trained DCNN to the testing tile library for Riley Creek. Values within the matrix show the percentage of the label library classified as the label indicated on the x-axis	88
72	Time series of river ice conditions at Riley Creek	88
73	Recommended ice-thickness measurement location at Windbag Marina	93

Tables

1	Pertinent AFD and Lake Pend Oreille data.....	3
2	Normal project discharge requirements.....	6
3	The FWPO BMP discharge requirements	7
4	Corps of Engineers data.....	11

5	Shore-based monitoring stations.....	11
6	USGS data.....	11
7	SNOTEL data.....	11
8	Ice-thickness parameters	20
9	HEC-RAS model error (in feet) at AFD tailwater stage (RS 89.02496). From all-season flows March 2003–March 2017.....	28
10	AFD tailwater stage-deviation statistics	35
11	AFD tailwater stage deviations exceeding 0.3 ft with a duration of 12 hours or more	37
12	Cusick River gage stage deviations exceeding 0.3 ft with a duration of 12 hours or more.....	37
13	Stage increase at AFD tailwater from 1 ft of downstream ice growth relative to open-water conditions.....	42
14	Effect of ice thickness on river stage	47
15	Stage increases relative to open water for 40 kcfs. Stage increases are reported in feet.....	53
16	Input data sources for the water-temperature model.....	57
17	Input data in water-temperature-model simulations where X represents observed values and C represents climatological values	59
18	Summary of errors of modeled hourly water temperatures at BCD, root-mean-square error (RMSE), mean absolute error (MAE), mean bias error (MBE), and Nash-Sutcliffe efficiency (NSE).....	60
19	Comparison of modeled and observed ice events for BCD using observed values for all model inputs (Simulation 1).....	62
20	Shoreline ice cameras located at Sandpoint, Idaho, 48.2758, -116.5398.....	65
21	Summary of days with ice for each Sandpoint shoreline ice camera	67

Preface

This study was conducted for U.S. Army Corps of Engineers, Seattle District, under Funding Account Code G3149647, AMSCO Code 000200, “Albeni Falls Water Management.”

The work was performed by the Terrain and Ice Engineering Group of the Remote Sensing / Geographic Information Systems Center of Expertise (CEERD-RS) and the Terrestrial and Cryospheric Science Branch (CEERD-RRG) and the Engineering Resources Branch (CEERD-RRE) of the Research and Engineering Division (CEERD-RR), U.S. Army Engineer Research and Development Center, Cold Regions Research and Engineering Laboratory (ERDC-CRREL). At the time of publication, Mr. Stephen Newman was lead, Terrain and Ice Engineering Group; Mr. David Finnegan was Chief, CEERD-RS; Dr. John Weatherly was Chief, CEERD-RRG; Dr. Caitlin Callaghan was Acting Chief, CEERD-RRE; and Mr. Jared Oren was Acting Chief, CEERD-RR. The Deputy Director of ERDC-CRREL was Mr. David B. Ringelberg, and the Director was Dr. Joseph L. Corriveau.

COL Teresa A. Schlosser was Commander of ERDC, and Dr. David W. Pittman was the Director.

Acronyms and Abbreviations

AFD	Albeni Falls Dam
AFDD	Accumulated Freezing Degree-Days
BCD	Box Canyon Dam
CRF	Conditional Random Field
CRREL	Cold Regions Research and Engineering Laboratory
DCNN	Deep Convolutional Neural Networks
DEM	Digital Elevation Model
ERDC	U.S. Army Engineer Research and Development Center
FOS	Factor of Safety
FWPO	Flexible Winter Power Operations
FWPO BMP	“Ice Best Management Practice, Flexible Winter Power Operation”
FWPO SOP	“Standard Operating Procedure for Fluctuating Lake Elevation, Flexible Winter Power Operations”
HEC-RAS	Hydrologic Engineering Center’s River Analysis System
MAE	Mean Absolute Error
MAF	Million Acre-Feet
MBE	Mean Bias Error
MCE	Minimum Control Elevation
NAVD88	North American Vertical Datum of 1988
NGVD29	National Geodetic Vertical Datum of 1929
NOAA	National Oceanic and Atmospheric Administration
NSE	Nash-Sutcliffe Efficiency
POPUD	Pend Oreille Public Utility District

RS	River Station
RMSE	Root-Mean-Square Error
SNOTEL	Snow Telemetry
USACE	U.S. Army Corps of Engineers
USGS	U.S. Geological Survey
WCM	Water Control Manual
WS	Water Surface
WY	Water Year

Unit Conversion Factors

Multiply	By	To Obtain
acres	4,046.873	square meters
acre-feet	1,233.5	cubic meters
cubic feet	0.02831685	cubic meters
degrees Fahrenheit	$(F-32)/1.8$	degrees Celsius
feet	0.3048	meters
gallons (U.S. liquid)	3.785412 E-03	cubic meters
inches	0.0254	meters
kips	0.4536	tonnes
miles (nautical)	1,852	meters
miles (U.S. statute)	1,609.347	meters
miles per hour	0.44704	meters per second
pounds (force)	4.448222	newtons
pounds (force) per square inch	6.894757	kilopascals
square feet	0.09290304	square meters
square miles	2.589998 E+06	square meters

Executive Summary

The Albeni Falls Dam (AFD) Water Control Manual includes separate wintertime operating criteria for the Pend Oreille River and Lake Pend Oreille. Exhibit 7-3 of the AFD Water Control Manual is titled “Flexible Winter Power Operations Ice Best Management Practice (FWPO BMP)” and applies to the Pend Oreille River downstream of AFD. Exhibit 7-4, “Flexible Winter Power Operations Standard Operating Procedure for Fluctuating Lake Elevation (FWPO SOP),” applies to Lake Pend Oreille.

Both criteria use accumulated freezing degree-days (AFDD) to indicate the likelihood of ice presence. The FWPO BMP restricts the outflow ramping rate from AFD during “Ice Hazard Conditions” to minimize potential ice jam formation and subsequent flooding and shoreline damage. The FWPO SOP specifies raising and lowering the lake elevation 0.1 ft/day over a 12-day cycle to create and maintain surface-ice *hinge cracks* to protect shoreline structures from ice damage.

The restrictions and specifications set forth in these wintertime criteria are challenging for water managers to implement given the other operational constraints placed on AFD. Specifically, the wintertime power generation is limited because of the restrictive ramping rates. In addition, the cycling of the Lake Pend Oreille surface elevation may conflict with other water uses and may not be feasible with the restricted outflow ramping rates.

This study evaluates the current wintertime operating criteria specified in the water control manual to determine if they are effective and required to reduce the ice jam flood risk downstream of AFD or potential ice damage to shoreline structures on Lake Pend Oreille. Additionally, this study developed and evaluated tools and methods that allow water managers to assess the potential risk from ice during real-time winter conditions.

The hydrology of Lake Pend Oreille and the Pend Oreille River is characterized by low flows during winter, a spring snowmelt freshet (April through July), and recession flow for the rest of the summer. There is a large year-to-year variability of the winter climate as measured by the AFDD recorded each winter. Typically there are relatively short, very cold periods when most ice formation occurs, especially on the river.

This study used a model of the river downstream of AFD to Box Canyon Dam (BCD), developed in the U.S. Army Corps of Engineers (USACE) Hydrologic Engineering Center's River Analysis System (HEC-RAS) software, as the primary modeling tool. The Seattle District originally built the HEC-RAS model as a planning tool for studies in the Pend Oreille River watershed. Previous calibration of the model focused on the freshet period (April through June) and was not representative of winter flow conditions. Therefore, we adjusted model parameters and the channel geometry to better represent winter flow conditions under steady and unsteady flow. The updated model was able to simulate observed stages downstream of AFD with good accuracy during the winter period. The flow in the river throughout most of its length is strongly controlled by the backwater created by the BCD. This backwater increases wintertime stages and reduces flow velocities, but the effect declines in the upstream direction. The HEC-RAS Water Quality Module was used to estimate water temperatures downstream of AFD. We evaluated the model by comparing the modeled temperature at BCD forebay with the observed temperature; and in general, the results were good to very good.

The study team investigated ice-cover formation in the Pend Oreille River by using images from two stationary cameras located along the river downstream of AFD and by using the HEC-RAS-modeled water temperatures. The river ice cover is formed by the growth of shore ice with the cover extending out into the river from both banks. Only during very cold periods is the river completely ice covered. We explored the impact of the shore ice on the tailwater stage at AFD. HEC-RAS simulations used two ice-growth scenarios. The first assumed border ice forms uniformly along the entire reach between AFD and BCD. The second scenario assumed border ice starts at the BCD forebay and grows completely across the river, moving upstream sequentially. The AFD tailwater stage values for both of these ice-growth scenarios were compared to the observed tailwater data. From this comparison, it is likely that both of these ice-growth scenarios can occur, depending on the nature of the cold weather event. The largest magnitude deviations between observed wintertime AFD tailwater stages and open-water stages are likely associated with complete ice cover from the BCD forebay upstream to Newport, Washington. Water managers can use the modeled stage-deviation results to approximate the ice extent and location downstream of AFD.

The study team also used HEC-RAS to evaluate ice jam formation on the Pend Oreille River. The strong downstream control provided by BCD reduced the severity of ice jams, as measured by their thickness and extent. One of the primary concerns with changes in discharge at AFD during winter is the potential to cause flooding if an ice jam were to occur. Based on both qualitative evidence (e.g., discussion with Seattle District water management) and quantitative hydraulic information (e.g., flow velocity), the potential for ice jams on the Pend Oreille River between BCD and AFD is in general is very low. If surface ice were to accumulate in a jam on the river, it would likely be near the Blue Slide section downstream of AFD. Assuming an ice jam were to occur at a discharge of 40 kcfs (about the maximum wintertime discharge that could be expected) at the Blue Slide location with 1 ft thick ice cover on the entire river, the resulting stage would be equivalent or less than an open-water stage of 75 kcfs. This open-water-equivalent stage is below the 90 kcfs limit used by water managers and far below the 100 kcfs maximum discharge limit specified in the water control manual. The risk of ice jams due to discharge changes from AFD, assuming a normal winter flow regime, is probably low.

Historical periods when ice was likely present on the Pend Oreille River were identified based on deviations between observed and modeled river stage at the AFD tailwater location. We established a base hydraulic model to represent open-water conditions for various AFD discharge levels. The base hydraulic model included updates to the hydraulic parameters for wintertime conditions to better match observed river stages. Using the base model, open-water simulations were performed with various AFD discharge rates. The resulting tailwater stages were compared with observed stages at AFD. When the difference between observed and modeled stage exceeded 0.3 ft, this indicated that the model assumption of open-channel flow was not valid and that ice was likely affecting the river hydraulics, resulting in a rise in the observed river stage. The presence of ice as determined by the imagery from stationary shoreline ice cameras correlated well with the stage deviations. A total of 19 ice-affected periods were identified between WYs (water years) 2002 and 2017 based on camera images and the stage-difference threshold. The two longest ice periods were 23 days during the winter of 2008–2009 and 10 days during the winter of 2016–2017.

This study also estimated the historical periods when ice was present on the Pend Oreille River by using the HEC-RAS Water Quality Module to identify

the periods when the water temperature of the river was less than 32.5°F. Water temperatures close to the freezing point (32°F) are an indication of the likely presence of ice on the river. Again, the presence of ice as determined by the imagery from stationary shoreline ice cameras correlated well with water-temperature estimates. However, the meteorological data requirements for the Water Quality Module are extensive, limiting its usefulness as an operational tool. This study evaluated the sensitivity and accuracy of the modeled water-temperature results by replacing the required meteorological parameters with average climatological values. This simplified the model's data requirements and will potentially allow for its use as an operational tool. We found that as long as the observed outflow temperature of AFD and the air temperature were provided, the model results were quite good. This suggests that the HEC-RAS Water Quality Module could be a useful tool for water managers for estimating ice formation.

The usefulness of AFDD to indicate the presence of ice in Lake Pend Oreille and the Pend Oreille River was investigated based on the 19 ice periods identified for the river and by the camera data for Lake Pend Oreille. In general, the AFDD criteria do not accurately identify ice periods. The 7-day AFDD, which accumulates the freezing degree-days over a running 7-day period worked much better. In addition, other approaches, such as identifying the stage deviations at the AFD tailwater by using HEC-RAS or identifying the periods of time when the water temperature of the river was less than 32.5°F by using the HEC-RAS Water Quality Module, can also determine with good accuracy when ice is present.

We investigated the restrictions on the outflow ramping rate from AFD by estimating the occurrence of shore ice fractures at a representative downstream location under the normal outflow ramping rate and the reduced ramping rate imposed during ice conditions. HEC-RAS was used to determine the rate of rise of the river stage during each outflow-rate scenario. We also developed a finite element model of the river ice cover that simulated the reaction of the sheet as the river stage increased. The material properties of the ice cover included the ability of the ice cover to *creep*, or strain indefinitely under constant stress, a well-known property of ice. The ability of ice to creep is what causes the ice cover to respond differently to different rates of rise of the water surface.

Four stationary shoreline ice cameras located at Windbag Marina in Sandpoint, Idaho, and a very limited number of satellite images observed

the ice formation on Lake Pend Oreille. This information, along with water-temperature measurements recorded by the Navy and personal anecdotes, strongly suggests that ice formation on Lake Pend Oreille is limited to shallow water depths generally located in the northern part of the lake and in isolated bays or inlets. There is no evidence that ice cover is formed on the main part of the lake south of the Clark Fork River inlet. Horizontal ice forces on shoreline structures are therefore likely to be minor as the ice fetch length is minimal. Ice damages in the lake are most likely to arise as a result of changes in lake levels, which have the potential to cause ice *jacking*, where piles are lifted out of the foundation material by forces transferred by ice.

We evaluated for both the lake and river operations the potential uplift forces that result in ice jacking. The FWPO SOP lake stage change criteria was compared against the open-water stage change limits. The results for the FWPO SOP indicate that the probability of ice jacking is low for well-constructed facilities that have closely spaced piles. Isolated piles will have a larger pullout force and increased probability of ice jacking, depending on the foundation depth. Development of a *hinge* crack to reduce stress on docks and marina facilities on Lake Pend Oreille was shown to be ineffective because the ice creep will reduce the stress and prevent the crack from forming. The FWPO BMP focuses on minimizing ice jam formation and flooding below AFD. The results of this study indicate that the risk for mobilizing ice, which results in ice jam, is similar whether using the restricted release changes specified in the FWPO BMP or using the open-water criteria. This is because the stress on the river surface ice is less sensitive to stage change rates but is primarily dependent on the total stage change.

Evaluation of the criteria specified in Exhibit 7-3 and 7-4 of AFD Water Control Manual indicates that the current practices for Lake Pend Oreille and the Pend Oreille River will not result in the intended risk reduction for ice damage of docks and marinas on the lake or ice jam formation on the river. Using the open-water operating criteria will result in very similar risk levels for each of these areas of concern. This report includes recommendations for eliminating or modifying the winter operating criteria.

Improvements to forecasting ice formation on Lake Pend Oreille and the Pend Oreille River include water-temperature modeling and adjustments to the shoreline-ice-camera image collection. The HEC-RAS Water Quality

Module was shown to be capable of accurately predicting water temperatures downstream of AFD by using only air temperature and forebay water-temperature forecasts. If this model were to be used operationally, air temperature forecasts are easily obtained from the National Weather Service products while AFD forebay temperature will require estimates using separate statistical or physically based models. In addition, the automated ice classification routine developed in this study will reduce time spent by water managers reviewing shoreline-ice-camera images before and during cold weather events. The automated classification can be used with the numerical modeling to validate where ice formation is occurring.

1 Introduction

1.1 Background

Albeni Falls Dam (AFD), a U.S. Army Corps of Engineers (USACE) dam, is located on the Pend Oreille River approximately 27 miles downstream of Lake Pend Oreille, Idaho. AFD regulates the flow out of Lake Pend Oreille and controls the Lake Pend Oreille water level during most of the year except during the freshet when the natural lake outlet often becomes the hydraulic control. Surface ice on Lake Pend Oreille and the Pend Oreille River downstream of AFD is a common occurrence in winter. The presence of ice can potentially cause operational issues for AFD, which the U.S. Army Cold Regions Research and Engineering Laboratory (CRREL) addressed in a previous investigation.* The focus of the previous effort was installation of four shore-based monitoring stations on the lake and river that included environmental monitoring equipment and shoreline ice cameras that regularly collected images of ice conditions. The previous effort provided recommendations for wintertime operations of AFD based on the evaluation of ice impacts and observations. These recommendations were incorporated into the AFD Water Control Manual (WCM) (USACE 2013) as Exhibit 7-3, “Ice Best Management Practice, Flexible Winter Power Operation” (FWPO BMP), and Exhibit 7-4, “Standard Operating Procedure for Fluctuating Lake Elevation, Flexible Winter Power Operations” (FWPO SOP).

The present study builds on the previous work by using the data collected at the four shore-based monitoring stations and more detailed ice analysis to revisit the current wintertime operating criteria for AFD. The restrictions and specifications set forth in these wintertime criteria are difficult for water managers to implement given the other operational constraints placed on AFD. Specifically, the wintertime power generation is limited because of the restrictive ramping rates. In addition, the cycling of the Lake Pend Oreille surface elevation may conflict with other water uses and may not always be feasible with the restricted outflow ramping rates. Furthermore, the damage to structures along the shoreline both upstream

* A. Tuthill and L. Zabilansky, “Effects of Large Flow Increases on Ice Processes Pend Oreille River: Albeni Falls to Box Canyon Dam” (Hanover, NH: U.S. Army Engineer Research and Development Center). Report prepared for the USACE Seattle District.

and downstream of AFD is an important consideration for water managers. This report recommends changes or modifications to the current operating criteria.

1.1.1 Albeni Falls Dam

The Albeni Falls Project was authorized by the Flood Control Act of 1950 and was part of the comprehensive plan of improvement for the Columbia River system (USACE 2013). Construction of the dam began in 1951 and was completed in 1955. The project purposes include power generation, navigation, flood risk reduction, recreation, fish and wildlife conservation, and water supply. The dam is located in Bonner County, Idaho, approximately 2 miles east of Newport, Washington, and 26 miles west of Sandpoint, Idaho. The dam site is located at approximately river mile 90.1 upstream of the confluence of the Pend Oreille and Columbia Rivers. The structure includes a powerhouse and spillway, which are separated by a natural rock island located near midchannel (Figure 1). The total dam length is 1080 ft, which includes the 300 ft for the powerhouse and 780 ft for the spillway structure. The powerhouse has three Kaplan-type turbines with a nameplate generation capacity of 42.6 MW and a design head of 22 ft. AFD is a base-load plant with hydraulic capacity that ranges from 4000 cfs to 35,000 cfs. Discharge through just the powerhouse is used to regulate Lake Pend Oreille storage except during flood events.

Figure 1. Albeni Falls Dam (USACE 2019).



The Lake Pend Oreille was glacially formed about 25,000 years ago and is located about 27 miles upstream of AFD. The water surface elevation difference between the AFD forebay and the Lake Pend Oreille water surface elevation determines the outflow from the lake. At low flows, the forebay stage is relatively high and the difference between the lake and AFD forebay elevations small. The AFD forebay water surface elevation drops with increasing lake outflows. At large outflows, the forebay stage is relatively low and the difference between the lake and AFD forebay elevations large. At very large outflows from the lake, the control passes from the AFD forebay upstream to a restriction in the Pend Oreille River at Dover, Idaho. At large outflows, often the water surface difference between the AFD forebay and tailwater is too small to support hydropower production. At this point, hydropower production ceases, the gates of the dam are opened wide, and the Pend Oreille River is essentially free flowing (USACE 2013). Table 1 summarizes relevant AFD and Lake Pend Oreille elevations.

Table 1. Pertinent AFD and Lake Pend Oreille data.

Albeni Falls Dam and Lake Pend Oreille Water Surface Elevation (ft)	
Maximum	2067.5
Normal Full	2062.5
Normal Minimum	2051.0
Minimum	2049.7
Albeni Falls Dam Hydraulic Capacity (cfs)	
Powerhouse Maximum	35,000
Powerhouse Minimum	4000
Spillway Maximum (at elevation 2085–2090 ft with gates removed)	350,000

1.1.2 Box Canyon Dam

The Pend Oreille River downstream of AFD is influenced both by releases from AFD and forebay elevations of Box Canyon Dam (BCD), located approximately 56 miles downstream. BCD is owned and operated by Pend Oreille Public Utility District (POPUD) and was constructed in 1956 with a major upgrade in 2015. The reach of the Pend Oreille River between AFD and BCD presents characteristics of both a river and reservoir, depending on the discharge. Therefore the tailwater for AFD can be significantly influenced by the BCD operations.

1.1.3 Wintertime operation

The current AFD WCM provides a complete summary of the project operation for all seasons, including winter. The regulation of Lake Pend Oreille follows a typical fill and drawdown cycle similar to other storage reservoirs in the Pacific Northwest. As discussed below, the inflow hydrology is driven by the snowmelt patterns in the northern Rocky Mountains. This pattern results in seasonal shifts for operating criteria for Lake Pend Oreille, which are consistent for many reservoir in the Columbia River basin. The fall drawdown usually begins after Labor Day and continues through mid-November until Lake Pend Oreille reaches an elevation of 2051.5 ft. Following the fall drawdown, the lake elevation is held to a 0.5 ft operating range to protect against dewatering of kokanee spawning and incubation areas. The 0.5 ft operating range is based on the Minimum Control Elevation (MCE), which is established on 1 December each year. The Winter-Spring Holding Period is from 1 January through 31 March each year. During this period, Lake Pend Oreille is usually operated in a 1 ft range above the MCE. Storage may be allowed to go above the MCE during this period to reshape high flow events or for unscheduled hydropower operations, but the lake elevation must not be drafted below the MCE.

In conjunction with the Winter-Spring Holding Period operation, there are currently special provisions that apply to operations when ice is anticipated or present. Regional winter cold fronts typically cause ice formation for Lake Pend Oreille and the Pend Oreille River, which presents challenges for water managers operating AFD. First of all, they must identify the time periods when ice is present in sufficient quantities and thicknesses to increase risks. Then they must operate AFD to meet the requirements for power generation, flood risk reduction, recreation, fish and wildlife conservation, and water supply as well as to minimize problems caused by ice. The potential ice problems will differ between Lake Pend Oreille and the Pend Oreille River. On Lake Pend Oreille, the primary challenges are ice impacts on shoreline recreational structures, such as docks and marinas. While ice impacts on these structures can result from several different modes of ice action, the primary mode of interest in Lake Pend Oreille is vertical uplift of piles caused by vertical motion of the ice cover reacting to increases in the lake water surface elevation. On the Pend Oreille River, ice movement presents potential risk for ice jams, ice jam flooding, and damage to structures and property along the Pend Oreille River downstream of AFD. In addition, operators at BCD reported ice accumulation on intake structures. Accumulation of surface ice that moves from upstream locations drives the ice

buildup at BCD. This requires POPUD to mechanically remove the ice in the forebay so as to limit the buildup on trash racks (Figure 2). This report does not specifically address ice issues at BCD.

Figure 2. POPUD mechanical removal of ice in BCD forebay.



1.1.3.1 Lake Pend Oreille

AFD operations during ice periods on Lake Pend Oreille are based on Exhibit 7-4, FWPO SOP, of the AFD WCM (USACE 2013). This SOP calls for ice operations when the number of accumulated freezing degree-days (AFDD) observed at Sandpoint, Idaho, exceeds 50 °F-days. It describes three different responses to ice, depending on the period of time that ice occurs: during kokanee spawning, the transition from kokanee spawning, and flexible winter power operation (FWPO).

Kokanee, an important fish species native to Idaho and introduced into Lake Pend Oreille, spawn starting in November, continuing through December. During this time, the lake level is held constant. The SOP recommends that the lake level be fluctuated by 0.1 ft/day to set “the stage for the hinge crack if the weather is cold.” Hinge cracks are cracks in the ice cover that pass from the surface to the bottom of the ice sheet and generally parallel the shore. They are located lakeward of any structure located

along the shore. Hinge cracks can isolate structures from the vertical motion of the ice cover lakeward of the crack and thereby reduce the uplift force on the structure piles.

During the transition from kokanee spawning, if ice is present, as verified by the shore-based cameras, the ice cover is to be inspected for the presence of hinge cracks and active cracks. If hinge cracks are present, the response of the next period, FWPO, can begin. If hinge cracks are not present, FWPO can begin “at the discretion of water management,” who will consider the lakeward extent of the ice cover, the forecasted air temperatures, the lake temperature, and other monitoring data.

Once FWPO begins, the lake level is to fluctuate “with alternating 6-day periods: 6 with $\sim 0.1'$ /day of increasing elevation, followed by 6 days with $\sim 0.1'$ /day decreasing elevation. These fluctuations will maintain the active and hinge cracks.”

These wintertime SOPs for ice can be compared to the AFD project operating limits for changes in the Lake Pend Oreille water surface elevation that are applicable during non-ice periods. In this case, when the lake level is less than 2058 ft, as it is during all winters (see Figure 7), the maximum change in elevation is 0.5 ft/day.

1.1.3.2 Pend Oreille River

AFD operations during ice periods for the Pend Oreille River are based on Exhibit 7-3, FWPO BMP, of the into AFD WCM (USACE 2013). In general, the FWPO BMP focuses on limiting the rate of change of discharge released by AFD in order to limit the risk of breaking up the ice cover downstream of AFD and causing ice jams, ice jam flooding, and damage to structures and property along the Pend Oreille River downstream of AFD. For comparison, Table 2 lists the normal AFD discharge requirements, which apply during non-ice periods.

Table 2. Normal project discharge requirements.

Discharge Requirements	cfs
Minimum instantaneous	4K
Maximum hourly change	5K
Maximum average daily change	10K

Table 3 summarizes the FWPO BMP discharge requirements. The FWPO BMP prescribes in much detail the operations that should be used during wintertime water management for the Pend Oreille River. The primary variable that is used for implementing these guidelines is the AFDD based on air temperature measurements at Sandpoint, Idaho. There are two operational categories defined by AFDD values: (1) less than 100 degree-days and (2) greater than or equal to 100 degree-days. If the AFDD is less than 100 degree-days and the 5-day air temperature forecast average is above 20°F, then open-water operating criteria should be used. If the 5-day forecast is below 20°F or if the outflow temperature from AFD (T_{w-AFD}) is below 34°F, then active monitoring of the river for border or frazil ice is recommended.

Table 3. The FWPO BMP discharge requirements.

AFDD (°F-Day)	Additional Criteria	Operating Condition	Max Flow Increase, ΔQ^*	1 Hour	24 Hours	48 Hours
			(cfs)			
≤ 100	Avg. 5-day forecast ≥ 20 °F	Normal Operation				
≤ 100	Avg. 5 day forecast ≤ 20 °F Or $T_{w-AFD} \leq 34 \text{ °F}$	Monitor for Ice				
≥ 100	Transition to modified winter operation	Ice Hazard Conditions	10K	2K	5K	10K
	24 hours w/o ice problems for $\Delta Q = 10K$ and Avg. 5-day forecast ≥ 25 °F		20K	2K	5K	10K
	24 hours w/o ice problems for $\Delta Q = 10K$ and Avg. 5-day forecast ≤ 25 °F		Suspend Ramp-Up			
	No ice problems for $\Delta Q = 20K$ and Avg. 5-day forecast ≥ 25 °F		30K	2K	5K	10K
	No ice problems for $\Delta Q = 30K$ and Avg. 5-day forecast ≥ 25 °F		44K	2K	5K	10K
	No ice problems for $\Delta Q = 30K$ and Avg. 5-day forecast ≤ 25 °F		Suspend Ramp-Up			

* The change in discharge is relative to the average discharge from AFD 1 week prior to meeting thresholds for modified winter operations.

Once the AFDD value is greater than 100 degree-days, then transition to “modified winter operations” occurs. In the modified winter operations,

the FWPO BMP recommends that discharge increases from AFD be no more than 10 kcfs followed by a period of monitoring for ice breakup, ice jams, and ice-related flooding on the river when the 5-day average temperature forecast is 25°F or higher. The ramping rate is also restricted during the modified winter operations. For all discharge increases, the ramping is limited to 2 kcfs/hr, 5 kcfs/24 hours, and 10 kcfs/48 hours. When the 5-day average temperature forecast is less than 25°F, no discharge increases should be made. If after 24 hours no ice problems are observed, then additional discharge changes can be made following the above criteria.

1.2 Objectives

Our objectives for this analysis are (1) to evaluate the winter operating criteria specified in the FWPO SOP and FWPO BMP to determine effectiveness and risk if modified, (2) to develop tools that can be used by water managers to identify and quantify ice impacts to AFD operations, and (3) to use the limited field information to estimate ice forces acting on those shoreline structures.

1.3 Approach

The approach for this study is to build upon the ice data that has been collected since 2011 when the shoreline ice cameras and water sensors were installed on both Lake Pend Oreille and the Pend Oreille River. This information along with both empirical and theoretical methods for ice hydraulics are used in determining the effectiveness of the winter operating criteria. The primary tool used in the ice hydraulics analysis is the USACE Hydrologic Engineering Center's River Analysis System (HEC-RAS), while ice forces were computed using a finite element model. These tools are also used to address the effectiveness of specific wintertime operating criteria to reduce risk of damage to shoreline structures by ice forces.

2 Pend Oreille River Watershed

The Pend Oreille River basin drains about 26,000 square miles in southern British Columbia, western Montana, northern Idaho, and northeastern Washington. The Clark Fork River, the major tributary to the Pend Oreille River, originates in the Rocky Mountains of western Montana and flows northeast about 350 miles to Lake Pend Oreille. Major tributaries to the Clark Fork include the Flathead River, Blackfoot River, and Bitterroot River. The Pend Oreille River begins at the outlet of Lake Pend Oreille, flows eastward for about 29 miles to AFD, and then flows to the northeast for about 90 miles to the confluence with the Columbia River in British Columbia. Major tributaries to the Pend Oreille River downstream of AFD include the Priest River, which flows out of Priest Lake (Figure 3) (Easthouse 2012). The study area for this analysis focused on Lake Pend Oreille and the Pend Oreille River from AFD downstream to BCD. Figure 4 shows the study area and shoreline-ice-camera locations.

Figure 3. Pend Oreille River watershed (Easthouse 2012).

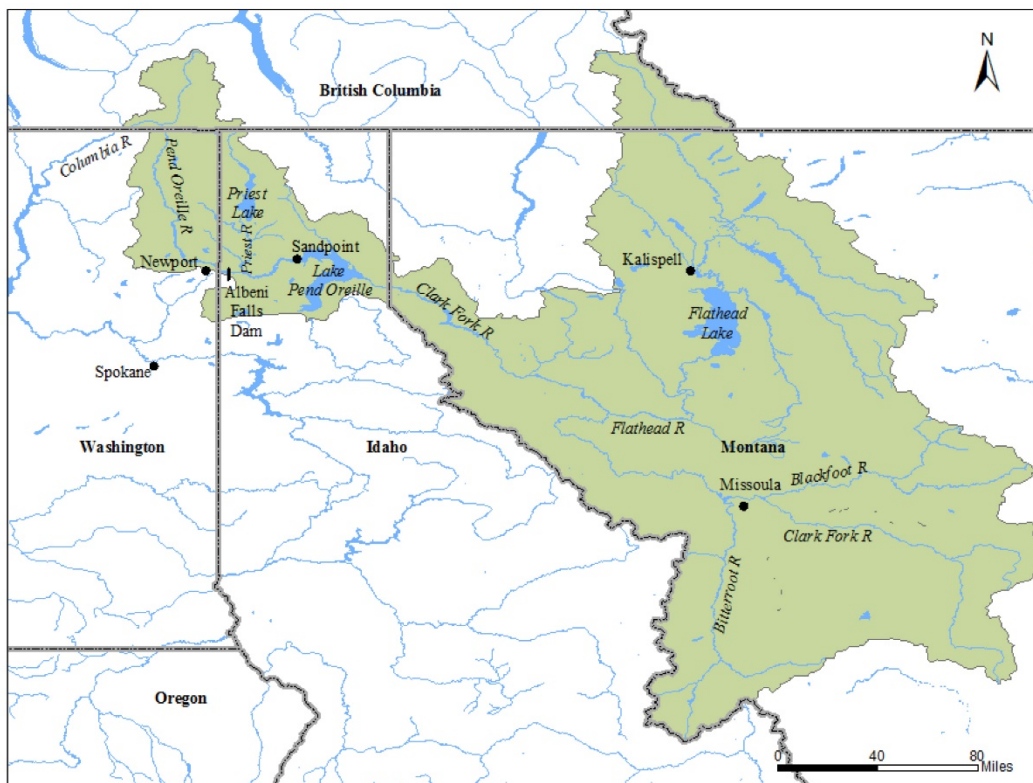
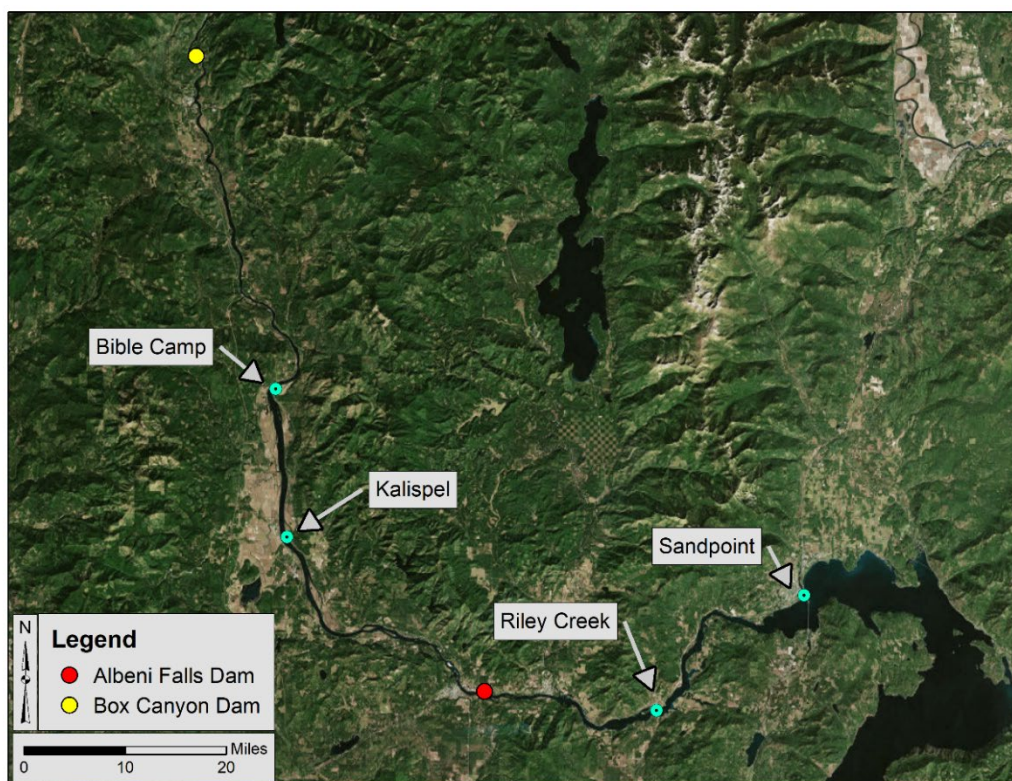


Figure 4. The study area including Lake Pend Oreille and the Pend Oreille River between Albeni Falls Dam and Box Canyon Dam.



2.1 Data sources

There are many sources of information on the hydrology and weather in the vicinity of Lake Pend Oreille and the Pend Oreille River, which are summarized in the AFD WCM (USACE 2013). The only data sources relevant to the present study and included in this study report are hourly stage, discharge, and water-temperature data at AFD and BCD (Table 4). The four shore-based monitoring stations established in the earlier study provide images of the shoreline ice conditions several times a day. Three of the stations also provide air temperature and water temperature; and the station located at Sandpoint, Idaho, provides wind speed and direction (Table 5). The U.S. Geological Survey (USGS) publishes daily water-level data for Lake Pend Oreille and discharge data for the Pend Oreille River and other tributary rivers (Table 6). A number of Natural Resource Conservation Service SNOTEL (Snow Telemetry) sites provide information on snow conditions, air temperature, and precipitation in the Pend Oreille vicinity (Table 7). Generally, these sites are located at elevations several thousand feet higher than Lake Pend Oreille or the Pend Oreille River.

Table 4. Corps of Engineers data.

Station	ID	Parameter	Start	End
Albeni Falls Dam	ALF	Forebay Stage	12/31/89 09:00	Present
		Tailwater Stage	11/2/74 08:00	Present
		Water temp	8/10/07 20:00	Present
		Outflow	9/30/89 24:00	Present
Box Canyon Dam	BOX	Forebay Stage	11/1/74 01:00	Present
		Water Temp	9/25/07 14:00	6/29/17 10:00

Table 5. Shore-based monitoring stations.

Station	ID	Images	Air Temp	Water Temp	Wind Speed	Wind Dir
Bible Camp	CUIW	1/11-5/16	12/15-9/17	11/15-9/17		
Riley Creek	RCRI	11/11-9/17	3/15-9/17	3/15-9/17		
Kalispel		9/11-9/17				
Sandpoint-Windbag	SAPI	12/12-5/17	4/15-9/17	4/15-9/17	4/15-9/17	4/15-9/17

Table 6. USGS data.

ID	Gage Location	Start	End
12391950	Clark Fork River below Cabinet Gorge Dam, ID	1995	Present
12395500	Pend Oreille River at Newport, WA	1903	Present
12392300	Pack River near Colburn, ID	1958	Present
12392500	Lake Pend Oreille near Hope, ID	1970	Present
12395950	Pend Oreille River at Cusick, WA	2015	Present
12395000	Priest River near Priest River, ID	1903	Present

Table 7. SNOTEL data.

SNOTEL SITE	ID	State	Elev. (ft)	Latitude	Longitude	Start	End
Bear Basin	319	ID	5350	44.952	-116.142	10/1/1979	Present
Schweitzer Basin	738	ID	6090	48.374	-116.639	10/1/1979	Present
Hidden Lake	988	ID	5040	48.893	-116.757	9/20/2000	Present
Myrtle Creek	1053	ID	3520	48.722	-116.463	10/1/2003	Present
Ragged Mountain	1081	ID	4210	47.855	-117.036	8/22/2006	Present
Banfield Mountain	311	MT	5600	48.571	-115.445	10/1/1968	Present
Garver Creek	918	MT	4250	48.975	-115.819	10/1/1968	Present
Hawkins Lake	516	MT	6450	48.972	-115.953	10/1/1968	Present
Poorman Creek	932	MT	5100	48.126	-115.623	10/1/1968	Present
Bunchgrass Mdw	376	WA	5000	48.686	-117.176	10/1/1979	Present
Mosquito Ridge	645	ID	5200	48.057	-116.230	10/1/1978	Present
Quartz Peak	707	WA	4700	47.879	-117.089	10/1/1985	Present

2.2 Hydrology

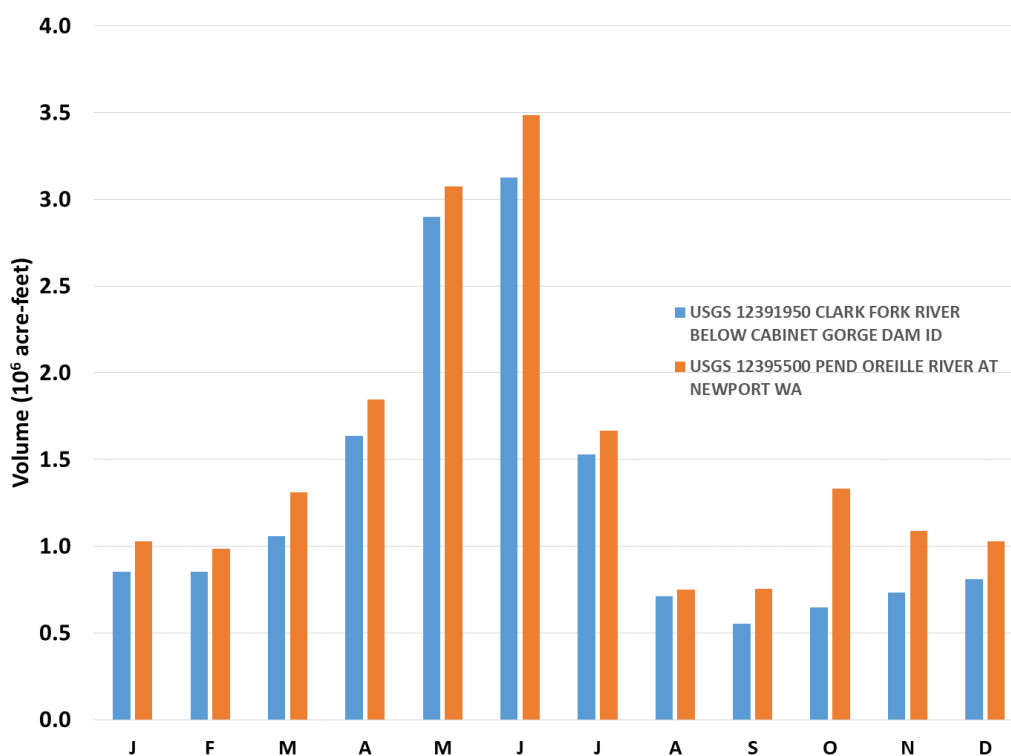
2.2.1 Lake Pend Oreille

Lake Pend Oreille is one of the largest and deepest natural lakes in North America. The lake's average depth is 545 ft, and its maximum depths are greater than 1150 ft. Its surface area is approximately 127.4 square miles, and its volume is 13 cubic miles (both at the elevation 2062 ft in the National Geodetic Vertical Datum of 1929 [NGVD29]) (Fields et al. 1996). The lake is relatively narrow and has a broad backwards S-shape in form when viewed from above. The bathymetry of most of the lake is deep with steeply sloping slide slopes. Shallow areas of the lake are limited to the northern portion of the lake, the inlet area of the Clark Fork River, and several relatively small bays and inlets.

The Clark Fork River is the major inflow to Lake Pend Oreille, and the Pend Oreille River is the major outflow. The average annual inflow of the Clark Fork River into Lake Pend Oreille for the period 1996–2017 was 15.582 MAF (million acre-feet) (USGS 2018), and the average annual outflow through the Pend Oreille River was 18.442 MAF (USGS 2018). On average, the Clark Fork River provides about 84% of the inflow into Lake Pend Oreille. The remainder of the inflow results from runoff from the watershed surrounding the lake. Water also flows out of Lake Pend Oreille as groundwater through the Spokane Valley-Rathdrum Prairie Aquifer at the southern end of the lake. The estimated flow rate is 43M gal. per day, a relatively minor flow amounting to about 0.05 MAF per year (Boese 2015).

The flows into and out of the lake vary throughout the year as shown in Figure 5. The peak flows occur in May and June as a result of snowmelt in the Clark Fork Watershed. The flows are generally low from August through February and increase starting in March to the peak flows in late spring. AFD controls the outflow from Lake Pend Oreille except when the flow rates are very high and the natural outlet becomes the hydraulic control as is discussed in section 1.1.1.

Figure 5. Monthly average Clark Fork River inflow (USGS 12391950) and Pend Oreille River outflow to Lake Pend Oreille (USGS 12395500).



The lake level is controlled to provide benefits to fisheries, flood control, and hydropower operation (USACE 2013) and follows an annual cycle shown in Figure 6 (USACE 2017). The cycle begins when the lake is drawn down in the fall and maintained at a more or less constant elevation during the winter. The wintertime elevation varies from year to year but is generally held at 2051.5 ft or 2055.5 ft NGVD29. The wintertime lake elevation is determined by conditions during the fall and is set to protect kokanee spawning and egg incubation (USACE 2013). The lake level must be at or below 2056 ft by 1 April to provide storage for flood control. The lake is allowed to rise starting in April until it reaches a maximum elevation of 2062.5 ft in June or later. This elevation is then held until the end of August. At this point, the lake level declines until the wintertime minimum is reached. Figure 7 shows the daily average lake levels for 1996–2017. The figure shows that both the wintertime minimum and summer maximums are held relatively constant with some small fluctuations.

Figure 6. Lake Pend Oreille summary hydrograph (USACE 2017).

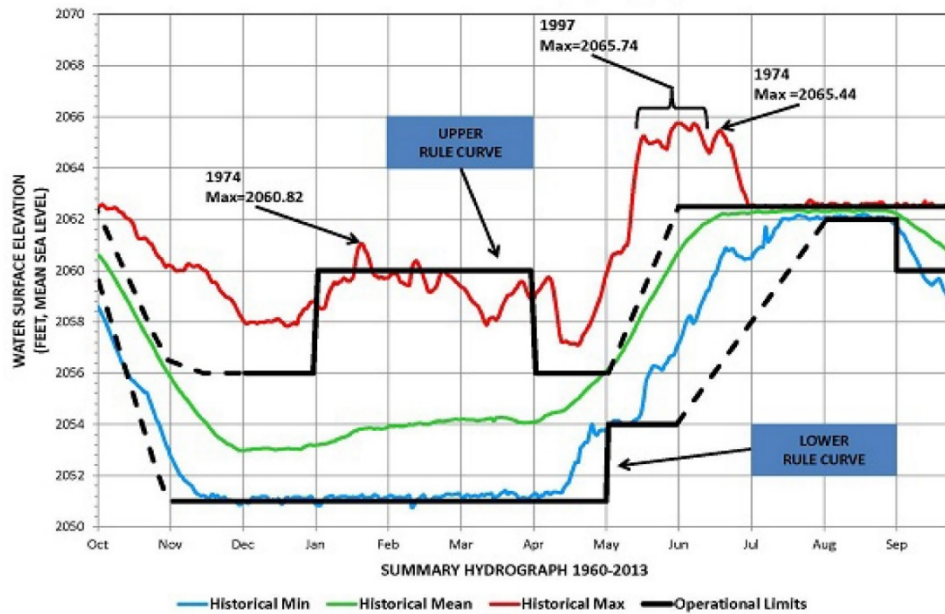
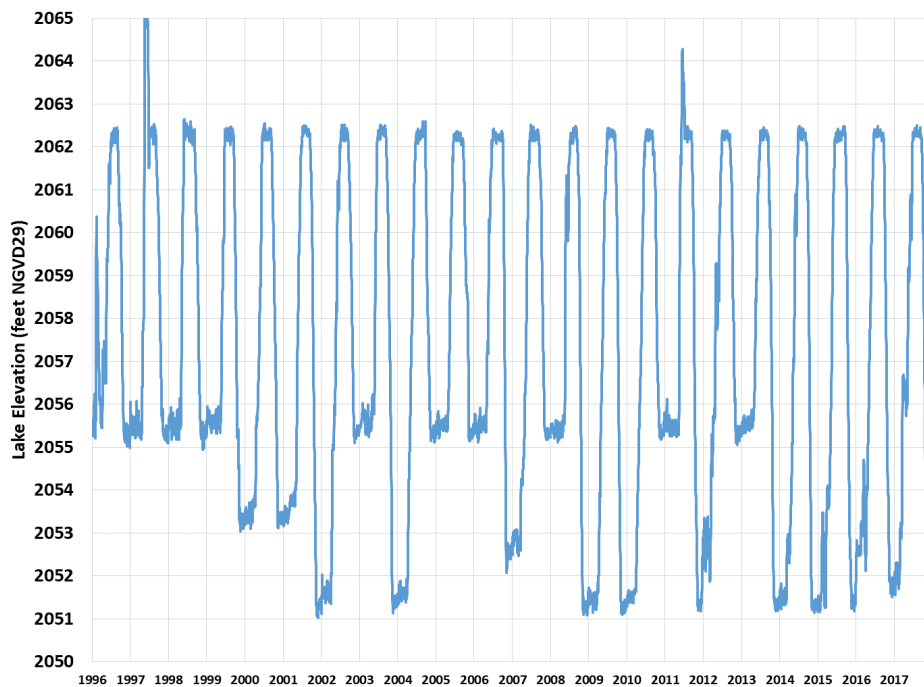


Figure 7. Lake Pend Oreille daily average lake elevation 1996–2017 based on the USGS 12392500 stage record.



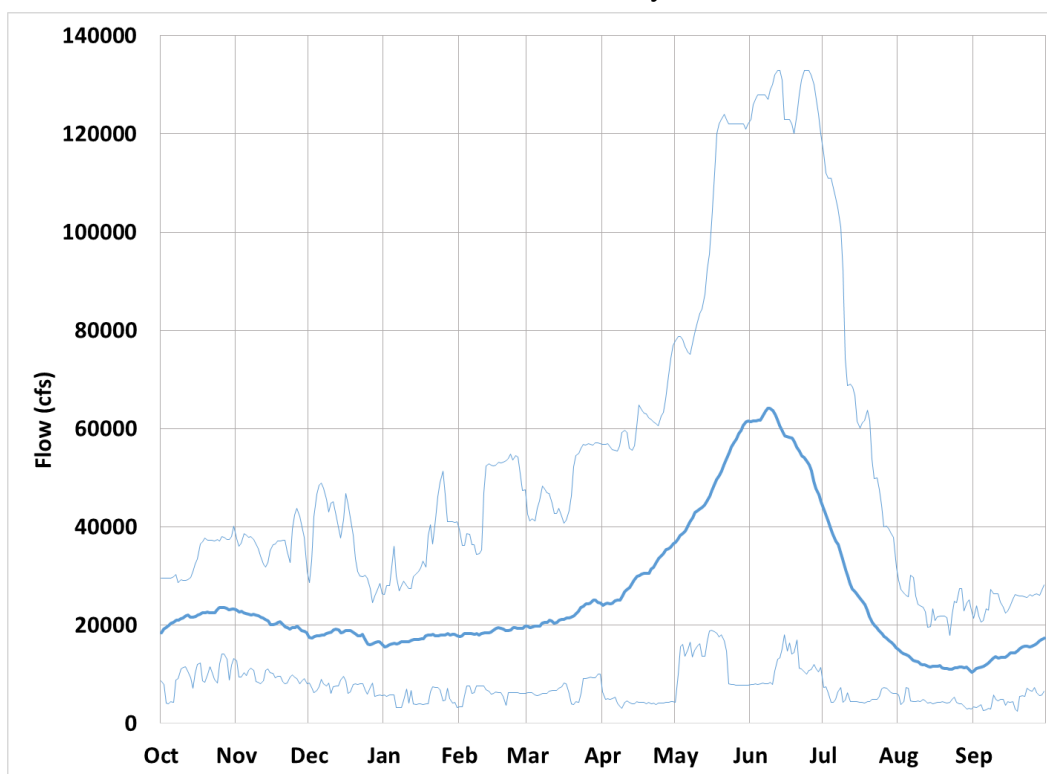
2.2.2 Pend Oreille River

The Pend Oreille River flows westerly out of Lake Pend Oreille at Sandpoint, Idaho; crosses into Washington; then flows north to the Canadian Border. The stream joins the Columbia River north of the border. Due

to the construction of AFD, a section of river upstream of the dam is now part of Lake Pend Oreille. This is commonly referred to as the “river” reach of the lake. The construction of BDC and AFD have transformed a natural river with a visible current to a relatively placid, slow moving system downstream of Sandpoint, Idaho.

The flow in the Pend Oreille River is characterized by low flows during winter, a spring snowmelt freshet (April through July), and recession flow for the rest of the summer. The flow rate in the period from May through July may be reduced somewhat due to storing water in Lake Pend Oreille in order to maintain its summer operating elevation range of 2062.0 to 2060.5 ft. The flow rate during the period of September through December may be increased slightly to lower the level of Lake Pend Oreille to its December minimum control elevation. Figure 8 shows the average, maximum, and minimum daily outflow from AFD on each day of the year. The figure shows that the maximum outflows are generally reached at the end of June while the minimum outflows occur during December, January, and February.

Figure 8. Average, maximum, and minimum daily outflow from AFD for each day of the year based on the USACE AFD daily record.



2.3 Climate

The climate in the vicinity of AFD has distinct variations between summer and winter. Summers are characterized by high air temperatures (Figure 9) with relatively large differences between the daily maximum and minimum air temperatures, lower relative humidity (Figure 10), and clear skies (Figure 11). Winters are characterized by low air temperatures (Figure 9) with relatively small differences between the daily maximum and minimum air temperatures, higher relative humidity (Figure 10), and cloudier skies (Figure 11). The monthly precipitation is greatest in November, December, and January, each with over 4 in. of precipitation on average (Figure 12). The monthly precipitation declines through the rest of the year, reaching a minimum of just over 1 in. in July and August (Figure 12).

There is limited wind data for the area around Lake Pend Oreille. The best resolution wind data is from the Sandpoint Airport, which has hourly observations available since 2007. Wind speed, wind direction, and solar radiation are other important variables when evaluating ice formation. The Sandpoint, Idaho, annual wind rose plot in Figure 13 indicates that the majority of wind as well as the higher wind speeds come from the north-northeast direction.

Figure 9. Daily average maximum and minimum air temperatures.

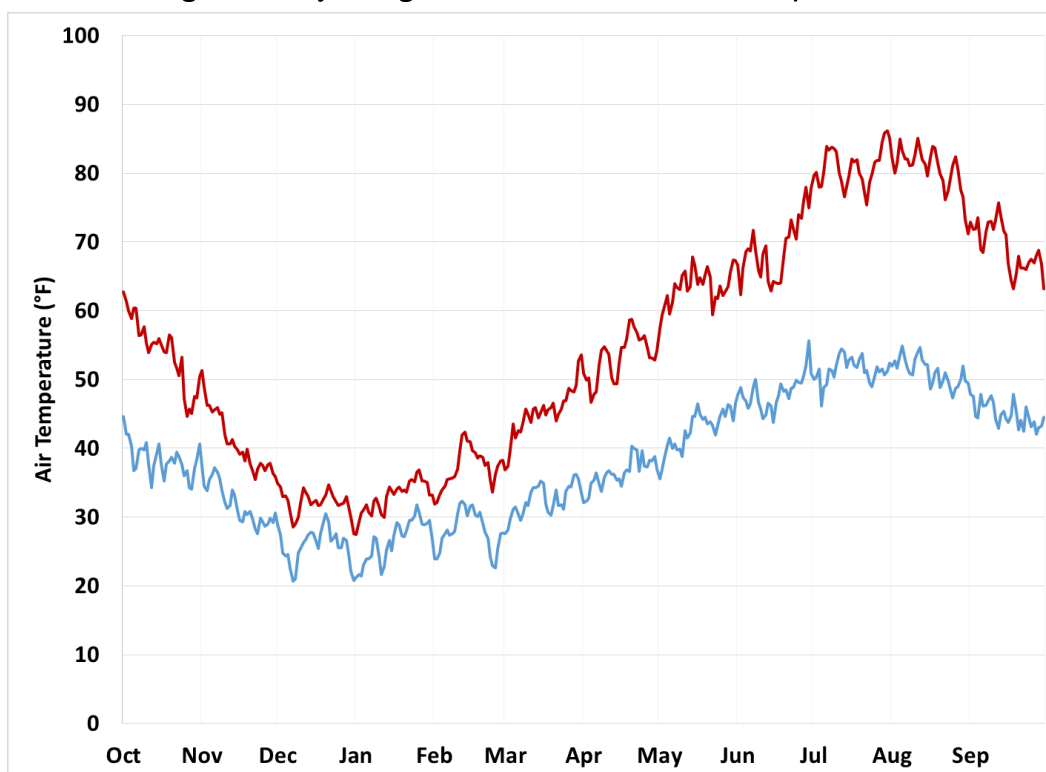


Figure 10. Daily average maximum, minimum, and average relative humidity.

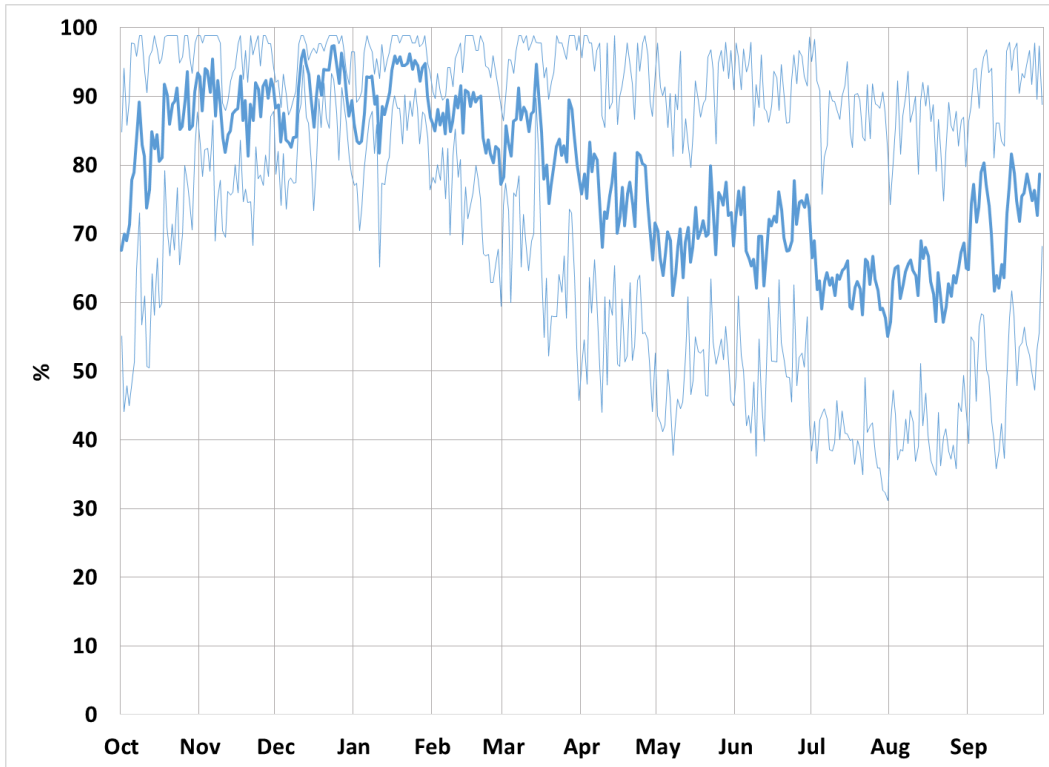


Figure 11. Daily average percent cloud cover.

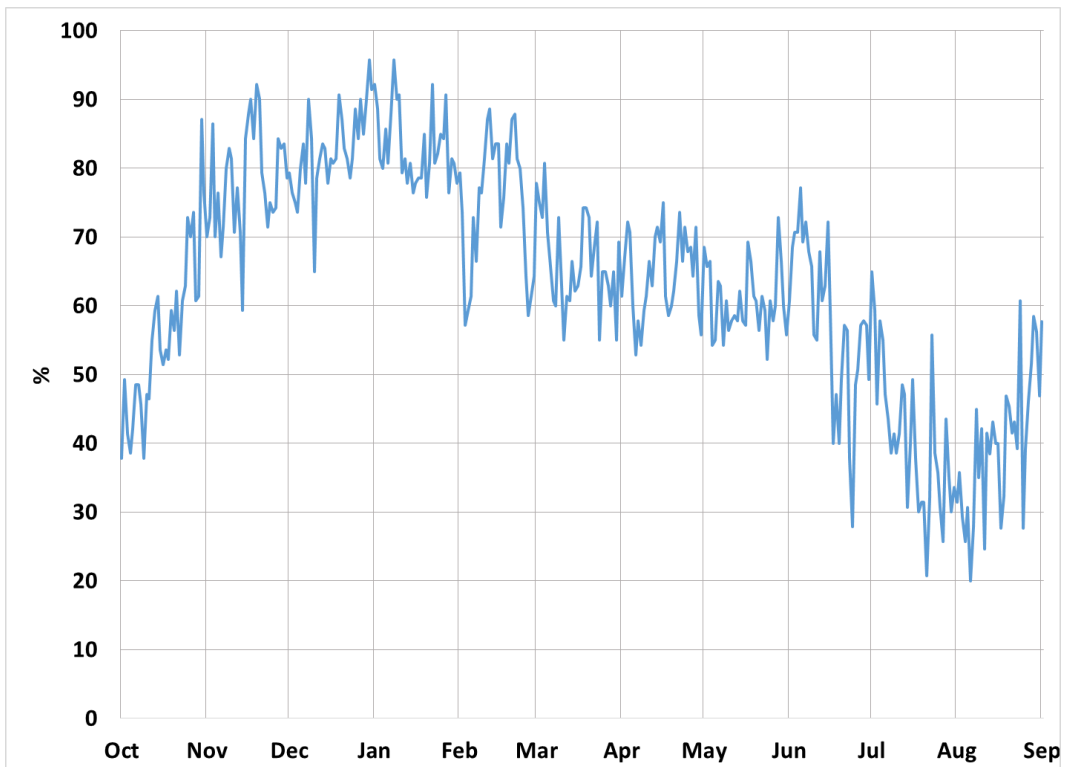


Figure 12. Average monthly precipitation for Sandpoint, Idaho, based on the Sandpoint Experimental Station.

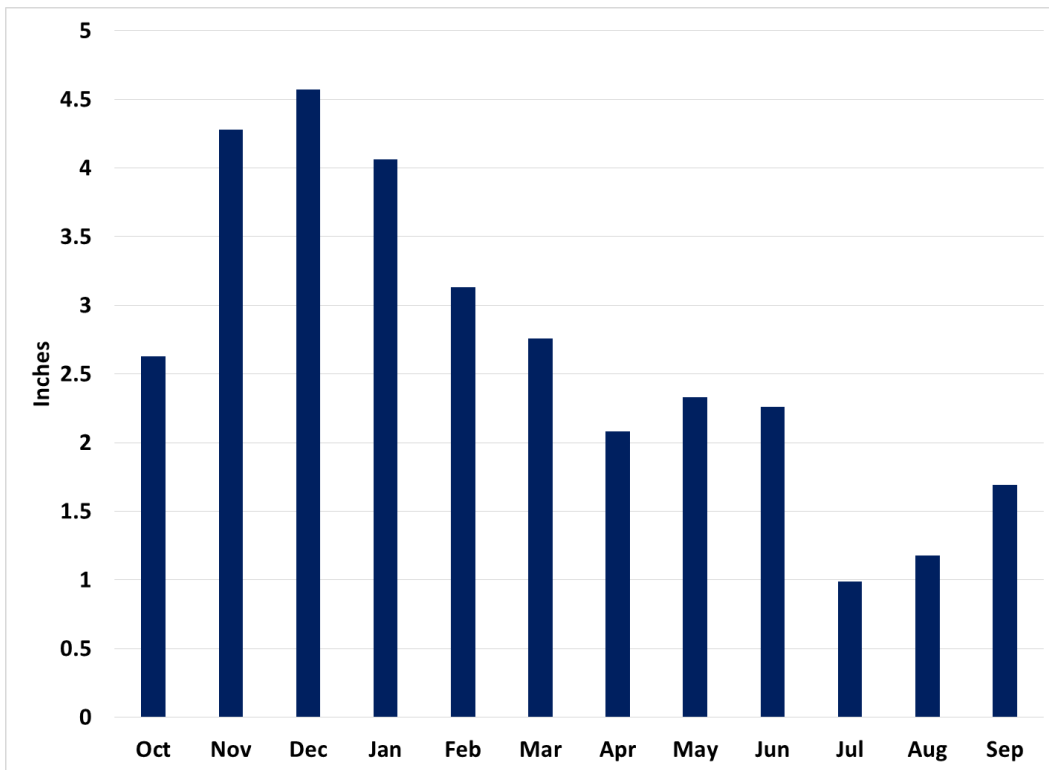
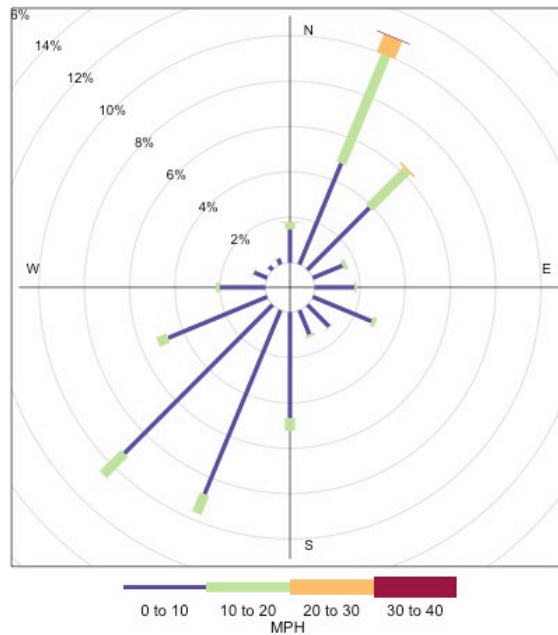


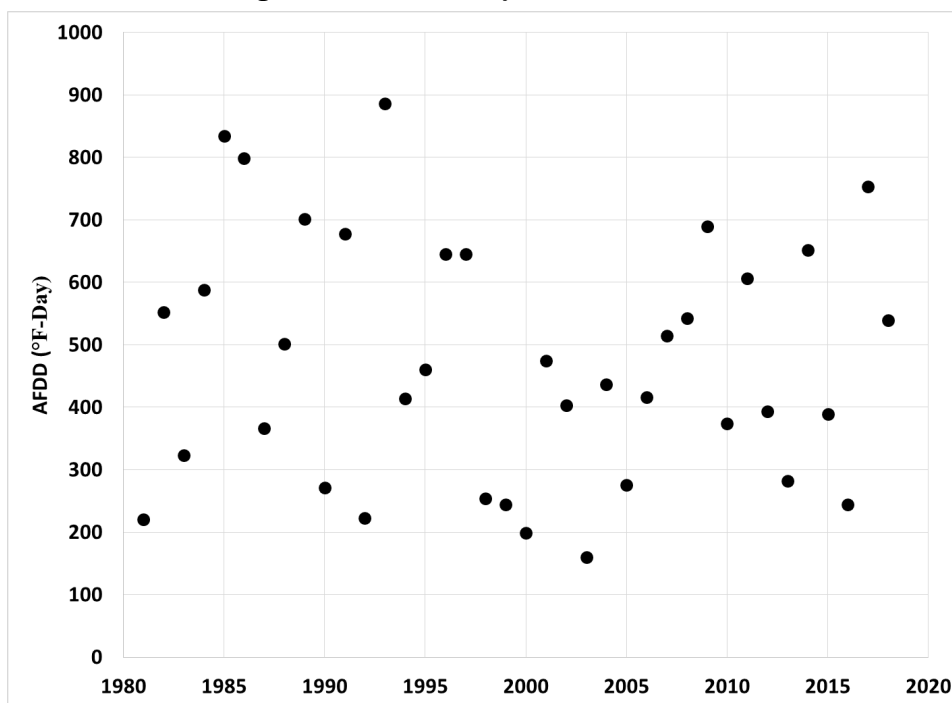
Figure 13. Annual wind rose for Sandpoint, Idaho, airport.



The winter weather is influenced by both the continental polar and maritime polar air masses. This results in periods of extreme cold followed by

relatively mild winter temperatures. As a result, the accumulation of freezing degree-days is event driven unlike other locations in the northern U.S. that have sustained periods of below freezing temperatures. Figure 14 plots the maximum AFDD values based on the Sandpoint, Idaho, Experimental Station data. The large range of AFDD values reflects the annual variability of cold air masses to the region.

Figure 14. AFDD water years 1981 to 2018.



2.4 Ice-thickness model

We estimated the ice growth for Lake Pend Oreille and the Pend Oreille River using the method described in Engineering Manual 1110-2-1612 (USACE 2002). This method (referred to as the ICETHK model in the Engineering Manual) uses daily average air temperature to estimate surface-ice growth. Our analysis used the Sandpoint Experimental Station daily air temperature from water years (WYs) 1981 through 2017. The air temperature values are used to compute the AFDD, which is then used to estimate the ice thickness on a daily time step. No ice-thickness observations for Lake Pend Oreille or the Pend Oreille River were available for this study. This presents challenges when calibrating the ice-growth parameters. Consequently parameters from other studies were used as reasonable estimates. Table 8 summarizes the parameters used for this analysis. $AFDD_{min}$ represents the accumulation of freezing degree-days it takes to cool the

water before ice formation occurs. The other parameters used for estimating ice growth and melt are α^* and β which represent heat transfer between the atmosphere and the ice.

Table 8. Ice-thickness parameters

Parameter	Value
$AFDD_{min}$	150 °C-days
α^*	2.3 cm (°C-day) ^{-1/2}
β	0.45 cm (°C-day) ^{-1/2}

Figure 15 presents the annual maximum of the ice thickness for Lake Pend Oreille and the Pend Oreille River. The average annual maximum ice thickness is approximately 7 in. for WYs 2003 through 2017. As discussed previously, the annual variability of cold periods can be large, which results in significant differences in ice thickness. The maximum ice thickness also varies between months. Figure 16 summarizes the average maximum ice thickness by month and compares that to the annual average maximum. The model estimates that peak ice thickness is generally in January or February for this area. It should be noted that there were three years in 2003–2017 where the model predicted ice in April. Based on information from project staff and the historical temperature records, the presence of ice in April is very unlikely.

Figure 15. Modeled maximum surface-ice thickness from WYs 2003 through 2017.

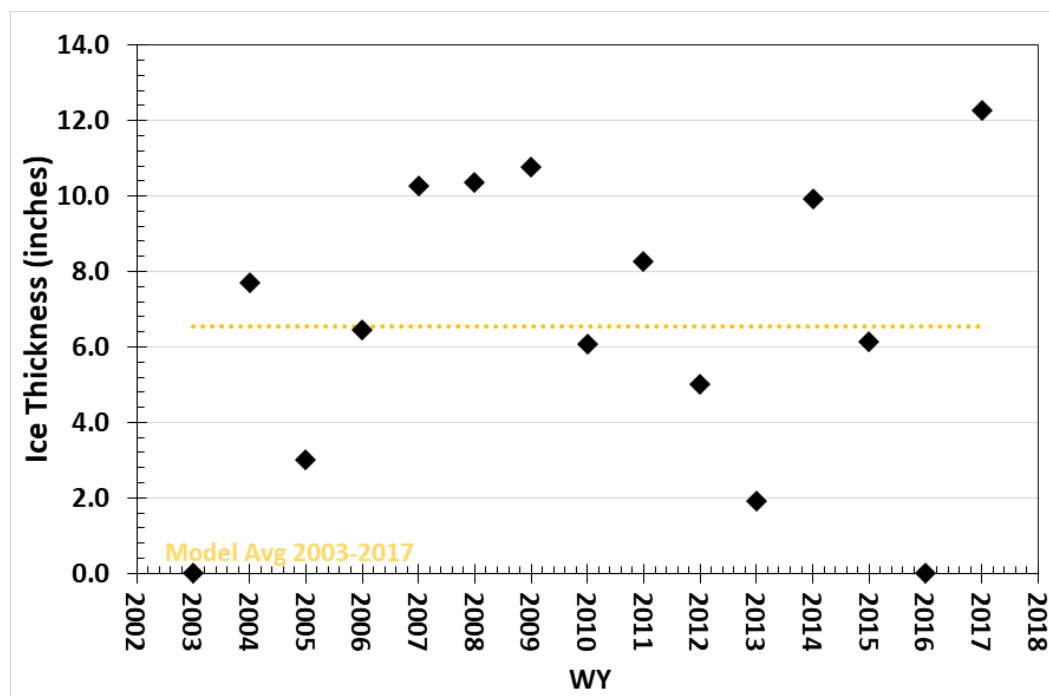
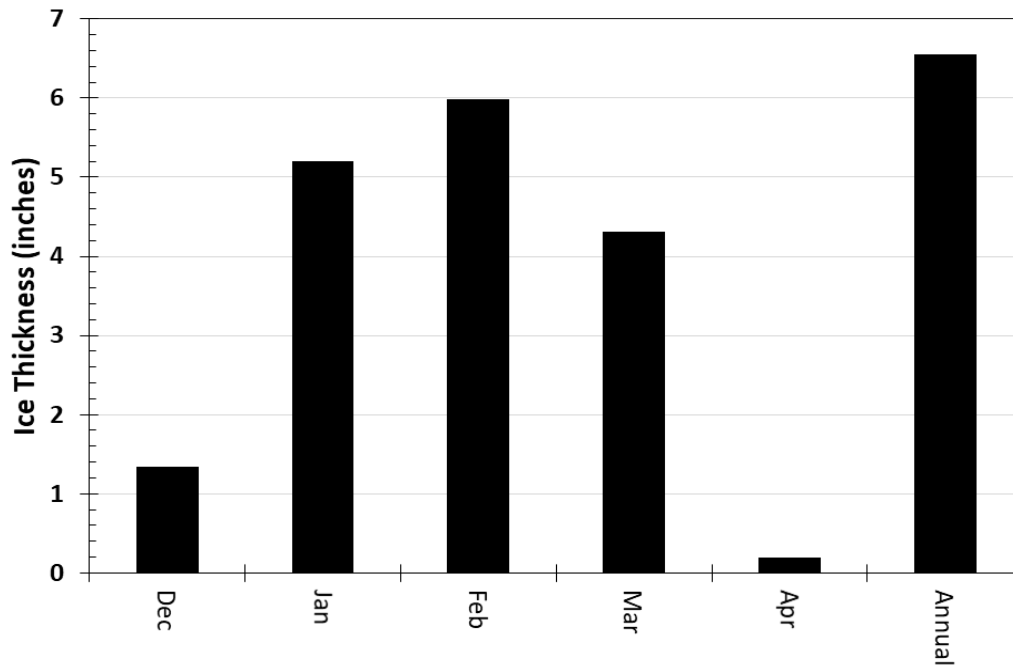


Figure 16. Average maximum ice thickness by month.



3 Pend Oreille River Hydraulics

3.1 Development of a wintertime hydraulic model

Modeling flow in the Pend Oreille River between AFD and BCD is complicated by the backwater effect of BCD. The forebay water surface elevation set at BCD impacts the stage of the entire 56-mile reach between the dams. The USACE Seattle District provided an existing one-dimensional open-water hydraulic model constructed with the USACE HEC-RAS. We modified this to evaluate dynamic effects of dam operations in conjunction with the effects of ice processes.

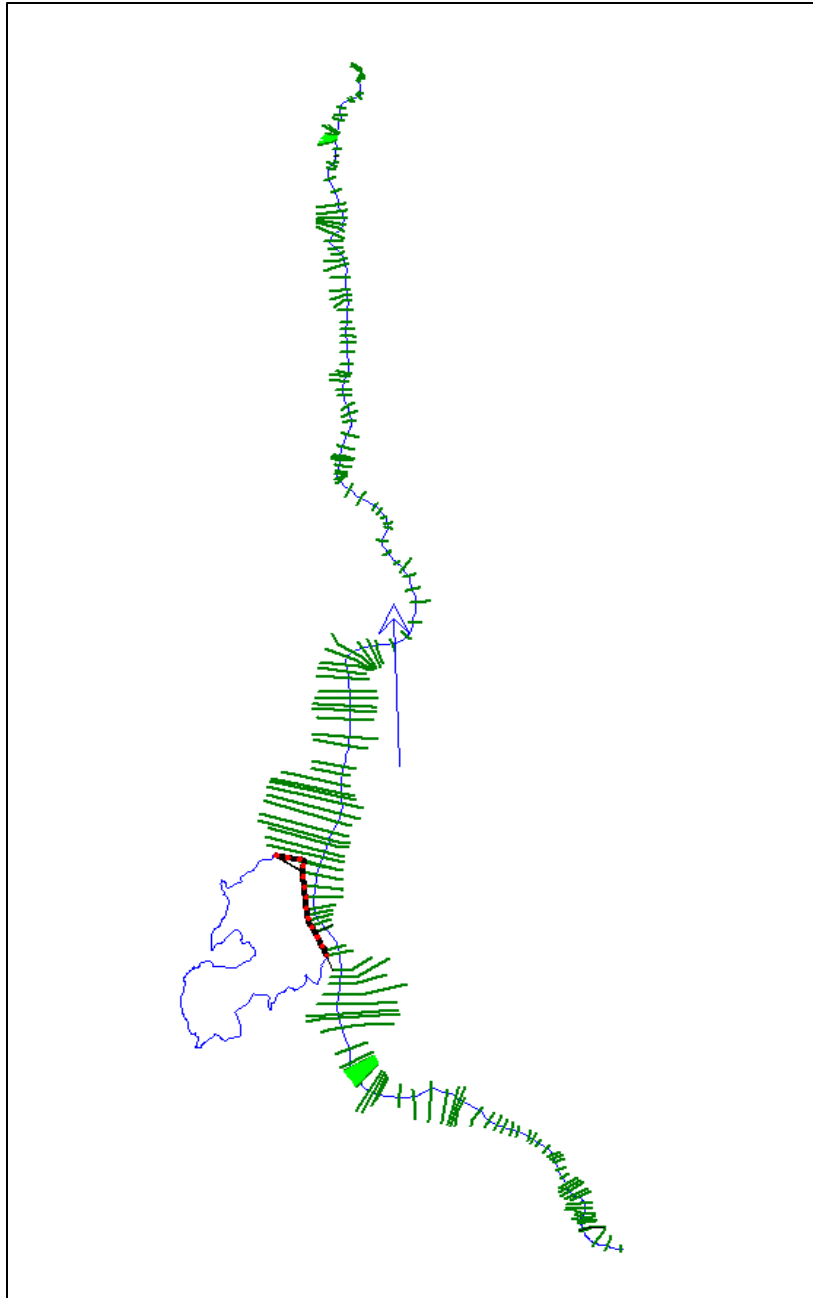
3.1.1 Existing hydraulic model geometry

For this study, geometry data used to model the Pend Oreille River were based on an existing one-dimensional HEC-RAS. The model covers the reach between AFD and BCD, shown in Figure 17. The upstream cross section of the model is immediately below AFD. The model's lower boundary is located approximately 56 river miles downstream in the forebay of BCD. The bed elevation ranges from 2019.42 ft to 1934.39 ft (referenced to the North American Vertical Datum of 1988, NAVD88) between the model boundaries with a total elevation change of 85.03 ft. The first 38.91 ft of bed elevation change occur in the upstream 54.21 miles (0.01% slope), while the remaining 46.12 ft of change occur in the last 1.75 miles of the model (0.5% slope) in the vicinity of Box Canyon Dam. The model consists of 220 cross sections with a mean spacing of 1350 ft; however, there is considerable variability in spacing, with several sections more than 4000 ft apart along straight reaches of river. Cross section data appear to be derived from a 16.404 ft (natively 5 m) digital elevation model (DEM) that accompanied the model. The DEM includes coarse bathymetric geometry of the channel bottom. The source of the DEM and the bathymetric data were not provided with the model. The river model contains six bridges, which, according to the model notes, were imported from a previous hydraulic model that was built using the USACE HEC-2 modeling software.

The overbank Manning's n values are 0.05 for the entire model. The channel Manning's n values are 0.033 for the upper 52.73 miles (from the model river station [RS] 89.02496 to RS 36.49329 in miles); change to 0.038 through a short 1.15 mile transition zone just downstream of Ione,

Washington (RS 36.49329 to RS 34.44691); and rise to 0.043 through the last 2.08 miles to end of the model (RS 34.44691 to RS 33.26100).

Figure 17. Pend Oreille River HEC-RAS model, Albeni Falls Dam to Box Canyon Dam.



We used a recorded time series of hourly releases from AFD as the upstream boundary condition of the model. Recorded forebay water surface elevations at BCD were used as the downstream boundary condition. The forebay elevations are reported as daily averages and were converted to

hourly time series to match the model's time step. Once the data was temporally synchronized, we simulated flow in the river for the time period between March 2003 and March 2017. The cross section immediately downstream of AFD (RS 89.02496) was used as a reference station where modeled stages were compared with observed tailwater stages to assess model performance. The Corps Water Management System provided both flow and observed stage data (USACE 2017). Figure 18 compares the modeled and observed results. In general, the model reproduces the observed tailwater stages well; but, prior to our modifications, the model is more accurate at higher flows. Figure 19 shows the difference between the computed and observed tailwater stage as a function of discharge. The model has the least error between 40,000 and 80,000 cfs but tends to under-predict stage between 5000 and 35,000 cfs. Figure 20 shows the model error as a function of season, with the least error occurring in May and June. This suggests that the model was built and calibrated for representing large spring flow events. We adjusted the model geometry and channel roughness to improve the wintertime low-flow performance.

Figure 18. Comparison of modeled and observed tailwater elevation at AFD from 2003 to 2018.

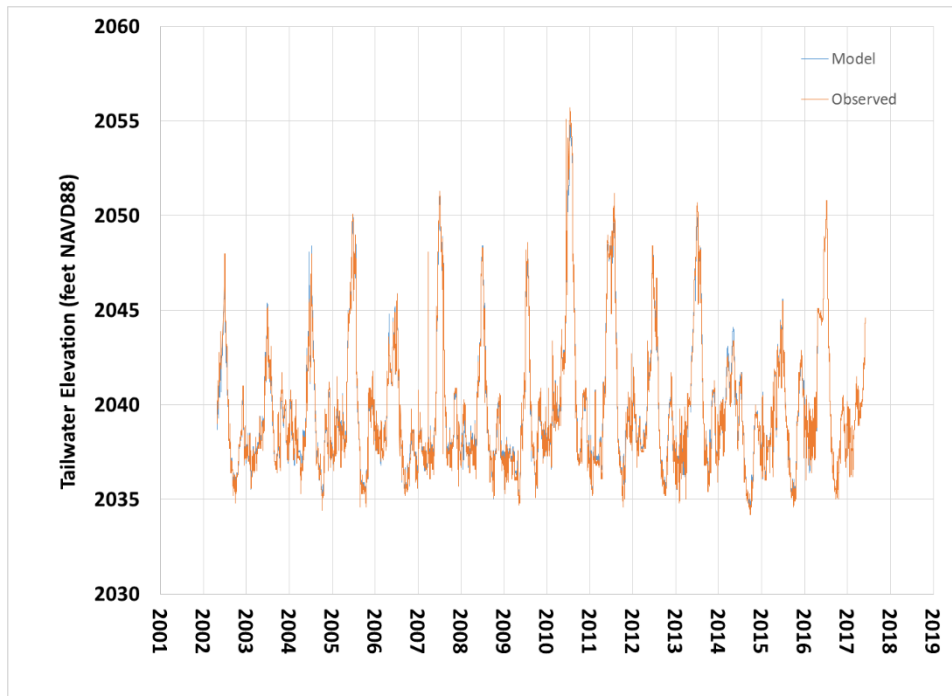


Figure 19. Difference between modeled and observed tailwater at AFD as a function of discharge.

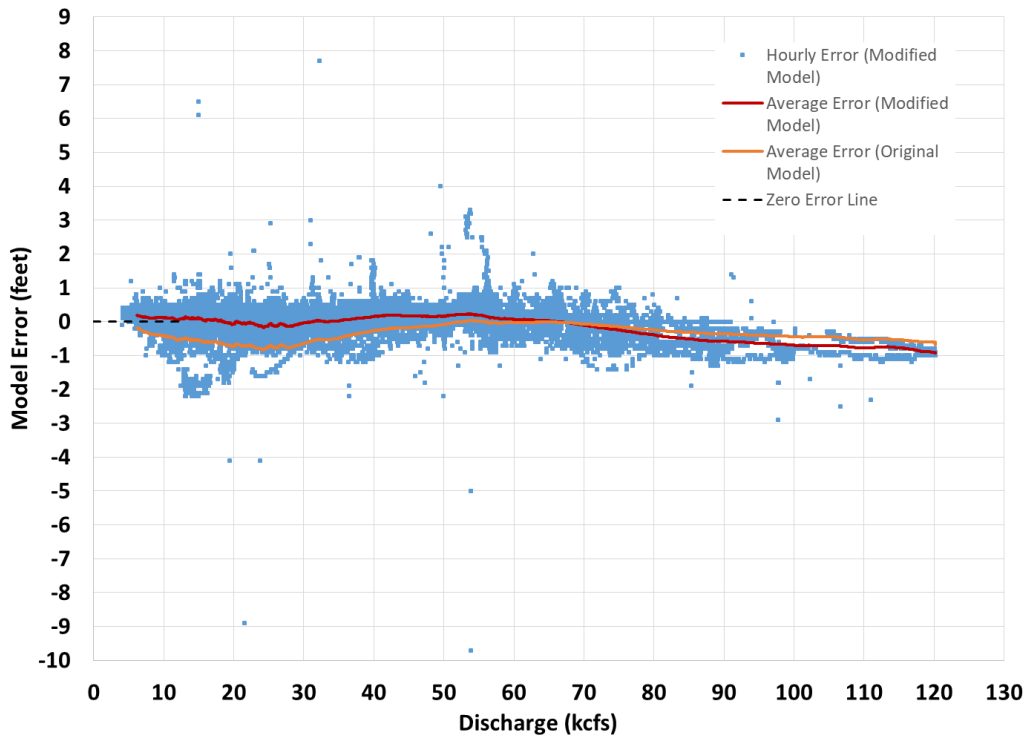
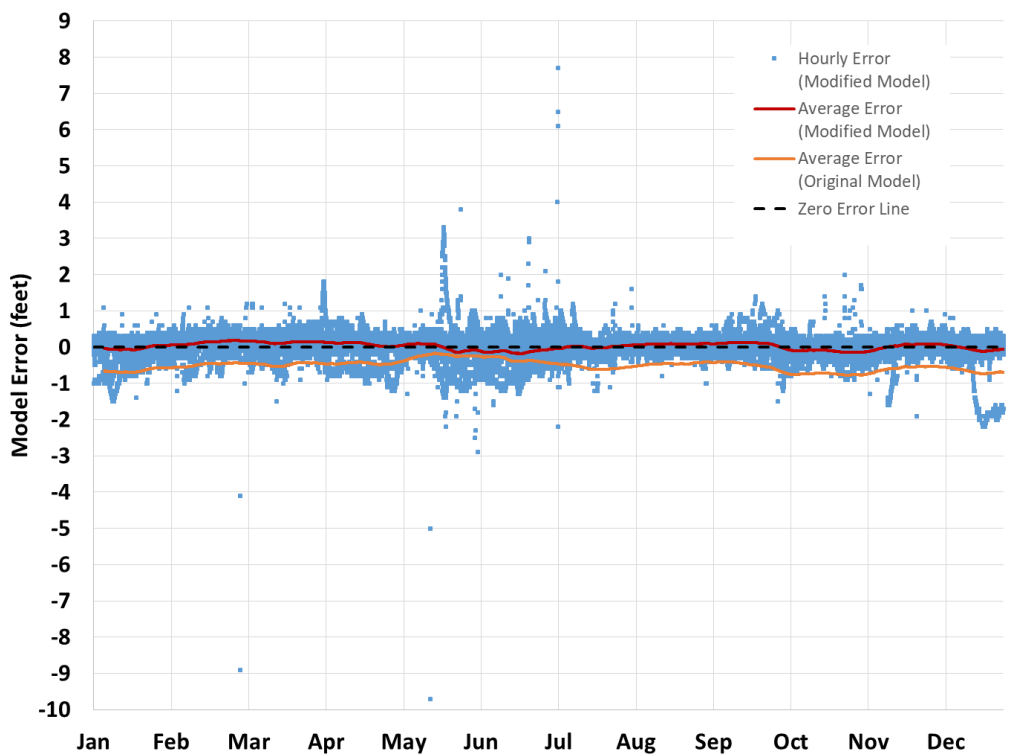


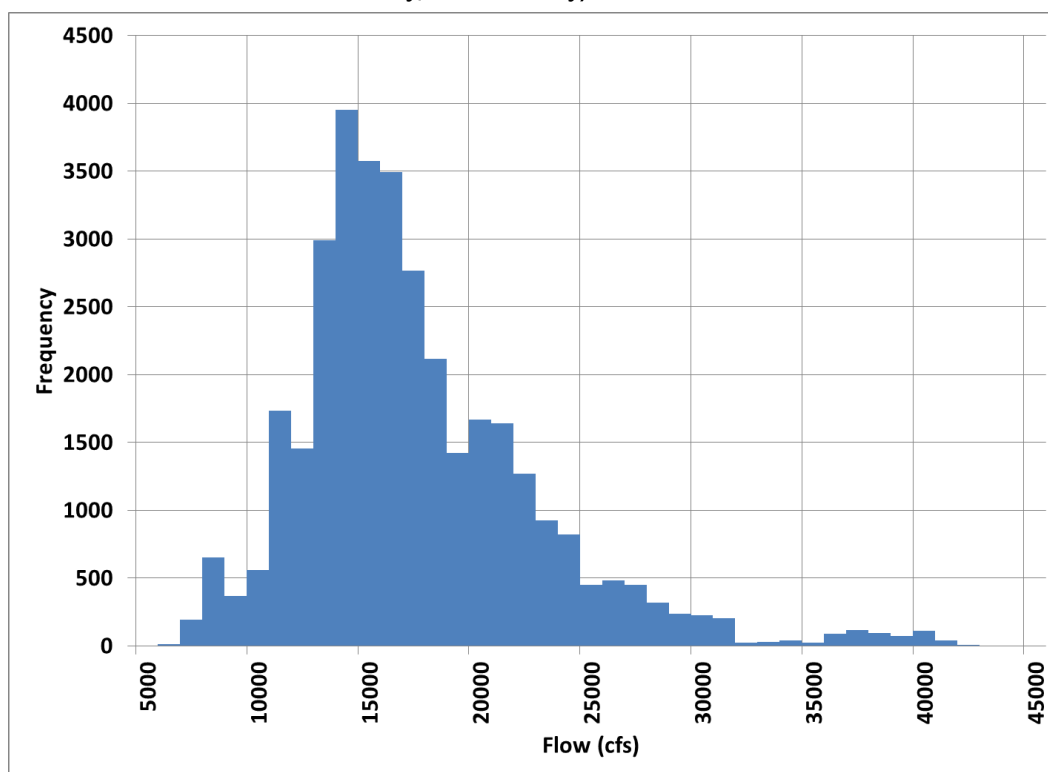
Figure 20. Difference between modeled and observed tailwater at AFD as a function of time of year.



3.1.2 Geometry modifications for winter flows

For the purposes of the hydraulic analysis, December through February was defined as the winter months when ice had the highest potential to be present on the river. Winter discharges from 2003 to 2017 ranged from 5000 to 40,000 cfs, with a mean of approximately 15,000 cfs. Figure 21 shows a histogram of winter flow distribution. Increasing the Manning's n values for the overbank and channel increased the modeled stages at Albeni Falls but did not remove the distinct "sag" pattern in the error plot centered around 25,000 cfs that is seen in Figure 19.

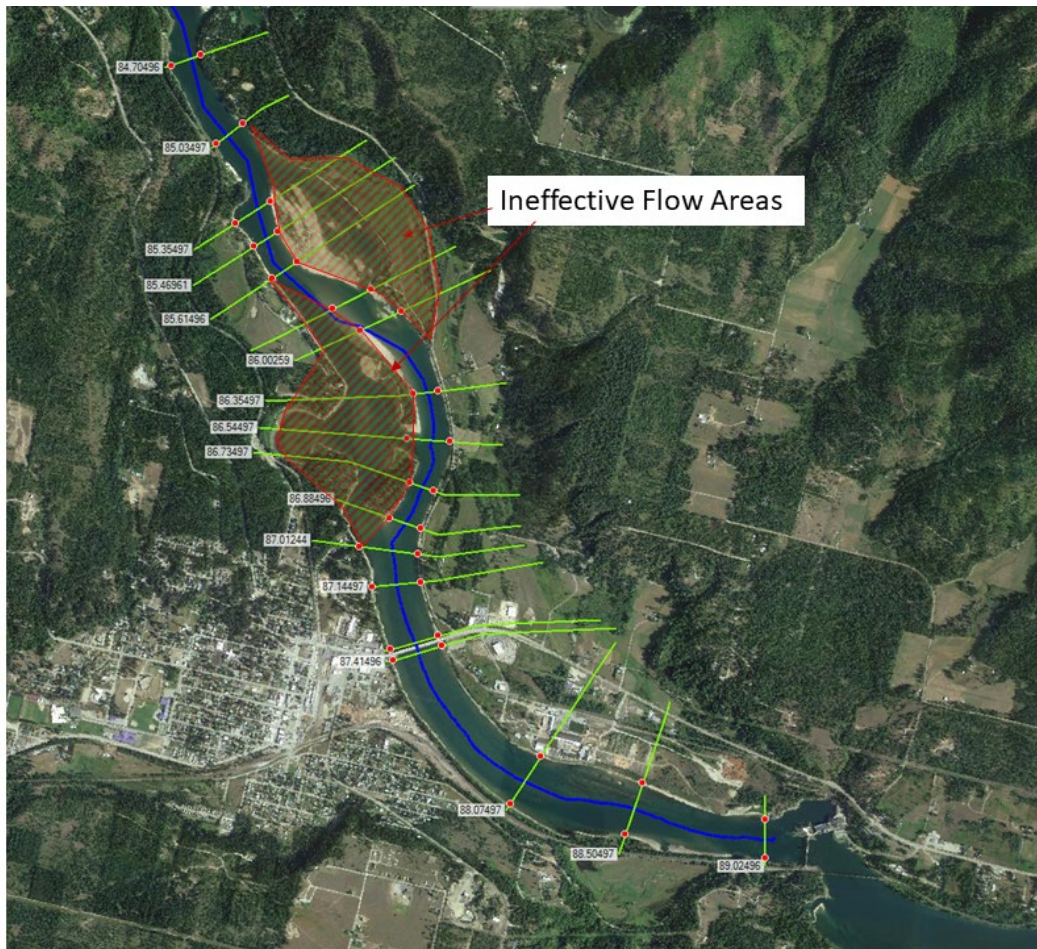
Figure 21. Histogram of hourly discharges for winter months (December, January, and February) 2003–2018.



Further review of the model revealed that the cross sections in the vicinity of several island groups downstream of AFD had much larger cross-sectional areas than those upstream due to the bifurcation of the river channel. Figure 22 shows the most upstream group of islands from RS 86.88496 to RS 85.35497. A similar group exists further downstream between RS 80.98497 to RS 79.07497. A review of aerial photographs suggests that, around these islands, there is a less dominant channel that contains more visible sediment deposited by slower-moving water and a more dominant channel that likely conveys most of the flow at lower stages. We modified

the model cross sections in these island groups by moving the bank stations to either side of the apparent dominant channel and isolating the less dominant channel with permanent ineffective areas. The height of the ineffective areas was adjusted iteratively along with modifications to the Manning's n values until the modeled tailwater errors were minimized. The overbank Manning's n values are 0.05 for the entire modified model. The channel Manning's n values are 0.019 for the upper 2.01 miles of the model (RS 89.02496 to RS 87.01244), then 0.020 for 15.01 miles (RS 87.01244 to RS 72.00497), 0.035 for 0.25 miles (RS 72.00497 to RS 70.25497), and 0.04 for the last 37.0 miles (RS 70.25497 to RS 33.26100).

Figure 22. Midchannel islands between RS 86.88496 and RS 85.35497.



3.1.3 Model performance for wintertime flows

The constrictions imposed by the ineffective flow areas placed in the island group cross sections create a moderate backwater effect that raises the computed AFD tailwater elevations for low flows.

Table 9 compares the root-mean-square error (RMSE) and the mean absolute error (MAE) of predictions of tailwater at AFD from the original and the modified model. Of note, the modifications do not significantly affect model performance at high flows.

Table 9. HEC-RAS model error (in feet) at AFD tailwater stage (RS 89.02496). From all-season flows March 2003–March 2017.

Models	All Flows		Flows < 40K cfs		Flows > 40K cfs	
	RMSE	MAE	RMSE	MAE	RMSE	MAE
Original Model	0.58	0.50	0.60	0.53	0.39	0.27
Modified Low-Flow Model	0.30	0.21	0.27	0.19	0.46	0.34

The difference between the original and modified geometry model results were also compared with stages measured at the Pend Oreille River at the Cusick, Washington, gage (USGS 12395950), located near RS 68.54497. Again, the modified model performed better than the original model over the range of flows expected during winter (less than 40,000 cfs) as measured by the MAE, which improved from 0.78 to 0.56 ft. Further adjustments would be needed to fully calibrate the model to observed winter stages. However, the limited adjustments that were made improved the low-flow performance of the model significantly.

3.1.4 Flow conditions

The modified model was used to evaluate flow conditions on the river over a range of steady open-water scenarios. The water surface profiles in Figure 23 show the river stages over the range of expected winter flows. Observations at BCD indicate that a fixed forebay water surface elevation is generally maintained even with varied inflows. The downstream boundary condition in these model runs was a fixed elevation, which causes the profiles to converge at the downstream end.

The construction of BCD profoundly changed the natural hydraulics between BCD and AFD. We modeled the natural flow condition by setting the downstream boundary condition to the normal depth of the natural cross section in the BCD forebay, essentially disregarding the effect of BCD. The profiles in Figure 24 demonstrate the difference between the natural water surface elevations and those affected by the BCD forebay. The profiles were calculated with a flow rate of 15,000 cfs, which is the approximate average winter flow, and 40,000 cfs, which represents the high end of expected flows. Figure 25 shows the effect of the BCD backwater on

water velocities upstream under average flow conditions. As with the water surface elevations, the largest impacts are seen closest to BCD; however, the trend of slower, deeper flow due to the BCD backwater is a persistent pattern along the entire reach.

As an independent check of the model, the natural rating curve from HEC-RAS was compared with a natural rating curve developed for the AFD tailwater and attributed to a 1983 power-loss agreement (USACE 2017). Figure 26 plots the 1983 rating curve overlaid with the modified HEC-RAS rating curve. The curves show strong agreement over the range of winter-time flows. The figure also shows the computed rating curves for the controlled condition, demonstrating that the presence of BCD produces higher stages at AFD versus natural conditions under all flow conditions considered. The rating curves are plotted again in Figure 27 along with the history of stages and flows from March 2003 to March 2017. Deviations from the rating curve are a combination of model error and hysteresis from the dynamic effects of the unsteady flow. Identification of model bias for the tailwater rating curves was important to ensure that accurate thresholds were developed for comparing modeled and observed stages below AFD.

Figure 23. Open-water surface (WS) profiles for flows ranging from 5000 to 45,000 cfs.

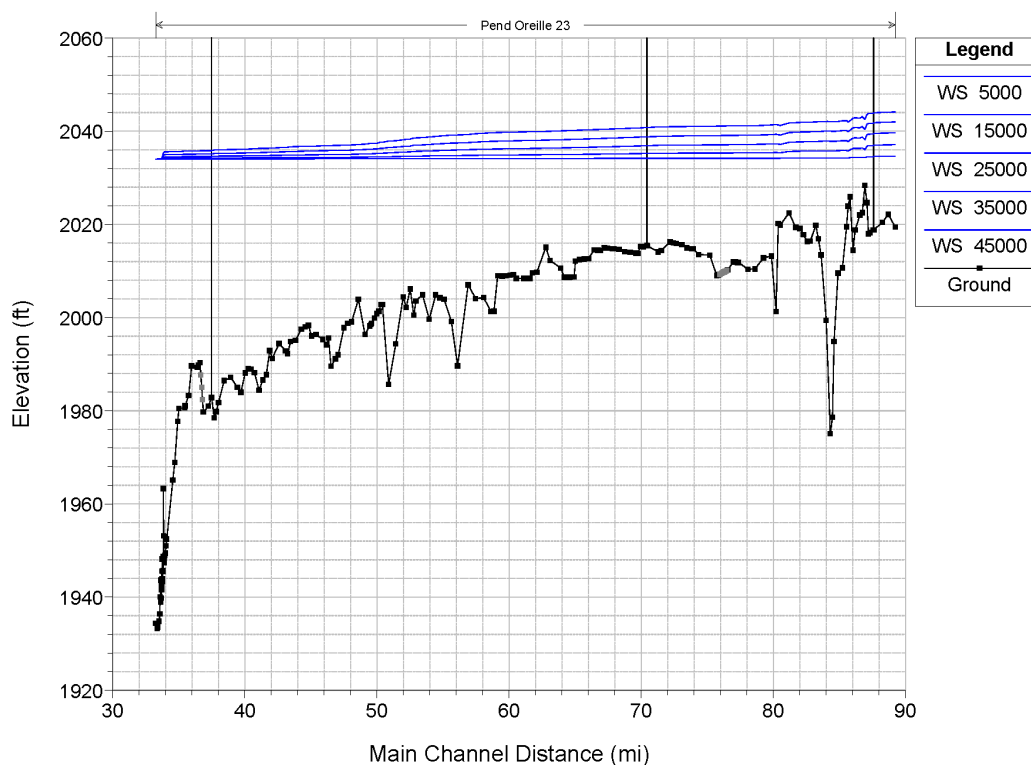


Figure 24. Open-water surface profiles showing the effect the BCD forebay at an elevation of 2034.0 ft has on upstream stage for flows of 15 and 40 kcfs. *Dashed lines show the stages without the effects of BCD for the same flows.*

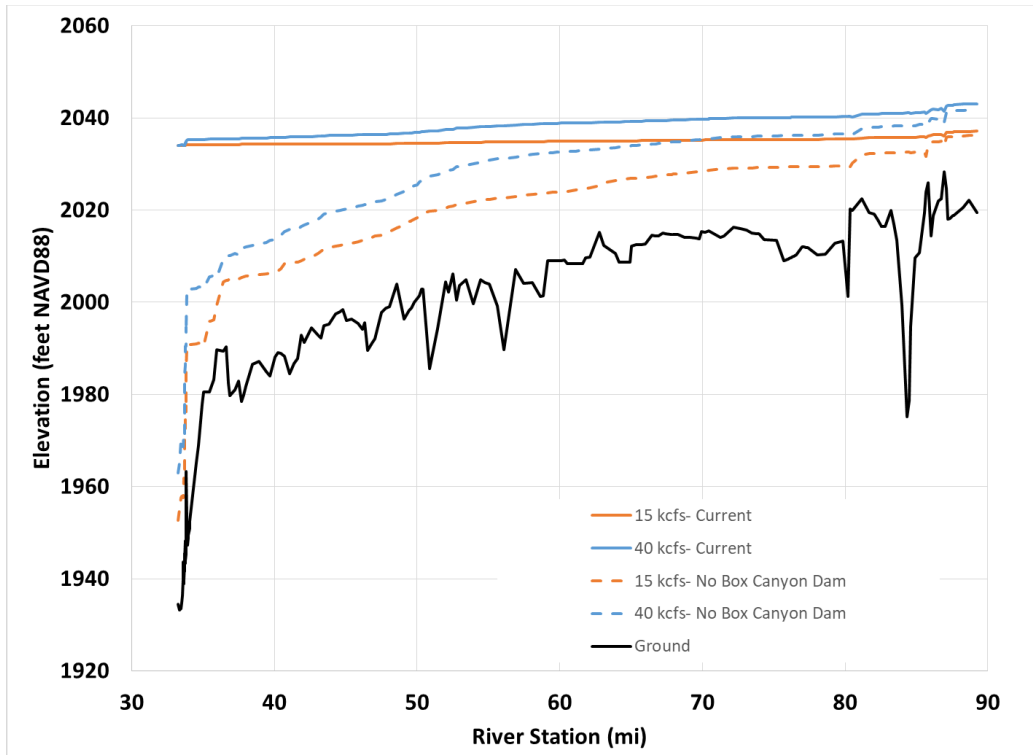


Figure 25. Open-water channel velocities for 15 kcfs under natural flow conditions and flow controlled by BCD forebay elevation at 2034.0 ft.

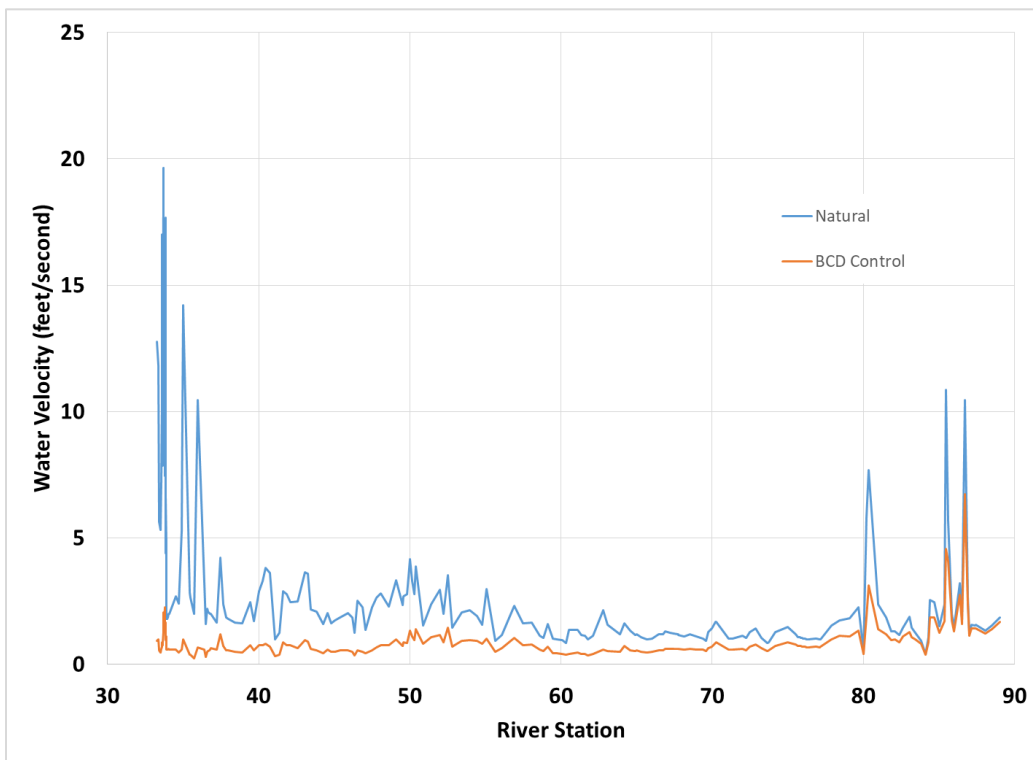


Figure 26. Comparison of AFD tailwater rating curves.

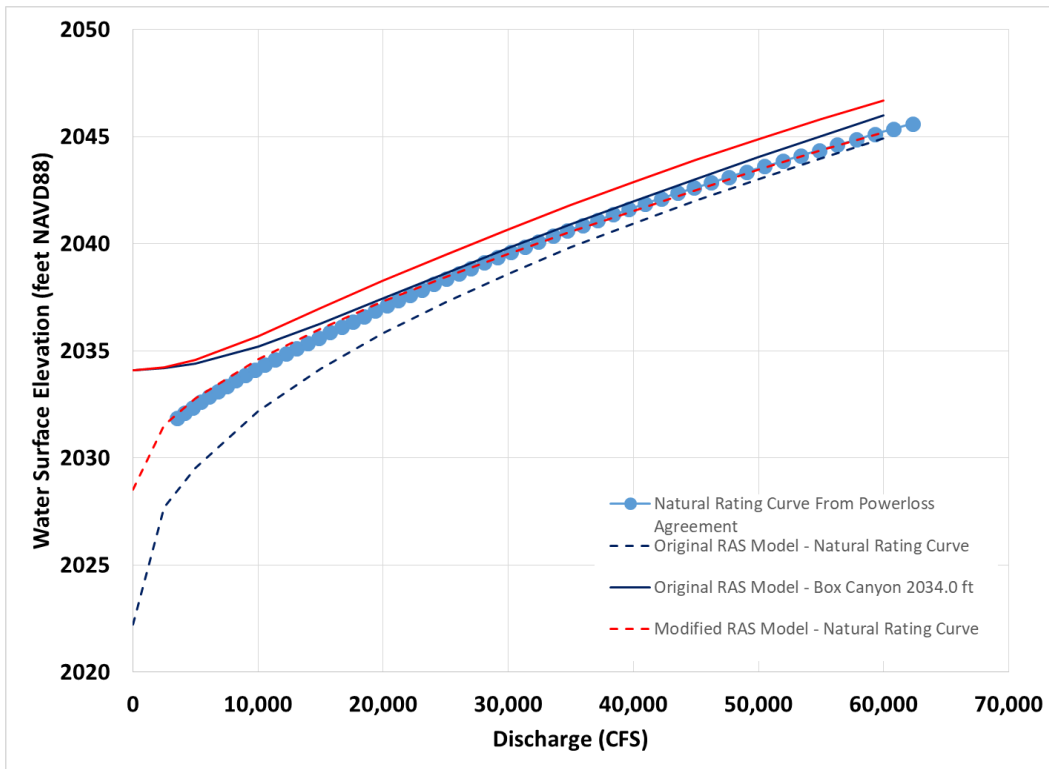
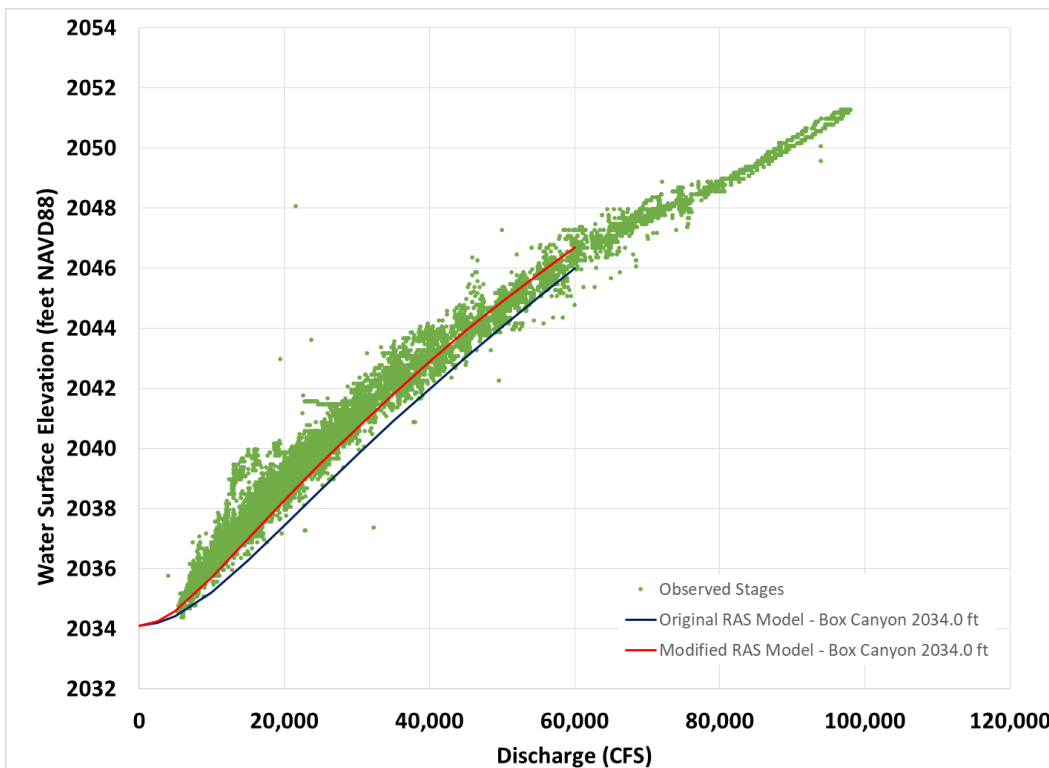


Figure 27. Albeni Falls Dam tailwater rating curves compared to observed stage and flow data.



4 Ice Formation in the Pend Oreille River

4.1 Shoreline camera ice observations

Figure 28 provides an overview of all the years when imagery was available for the Pend Oreille River downstream of AFD. Generally, the imagery was available for the winter only. Figure 29 shows the ice conditions during the winter of 2014–2015; Figure 30 shows the winter of 2015–2016; and Figure 31 shows the winter of 2016–2017. We determined the ice conditions based on a visual inspection of each image. The ice codes used were (1) some ice in image but no well-developed shore ice, (2) developed shore ice visible but open water in the center of the channel, and (3) complete ice cover across the channel.

Figure 28. Overview of imagery data collected along the Pend Oreille River.

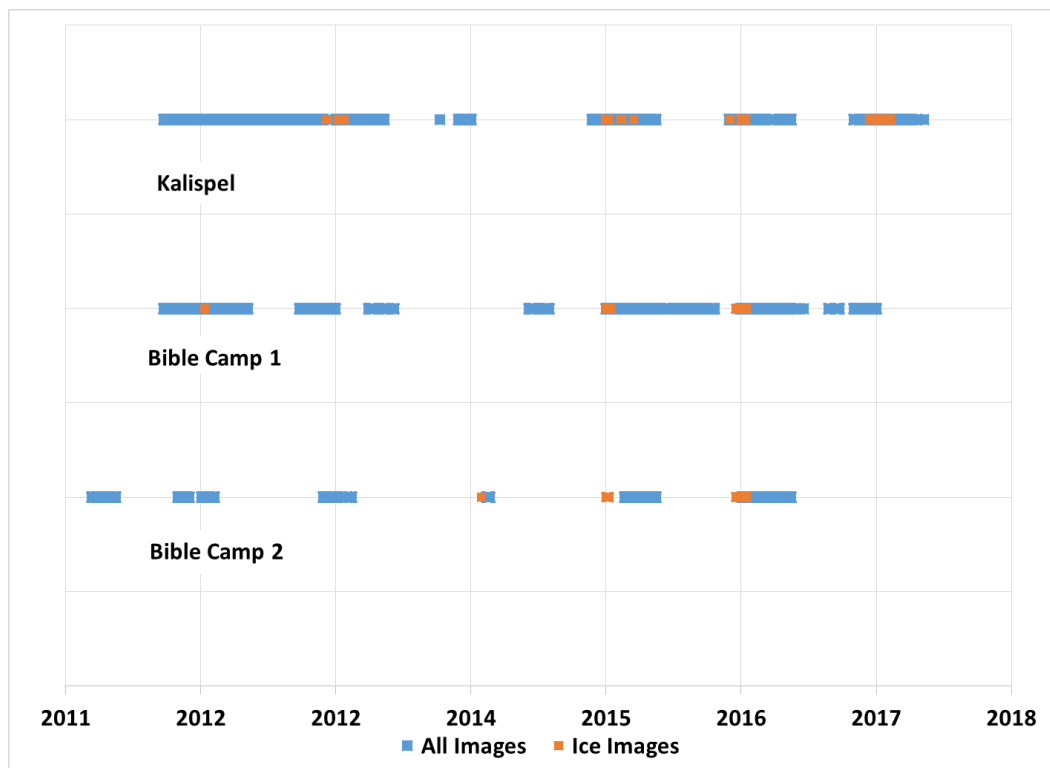


Figure 29. Ice cover on the Pend Oreille River for winter 2014–2015.

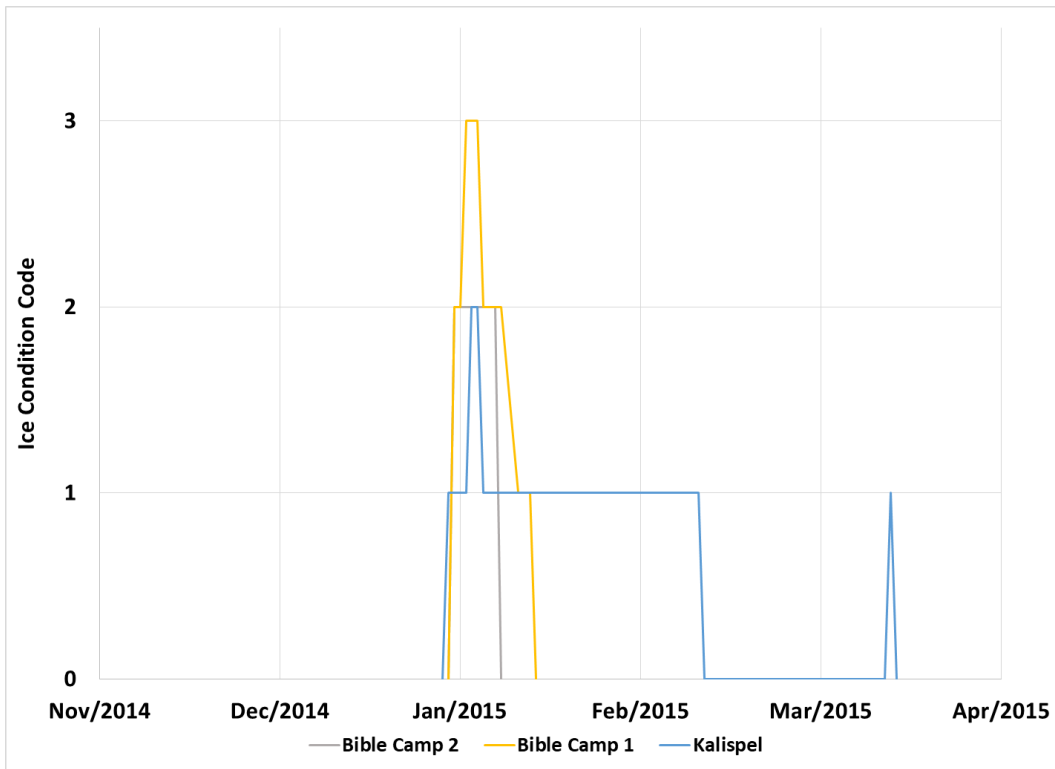


Figure 30. Ice cover on the Pend Oreille River for winter 2015–2016.

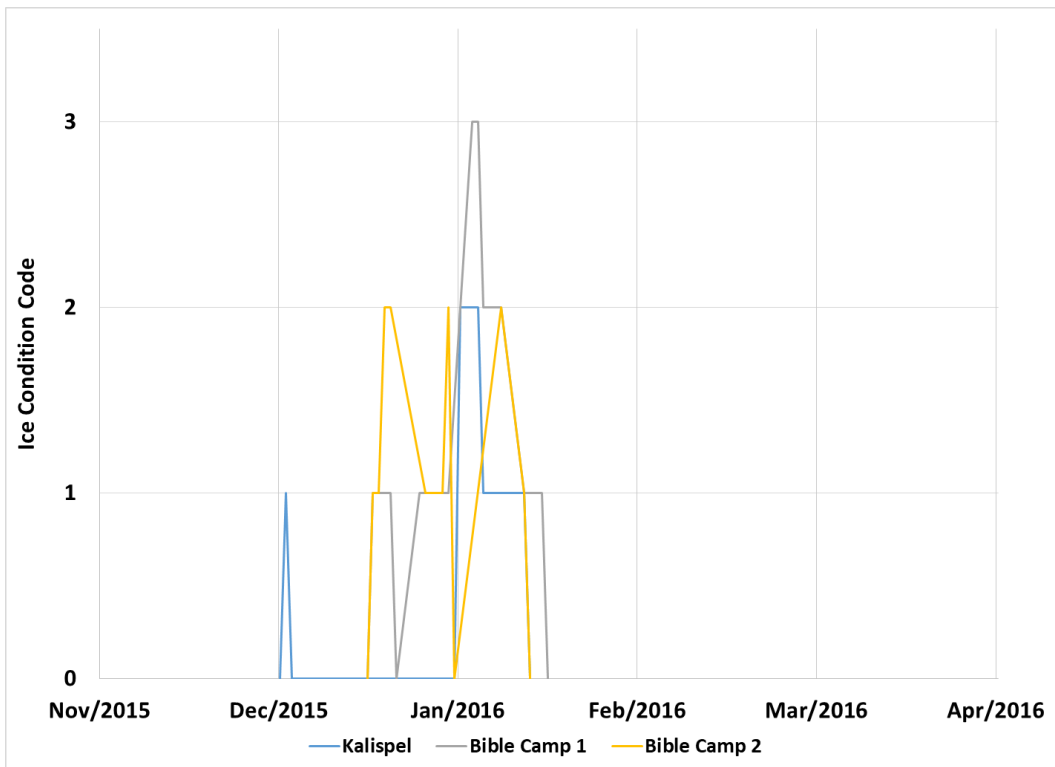
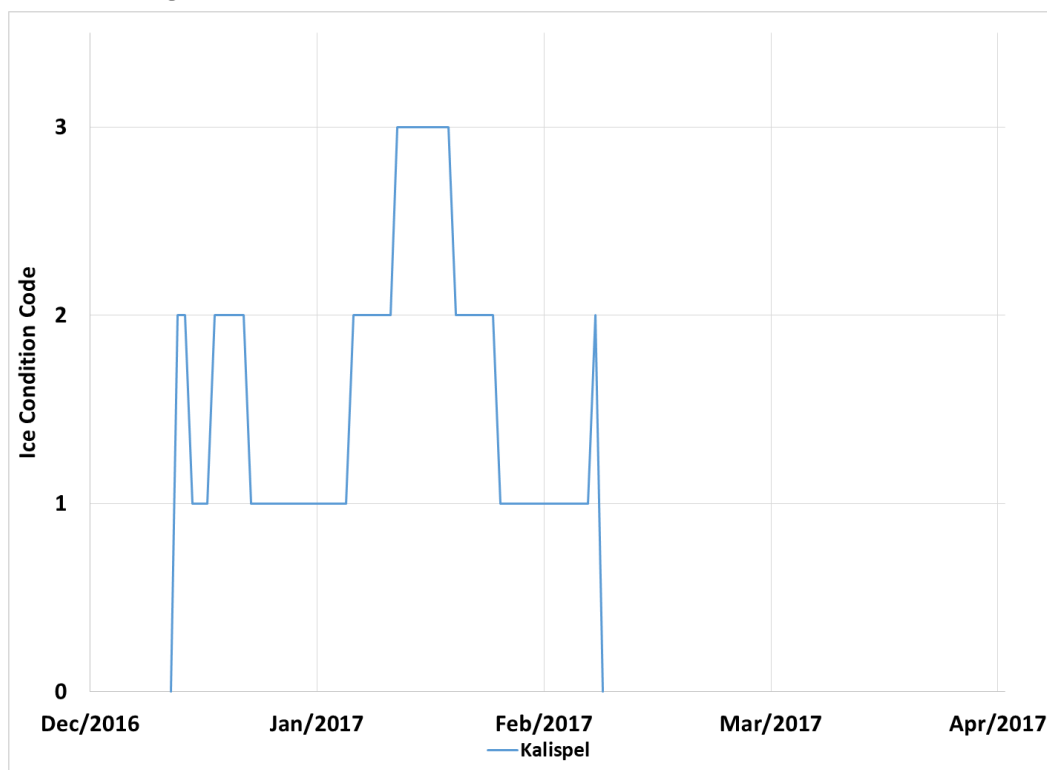


Figure 31. Ice cover on the Pend Oreille River for winter 2016–2017.



4.2 Ice hydraulics

The photographs collected by shore-mounted cameras show intermittent partial or complete ice cover on the river during the winter. Complete ice-cover events are absent during some winters. We calibrated the Seattle District's HEC-RAS model to open-water flows, which appears to be the predominant winter flow regime. However, it is of interest to understand the effect intermittent ice growth has on the river hydraulics, particularly stage. In most river systems, ice growth increases stage due to decreases in flow velocity from the additional flow boundary of the ice cover and from the displacement of water from floating ice. The historical record provides evidence of increased stage due to ice cover on the Pend Oreille River below AFD. Deviations between the open-water stage computed with the HEC-RAS model and measured tailwater stages can be used as an indicator of ice growth downstream. Subsequent sections discuss additional information regarding how this can be used in real-time water management.

We computed the impact of river ice growth on river stage by adding ice cover to the open-water steady hydraulic model over a range of flows and hypothetical ice-cover extents. The addition of ice cover raises the river stage for a given flow and produces a range of expected stage increases at

the AFD tailwater based on the extent of downstream ice cover. The computed stage increases can be used to create ice-affected AFD tailwater rating curves. When the observed AFD tailwater stages are higher than the results of the open-water HEC-RAS model, the deviation in stage can be compared to the ice-affected tailwater rating curves to estimate the amount of ice cover during that event. This approach was used to build a record of past ice-affected hydraulic events solely from the difference between the observed stage record at AFD tailwater and the modeled stage based on historical flows. This method could also be used as a near-real-time tool to detect ice formation downstream by monitoring deviations between observed AFD tailwater stages and those computed by the open-water HEC-RAS model.

4.2.1 Identifying ice-covered periods

We identified periods that were likely ice affected between WYs 2003 and 2017 by using hourly records of flow and tailwater stage at AFD. The flows were run through the unsteady open-water HEC-RAS model to create a time series of computed AFD tailwater stages. The computed tailwater stages were subtracted from the observed tailwater stages to create a new time series of deviations between the modeled and observed results. The mean average all-season hourly stage deviation was approximately -0.05 ft, meaning the HEC-RAS model, which was modified to improve low-flow performance as described previously, slightly overestimates stage on average. The standard deviation of hourly stage deviations of the same data set was 0.30 ft. Winter conditions were evaluated by isolating hour deviations from the months of December, January, and February from each water year. Wintertime deviation statistics were strikingly similar to the all-season and nonwinter periods, shown in Table 10. This similarity suggests that the calibration of the hydraulic model is not significantly seasonally biased and supports the assumption that, during winter, open-water flow is predominant.

Table 10. AFD tailwater stage-deviation statistics.

Season	Mean (ft)	Standard Deviation (ft)
All-Season	-0.05	0.30
Winter	-0.04	0.30
Nonwinter	-0.05	0.30

A stage deviation of greater than one standard deviation, 0.3 ft, was used as the base criterion for identifying potentially ice-affected events. To avoid misclassification of noise in the data set, the deviation was required to persist for 12 hours or more to be classified as a potential ice-affected event. Figure 32 shows an example of a significant stage-deviation event that occurred in January 2017. A total of 18 stage deviations were found between WYs 2003 and 2017 and are tabulated in Table 11. The largest deviation is approximately 2.2 ft, which occurred during the event with the longest duration, spanning 23 days in December 2008 through January 2009. There does not appear to be a strong correlation between flow and magnitude of deviation. There is a noticeable break in the occurrence of stage deviations between 2010 and 2013, which on average were not exceptionally mild winters; however, they are characterized by an absence of consecutive days with an average temperature at or below 10°F.

The same stage-deviation analysis was conducted on the Cusick gage (RS 68.5) using 15 minute stage data from fall 2015 to spring 2017. Table 12 and Figure 33 show limited results, which generally agree with the AFD tailwater deviations, with a few additional events likely due to ice processes occurring downstream that do not affect AFD.

Figure 32. Comparison of open-water model stage and observed AFD tailwater stage during an ice-affected event.

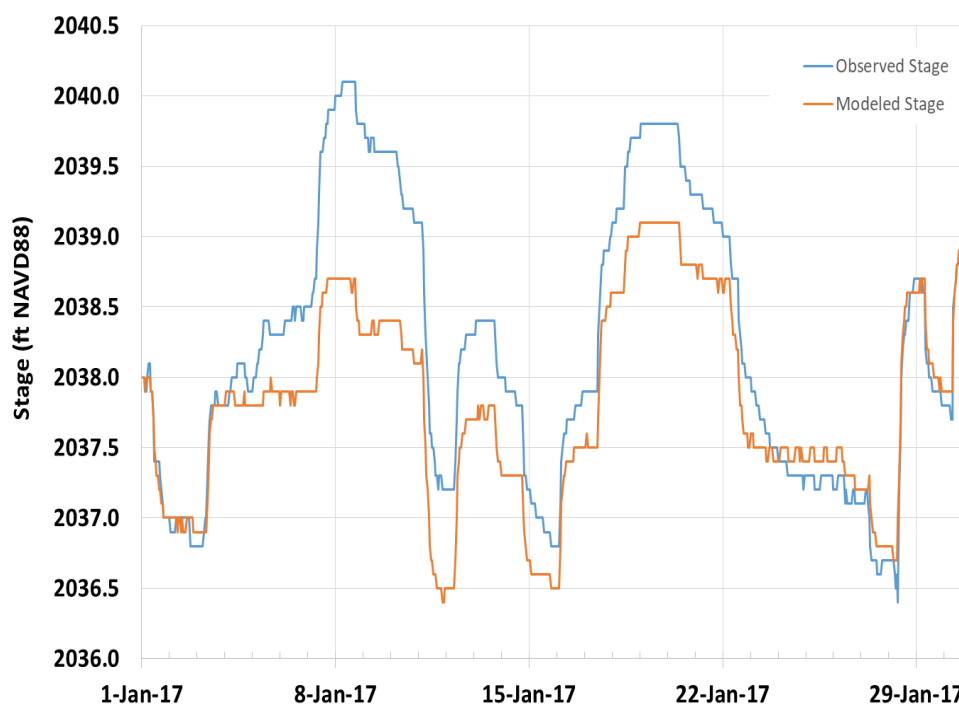


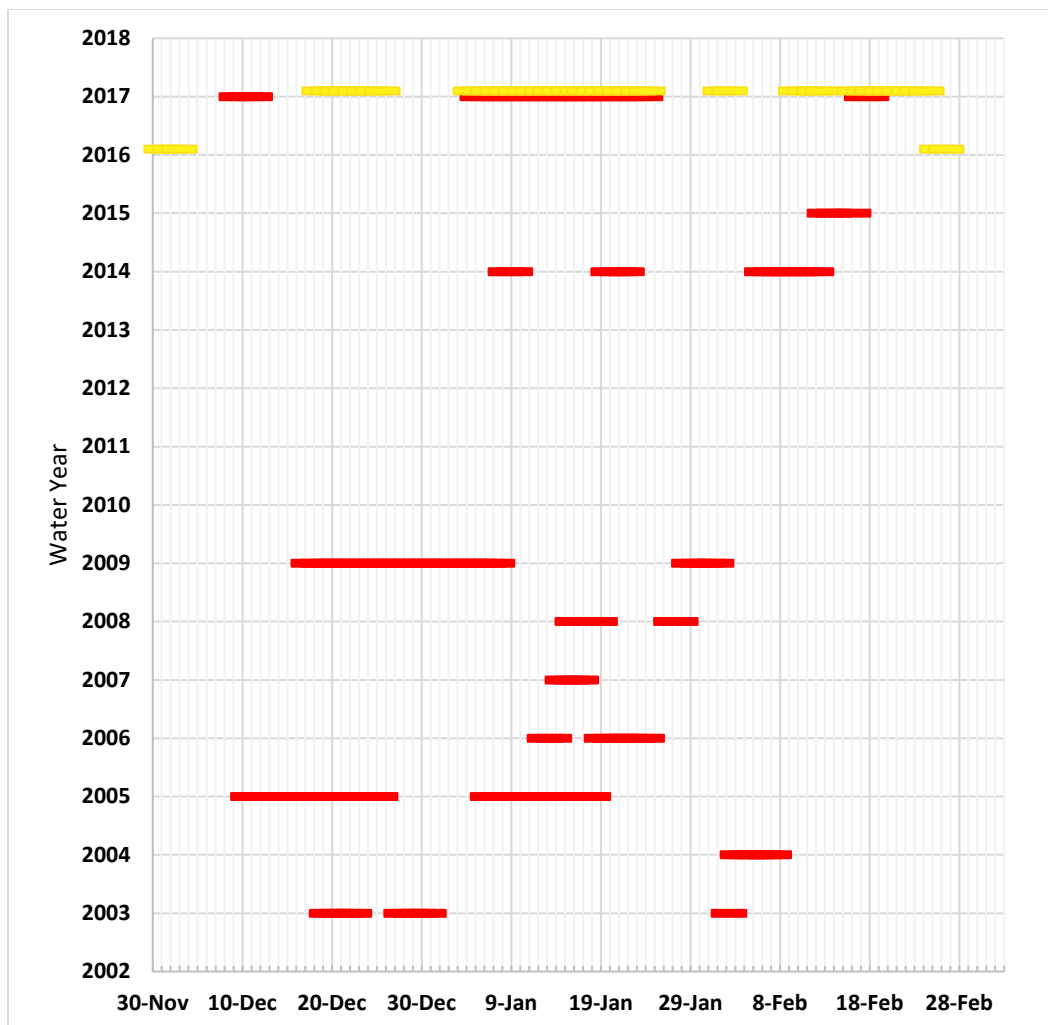
Table 11. AFD tailwater stage deviations exceeding 0.3 ft with a duration of 12 hours or more.

Event Number	Begin Date	End Date	Duration (days)	Mean Flow (cfs)	Mean Deviation (ft)	Max Deviation (ft)
1	19-Dec-02	21-Dec-02	2	16142	0.43	0.63
2	27-Dec-02	30-Dec-02	2	16572	0.36	0.49
3	2-Feb-03	7-Feb-03	5	19122	0.59	0.92
4	6-Jan-04	10-Jan-04	4	11735	0.69	1.13
5	10-Dec-04	14-Dec-04	4	23043	0.36	0.47
6	17-Dec-04	18-Dec-04	1	24000	0.33	0.35
7	20-Dec-04	21-Dec-04	1	20000	0.33	0.42
8	24-Dec-04	24-Dec-04	1	18308	0.45	0.90
9	14-Jan-05	23-Jan-05	9	16710	0.49	0.79
10	12-Jan-06	17-Jan-06	5	24911	0.46	0.85
11	15-Jan-07	17-Jan-07	2	13349	0.41	1.34
12	26-Jan-08	31-Jan-08	5	12034	0.39	0.54
13	17-Dec-08	9-Jan-09	23	17205	1.30	2.20
14	19-Jan-11	20-Jan-11	1	40138	0.32	0.41
15	6-Feb-14	13-Feb-14	7	12640	0.62	0.94
16	16-Feb-14	17-Feb-14	1	22345	0.47	0.65
17	9-Dec-14	10-Dec-14	2	22368	0.45	0.56
18	5-Jan-17	15-Jan-17	10	15513	0.79	1.48
19	16-Jan-17	23-Jan-17	6	18594	0.51	0.71
20	19-Feb-17	21-Feb-17	2	23907	0.61	0.73

Table 12. Cusick River gage stage deviations exceeding 0.3 ft with a duration of 12 hours or more.

Event Number	Begin Date	End Date	Duration (days)	Mean Deviation (ft)	Max Deviation (ft)
1	1-Dec-15	2-Dec-15	1	0.58	0.66
2	25-Feb-16	26-Feb-16	1	0.33	0.35
3	18-Dec-16	25-Dec-16	6	0.36	0.48
4	4-Jan-17	12-Jan-17	8	0.63	1.21
5	13-Jan-17	15-Jan-17	3	0.49	0.62
6	17-Jan-17	24-Jan-17	7	0.79	1.14
7	1-Feb-17	2-Feb-17	1	0.40	0.45
8	9-Feb-17	12-Feb-17	3	0.49	0.59
9	16-Feb-17	23-Feb-17	7	0.64	0.99

Figure 33. AFD tailwater stage-deviation time series in *red bars*. *Yellow bars* show stage deviations at the Cusick gage (near RS 68.5) for WYs 2016 and 2017.



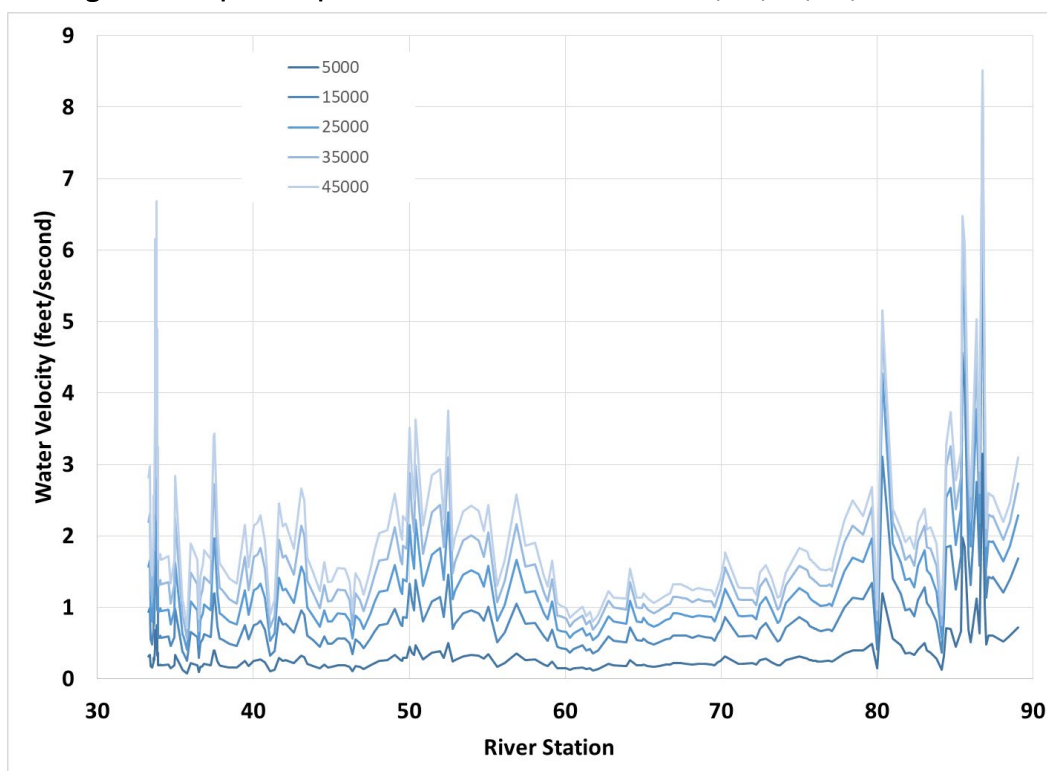
4.2.2 Ice-growth effect on hydraulics

A floating ice cover exerts three primary effects on flow. The first is that a portion of the channel flow area is blocked by the area of the ice cover beneath the water surface. The second results from the increase in the channel wetted perimeter because of the presence of the stationary ice cover. The third is the modification of the effective channel hydraulic roughness. Generally, these effects combine to cause the river stage to increase. The shoreline-ice-camera photo record indicates that ice cover in the Pend Oreille River generally forms as border ice that initiates at the shore and grows outwards towards the center of the channel. Project staff at AFD generally have observed border ice in lower-velocity sections of the river (e.g., outside river bends). While border ice is common, it appears that melting from increasing air or water temperature limits growth, and the

establishment of complete ice cover that spans from bank to bank is rare. When a complete ice cover does form, it likely originates at the downstream end of the river immediately upstream of BCD. Channel geometry and water velocity impact the ice-cover closure initiation and growth rate, with narrow, slower moving areas likely to bridge first. If water and air temperatures remain suitable for ice growth, the cover extents will progress in the upstream direction.

The formation rate of border ice is sensitive to water velocity but has been observed growing in velocities of 10 ft/s (3 m/s). However, closure generally will not occur unless velocities are less than about 1.3 ft/s (0.4 m/s) (Beltaos 2013). Figure 34 shows the expected open-water velocities between BCD and AFD over the range of wintertime flows (5–45 kcfs). For flows of 15 kcfs and lower, water velocities are suitable for the formation of ice along nearly the entire reach.

Figure 34. Expected open-water velocities from flows of 5, 15, 25, 35, and 45 kcfs.



We conducted simulation experiments using the HEC-RAS model discussed in previous sections. These experiments were meant to test the sensitivity of the river reach to ice growth and envelope conditions that caused

the historical stage deviations. The first simulations were set up with complete ice cover across the river channel but with varying longitudinal extents upstream of BCD. The second set of simulations assumed uniform border-ice growth for the entire reach. The border-ice growth was incrementally increased from the shoreline to the centerline of the river.

4.2.3 Spatially varying complete ice cover

We calculated the effect of complete ice cover on the water surface elevation of the Pend Oreille River by applying a uniform 1 ft thick ice cover to the entire study reach (AFD to BCD) under steady flow conditions. The ice thickness was selected to represent a conservatively thick but reasonably possible river ice thickness. Calculations based on freezing degree-days suggest that the average annual maximum thickness is approximately 7 in. A Manning's n value of 0.02 was assumed for the underside of the ice cover. The water surface rise under full ice-cover conditions was compared to the rise from a series of less extensive ice covers extending from BCD to several intermediate points on the river (i.e., Newport RS 87.1, downstream of the island groups near Newport RS 78.1, Cusick RS 68.5, Bible Camp RS 59.1, and Ione RS 36.6). A fixed water surface elevation at BCD was assumed to be 2034.0 ft (NAVD88) and was applied as the model's downstream boundary condition.

Figures 35 and 36 show examples of the difference between open-water surface profiles from ice cover extending from BCD to Newport and from BCD to approximately halfway up the reach to Cusick. The profiles are of 15 and 40 kcfs, respectively, representing average and high wintertime flows. While the stage at AFD is affected by ice cover on the river (Table 10), Table 13 shows that the magnitude of those effects is less when the flows are lower and when the ice cover does not extend as far upstream.

Figure 37 summarizes the effects of 1 ft of ice cover on the AFD tailwater rating curve. The points shown on Figure 37 are probable ice-affected hydraulic events based on the historical flow record between WYs 2003 and 2017. The individual lines represent ice covers extending from BCD to upstream locations, showing the effects of a cover growing from downstream to upstream. This type of ice-growth affects AFD tailwater in a relatively uniform fashion until ice cover reaches the island groups upstream of RS 78.1. The ineffective flow areas added to the island channels geometry to improve open-water model performance constrict flow, producing a local backwater effect extending from the islands to AFD. The presence of ice in

the islands causes a major change in the backwater effect seen in the Newport curve in Figure 37.

Very little is known about the ice processes in the channels around the islands, so the results of the ice effects on the reach between AFD and 10 miles downstream should be interpreted carefully. It is likely that the tailwater is very sensitive to ice cover in this reach, but the response predicted by the model is based on simplified assumptions that cannot be confirmed or improved without more specific documentation of the ice processes.

Figure 35. Comparison of open-water and ice-affected river stages. Ice cover from BCD to AFD, ice thickness 1 ft, flows 15k and 40k cfs.

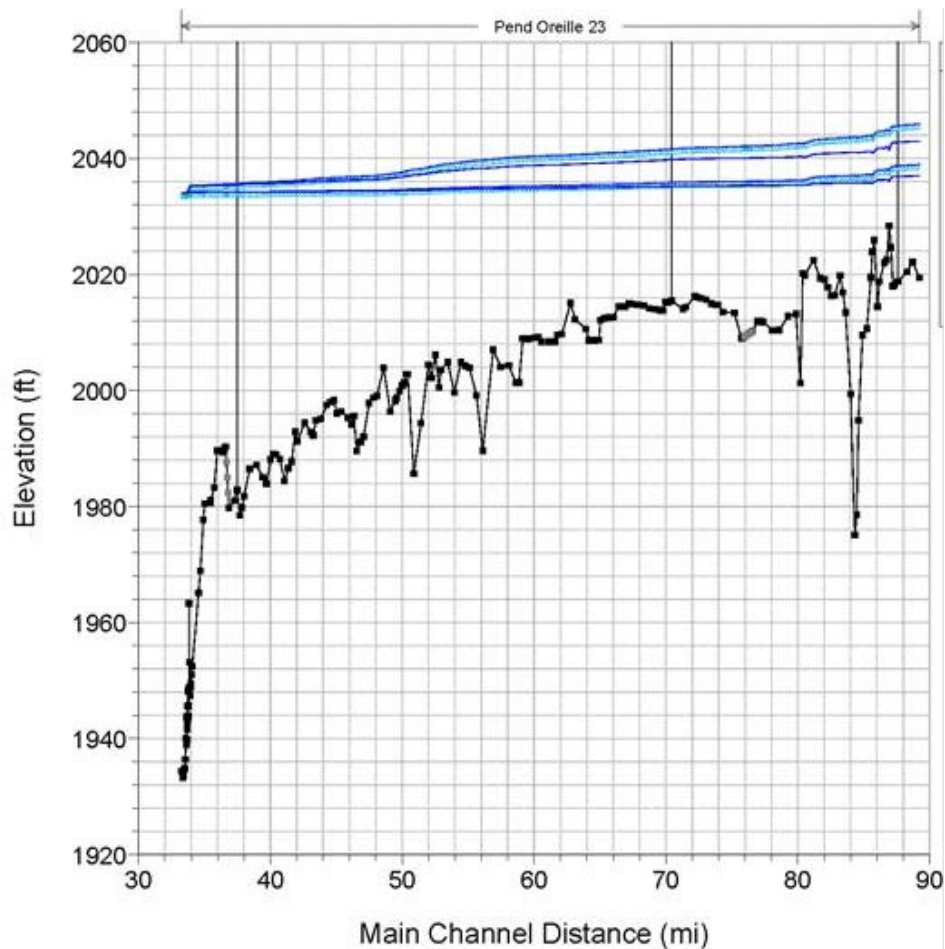


Figure 36. Comparison of open-water and ice-affected river stages. Ice cover from BCD to Cusick (RS 68.54497), ice thickness 1 ft, flows 15 and 40 kcfs.

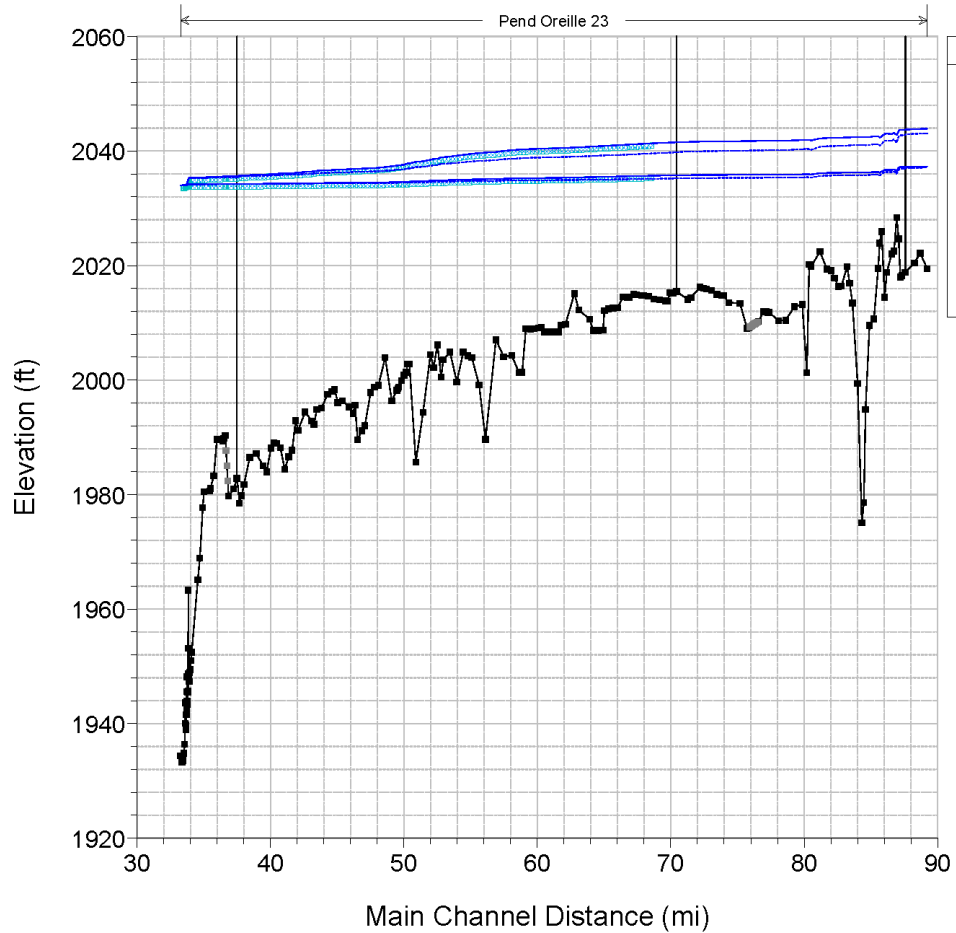
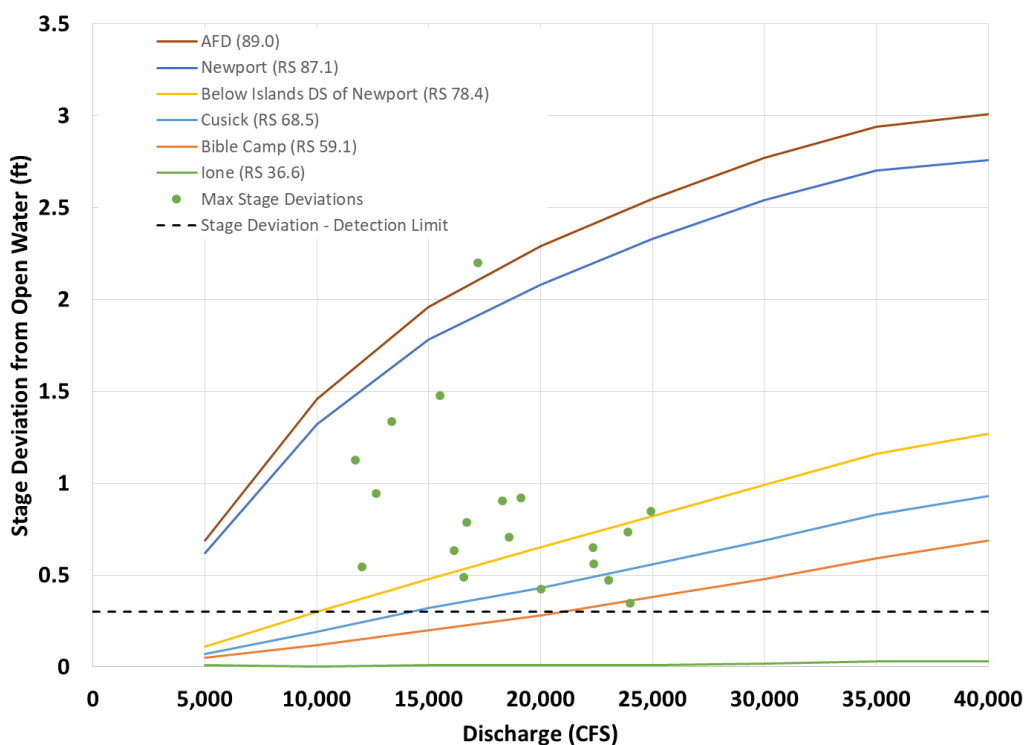


Table 13. Stage increase at AFD tailwater from 1 ft of downstream ice growth relative to open-water conditions.

Ice Extent from BCD	Stage Increase (ft)	
	15 kcfs flow	40 kcfs flow
Ione (RS 36.6)	0.01	0.03
Bible Camp (RS 59.1)	0.20	0.69
Cusick (RS 68.5)	0.32	0.93
Below Islands (RS 78.4)	0.48	1.27
AFD (RS 89.0)	1.96	3.01

Figure 37. Effects of ice-cover extent (from BCD to upstream points) and flow rate on AFD tailwater elevation.



The results of this analysis show the modeled effects of a channel-spanning ice cover extending from BCD to a series of points upstream. While the process of ice growth from downstream to upstream is typical, the assumption of a clear line between downstream ice cover and upstream open-water conditions is a major simplification of likely field conditions. However, the model is useful in showing that AFD tailwater is relatively insensitive to ice presence below RS 78. It also suggests that the maximum effect that an intact ice cover would have on AFD tailwater is approximately 2 ft under average flow conditions of 15 kcfs. At higher discharge, the maximum can reach 3 ft at AFD.

4.2.4 Flow velocities with ice cover

Elevated water surfaces are typically accompanied by a reduction of water velocity once an ice cover is established. Ice cover on a broad, shallow river approximately doubles the wetted perimeter and therefore approximately halves the hydraulic radius. The composite Manning's roughness with ice cover is calculated in HEC-RAS using the Belokon-Sabaneev formula, shown in the following equation:

$$n_c = \left(\frac{n_b^{3/2} + n_i^{3/2}}{2} \right)^{2/3}, \quad (1)$$

where

- n_c = composite roughness,
- n_b = bed Manning's n roughness, and
- n_i = ice Manning's n roughness.

The Manning's n value associated with an established ice cover is typically less than the bed value, so the composite roughness for the entire cross section usually becomes smaller with an ice cover. The decrease in composite roughness is generally not as significant as the decrease in hydraulic radius with ice cover, which results in the decreased cross-sectional average velocity. A frazil ice cover can increase the composite roughness; however, this is unlikely in the Pend Oreille River due to low velocities.

Manning's equation, shown next, can be used to estimate velocity and stage changes for ice-covered conditions under uniform flow:

$$Q = AV = \frac{1.49}{n} AR^{2/3} \sqrt{S}, \quad (2)$$

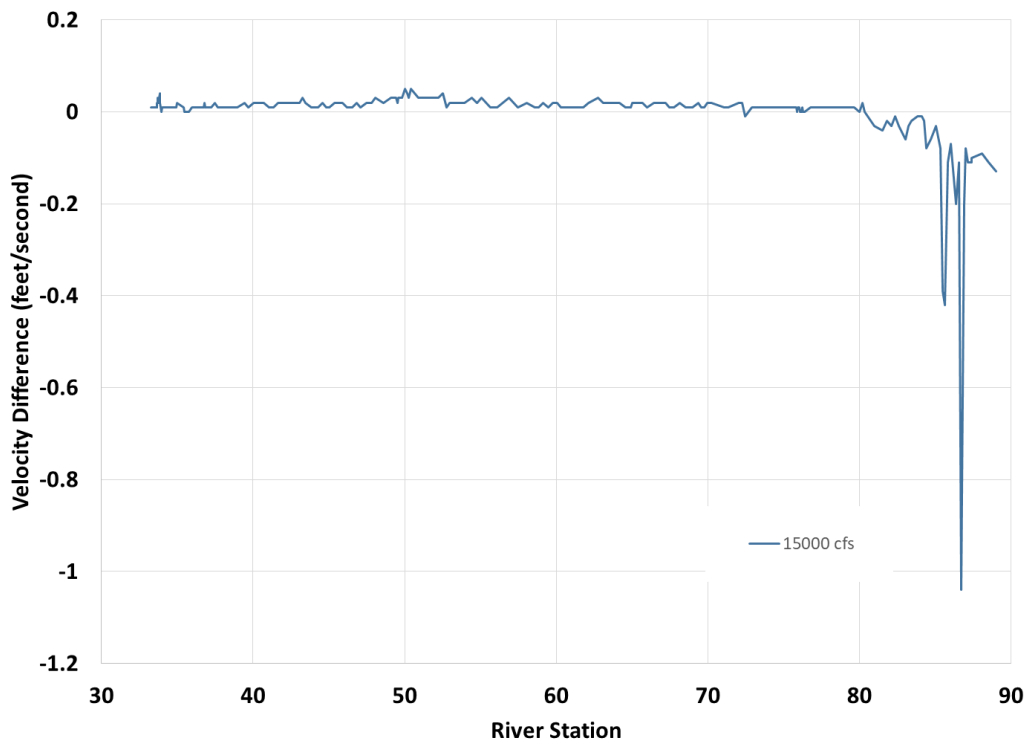
where

- Q = flow rate (ft³/s),
- V = water velocity (ft/s),
- A = flow area (ft²),
- n = Manning's roughness,
- R = hydraulic radius (ft), and
- S = Channel slope (ft/ft).

On the Pend Oreille River, the backwater from BCD significantly influences the water surface profile, resulting in flatter hydraulic gradients and slower water velocities than would be present under natural conditions prior to BCD construction. The velocities are much lower than the natural condition velocities due to the backwater effect, which flattens the open-water energy grade line from an average slope of approximately 0.00086 ft/ft to 0.00001 ft/ft. A less intuitive finding from the model is that the presence of ice cover slightly increases the water velocity and stage along a

majority of the reach. Figure 38 shows the effect of 1 ft of ice cover on velocities for a flow of 15 kcfs. The velocity increase is due to the assumption of a fixed water surface elevation at BCD. With the water surface held constant at the downstream end, the displacement from 1 ft of ice obstructs the top 0.92 ft of the fixed flow area directly upstream of the dam, reducing the effective flow area. With no change in flow rate and a smaller flow area, the water velocity must increase to maintain continuity. In this case, the increase in velocity is very small because the ice encroachment from 1 ft of ice reduces only around 1% of the flow area in the cross sections immediately upstream of BCD.

Figure 38. Difference between water velocities under open-water and complete-ice-cover conditions (15 kcfs and 1 ft of ice) with BCD control. Difference calculated as ice-covered conditions minus open-water conditions.



The reduction of flow area due to ice cover also reduces the conveyance, K , defined in equation (3). The composite n_c , which includes the effects of the ice roughness, is generally lower than the bed roughness; however, its effect of increasing the conveyance is outweighed by the reduction of the hydraulic radius due to the ice cover. Combining Manning's equation (equation 2) with the conveyance expression (equation 3) yields the equation for the slope of the energy grade line, equation (4). From equation (4), it can be seen that a reduction in conveyance will increase the slope of the energy

grade line. This results in a steeper water surface profile for the ice-covered case as friction losses from the ice result in more head loss between cross sections than the open-water condition.

$$K = \frac{1.49}{n} AR^{\frac{2}{3}}. \quad (3)$$

$$S_f = \left(\frac{Q}{K}\right)^2. \quad (4)$$

An ice thickness of 1 ft was selected for the model runs in this report as a representative condition for the Pend Oreille River, but ice thicknesses over a range of thicknesses is obviously possible. Figure 39 shows the effects on river stage from a complete ice cover extending from BCD to AFD over a range of thicknesses, at various locations along the river. There is generally a linear increase in stage at each location with increasing ice thickness; however, the effect is more significant nearer to AFD where the flow is approaching normal depth. For flow at normal depth, the slope of a line in Figure 39 would be approximately 0.92 ft/ft where additional stage increase is due to additional displacement from the buoyant ice. The influence of ice thickness on stage is also shown in Table 14.

Figure 39. Effect of ice thickness on river stage, relative to open-water conditions (15 kcfs).

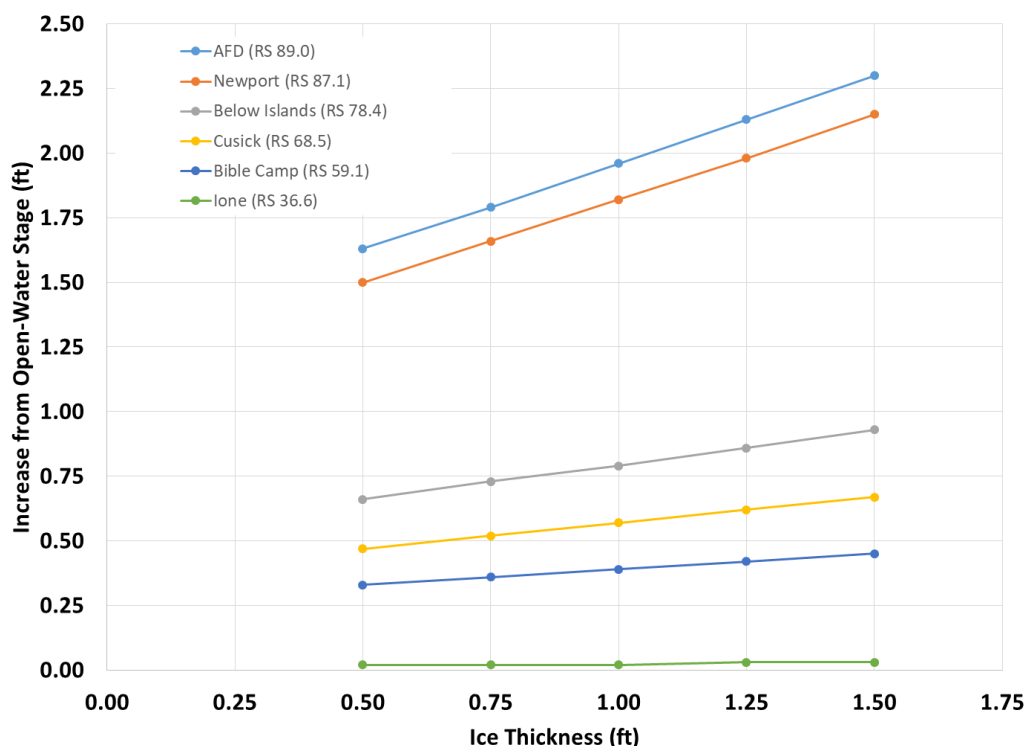


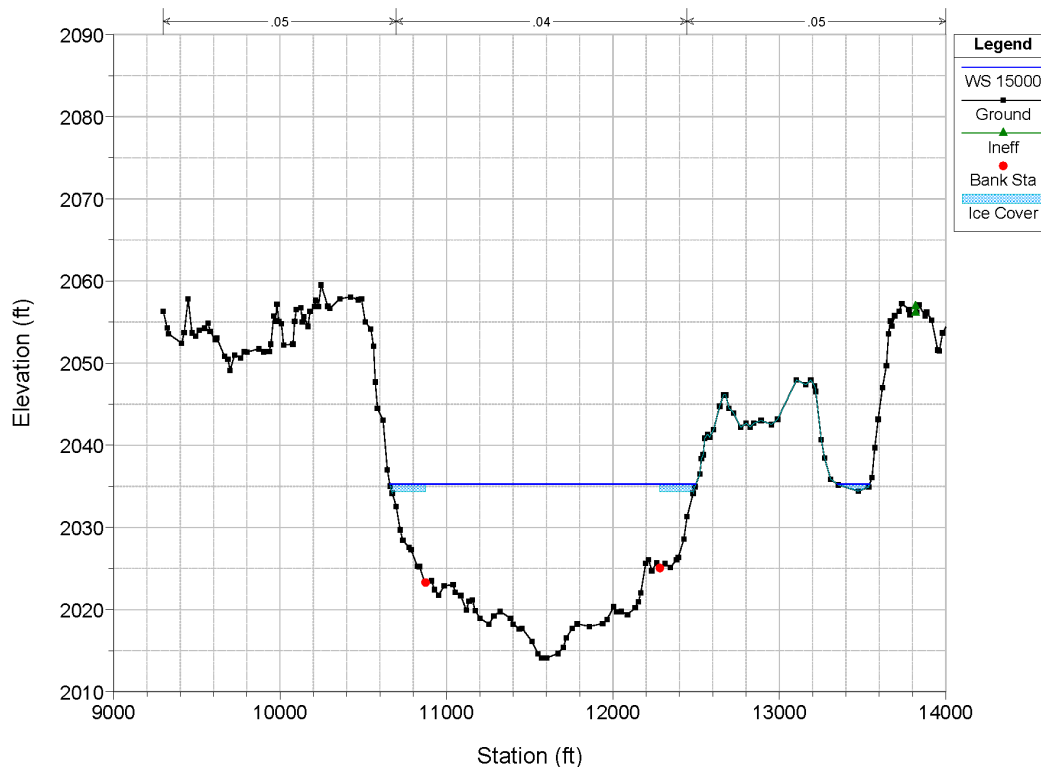
Table 14. Effect of ice thickness on river stage.

River Station	Ice Thickness (ft)	Water Surface Elevation (ft NAVD88)	Stage Change From Open Water (ft)
Ione (RS 36.6)	Open Water	2034.20	0.00
	0.50	2034.22	0.02
	0.75	2034.22	0.02
	1.00	2034.22	0.02
	1.25	2034.23	0.03
	1.50	2034.23	0.03
Bible Camp (RS 59.1)	Open Water	2034.85	0.00
	0.50	2035.18	0.33
	0.75	2035.21	0.36
	1.00	2035.24	0.39
	1.25	2035.27	0.42
	1.50	2035.30	0.45
Cusick (RS 68.5)	Open Water	2035.12	0.00
	0.50	2035.59	0.47
	0.75	2035.64	0.52
	1.00	2035.69	0.57
	1.25	2035.74	0.62
	1.50	2035.79	0.67
Below Islands (RS 78.4)	Open Water	2035.33	0.00
	0.50	2035.99	0.66
	0.75	2036.06	0.73
	1.00	2036.12	0.79
	1.25	2036.19	0.86
	1.50	2036.26	0.93
Newport (RS 87.1)	Open Water	2036.86	0.00
	0.50	2038.36	1.50
	0.75	2038.52	1.66
	1.00	2038.68	1.82
	1.25	2038.84	1.98
	1.50	2039.01	2.15
AFD (RS 89.0)	Open Water	2036.99	0.00
	0.50	2038.62	1.63
	0.75	2038.78	1.79
	1.00	2038.95	1.96
	1.25	2039.12	2.13
	1.50	2039.29	2.30

4.2.5 Border ice

While the photo record from the shoreline ice cameras suggests that it is uncommon for the river to freeze over with complete ice cover, the presence of border ice is common. The previous section evaluated the spatial effect of ice growth extending from BCD upstream as uniform ice cover over the entire channel width. This section evaluates the impacts of border-ice growth. HEC-RAS is limited in its ability to simulate the effects of border ice on river hydraulics because ice cover is defined in the model by specifying its thickness in only the channel or in the right or left overbank. However, the geometry of a margin of ice extending from the shore can be approximated by moving the bank stations into the channel and applying ice to the overbank areas, as shown in Figure 40.

Figure 40. Water-surface profile (WS) for border-ice simulation in HEC-RAS at 15 kcfs. Border-ice growth of 200 ft from the right and left shore.



To simulate the effects of growing border ice, we wrote a Python script to iteratively edit the HEC-RAS geometry file and incrementally advance the bank stations towards the center of the channel for all 217 cross sections, from RS 33.26100 to RS 89.02496. Ice was applied to the right and left overbanks with a thickness of 1 ft and a Manning's n value of 0.02. The

script generated new plans for each geometry, ran them, and exported results to a file. Each model represented a 100 ft increase in distance of border-ice growth from the shore. Figure 40 and Figure 41 show a cross section near Cusick (RS 68.5) with 200 and 600 ft of ice growth from each shore. Approximately 17 individual plans were required to represent the range of conditions between open water and complete river ice cover. Figure 42 shows the effects of increasing border-ice growth on tailwater stage at AFD during average winter flows of 15 kcfs. The “percent of reach covered” is the ratio of ice-cover surface area to total river surface area. Figure 43 shows the effects of border-ice growth on the AFD rating curve for 25%, 50%, 75%, and 100% reach coverage. This plot is similar to the AFD rating-curve effects shown in Figure 37 representing effects from ice growing from downstream to upstream.

Figure 41. Water surface (WS) profile for border-ice simulation in HEC-RAS at 15 kcfs. Border-ice growth of 600 ft from the right and left shores.

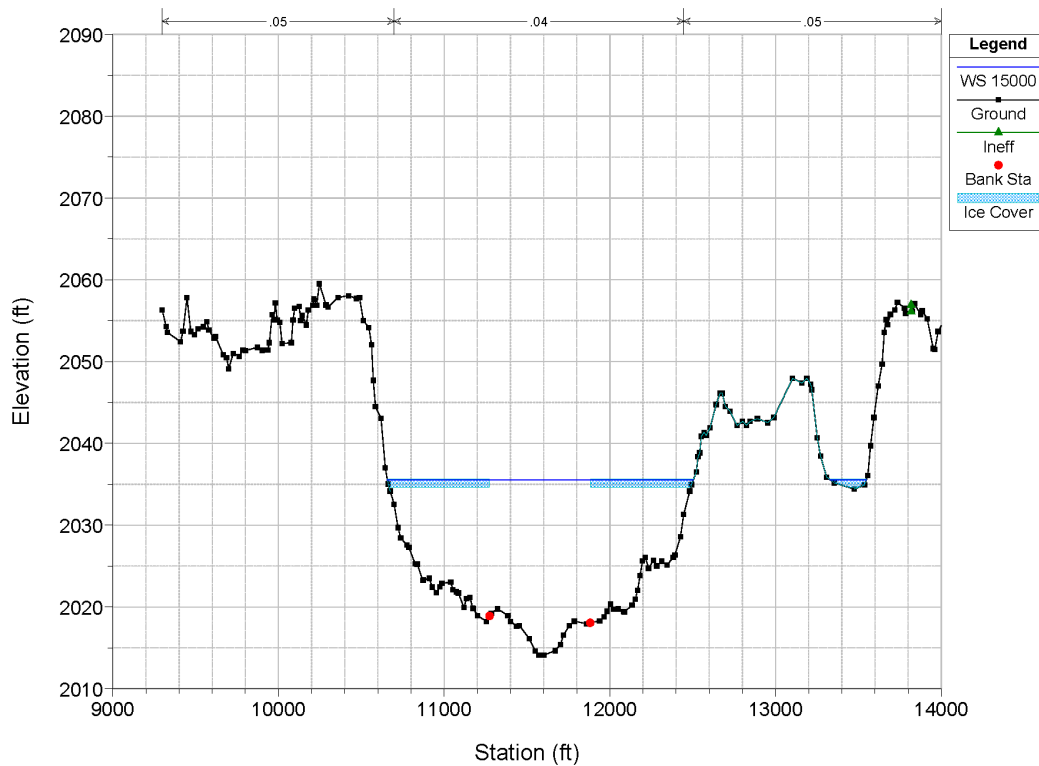


Figure 42. Effect of increasing border-ice growth on the AFD tailwater stage for 15 kcfs. The percent of reach covered is the ratio of ice-cover surface area to total river surface area.

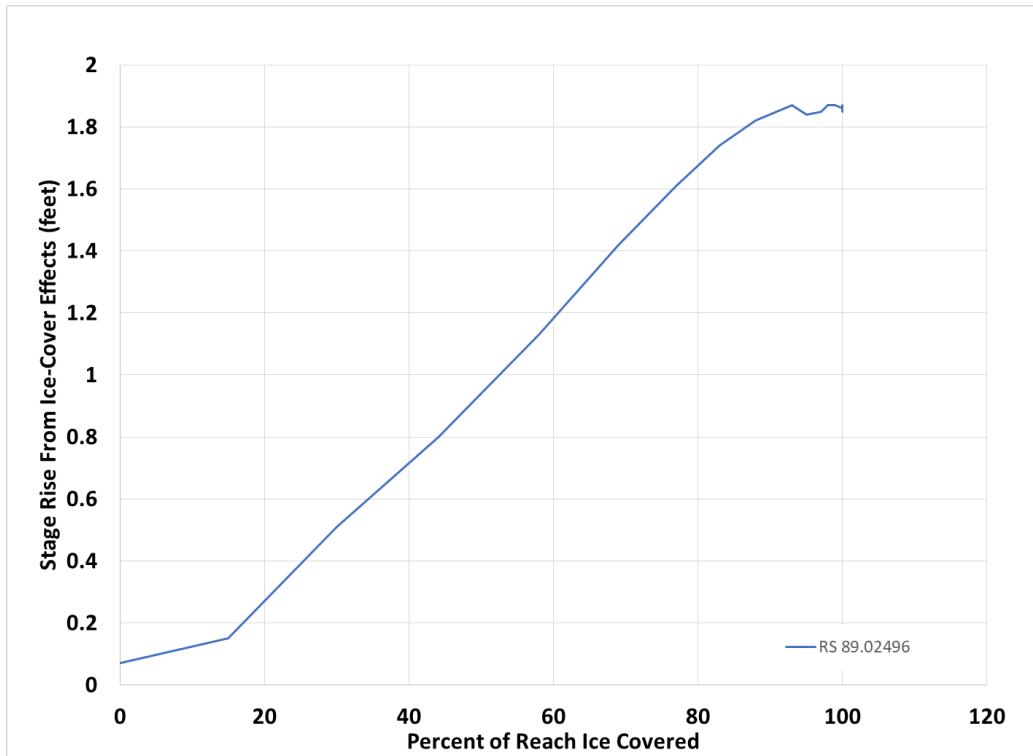
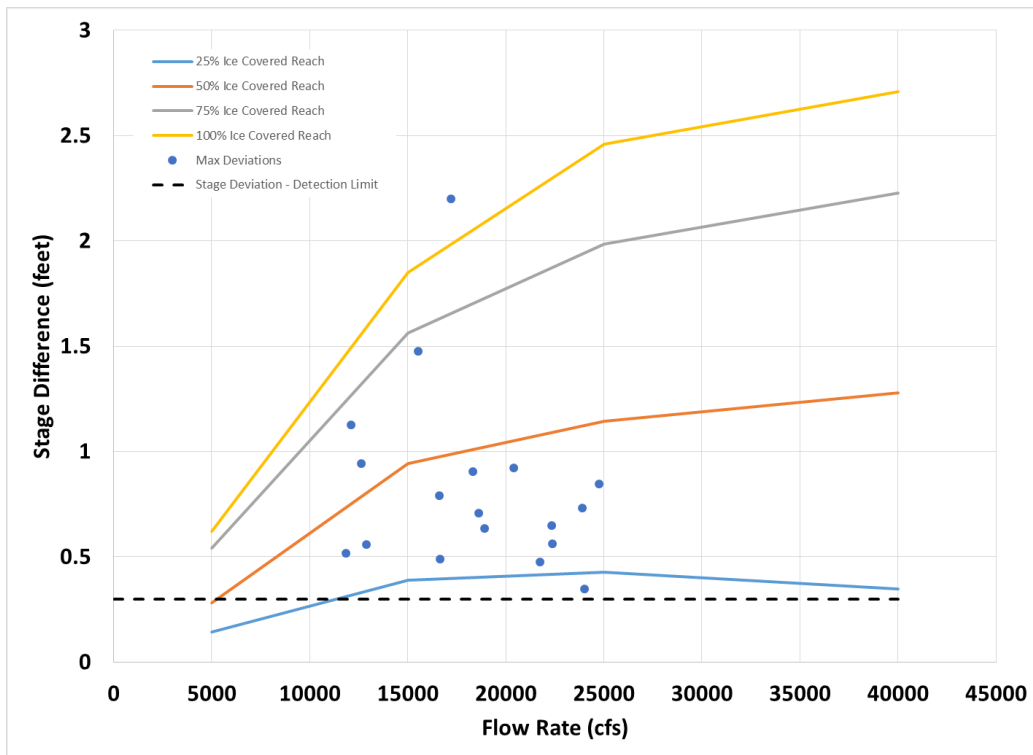


Figure 43. Effect of border-ice growth on the AFD rating curve. Individual *lines* represent 25%, 50%, 75%, and 100% reach coverage. *Dots* represent maximum stage deviations from 2003 to 2017.



4.3 Ice jams

A large ice jam was reported upstream of Usk in 1928 (*Spokane Daily Chronicle* 1928); but since the construction of BCD, no major ice jams have been reported. This is most likely due to the major changes to the hydraulic conditions caused by the BCD backwater. Without appreciable water velocities to drive ice thickening during breakup and a limited ice supply, the reach is not particularly susceptible to the formation of ice jams.

We used the HEC-RAS hydraulic model to evaluate the effects of a potential jam by using the software's built-in force-balance routines. The jams were simulated assuming the breakup of a 1 ft thick ice cover over the entire reach. The roughness of the underside of the jam was computed using Nezhikovsky's empirical relationship, which is a function of water depth and jam thickness (Brunner 2016).

Figure 44 shows the effects of an ice jam occurring under average winter flows of 15 kcfs. The ice does not thicken appreciably, and the result is a thin jam similar in thickness to the initial 1 ft ice cover. Figure 45 shows the effects of the same 1 ft ice cover breaking up and jamming during a high wintertime flow of 40 kcfs. In this case, a channel constriction around Blueslide (RS 50.4) generates velocities high enough to cause significant thickening and formation of a moderate ice jam.

The effect of the ice jam on stage was compared with open-water elevation profiles to gauge the severity of the event. Table 15 shows the impact of the jam on stage at several locations along the river. The 75 kcfs open-water profile envelopes the 40 kcfs ice jam water surface profile (Figure 46). Figure 47 shows the effects of ice cover and ice jamming relative to open-water conditions during high winter flows. The AFD WCM (USACE 2013) states that, for discharges of 100 kcfs, no downstream damages are expected and that flooding is limited to low-lying pastures and hay fields. This indicates that the modeled ice jam, representing a conservative combination of ice supply and wintertime flow, would be unlikely to cause flood damages along the river. A full Monte Carlo analysis would be necessary to quantify the risk of flooding due to an ice jam between AFD and BCD.

Figure 44. Ice jam during average winter flows of 15 kcfs.

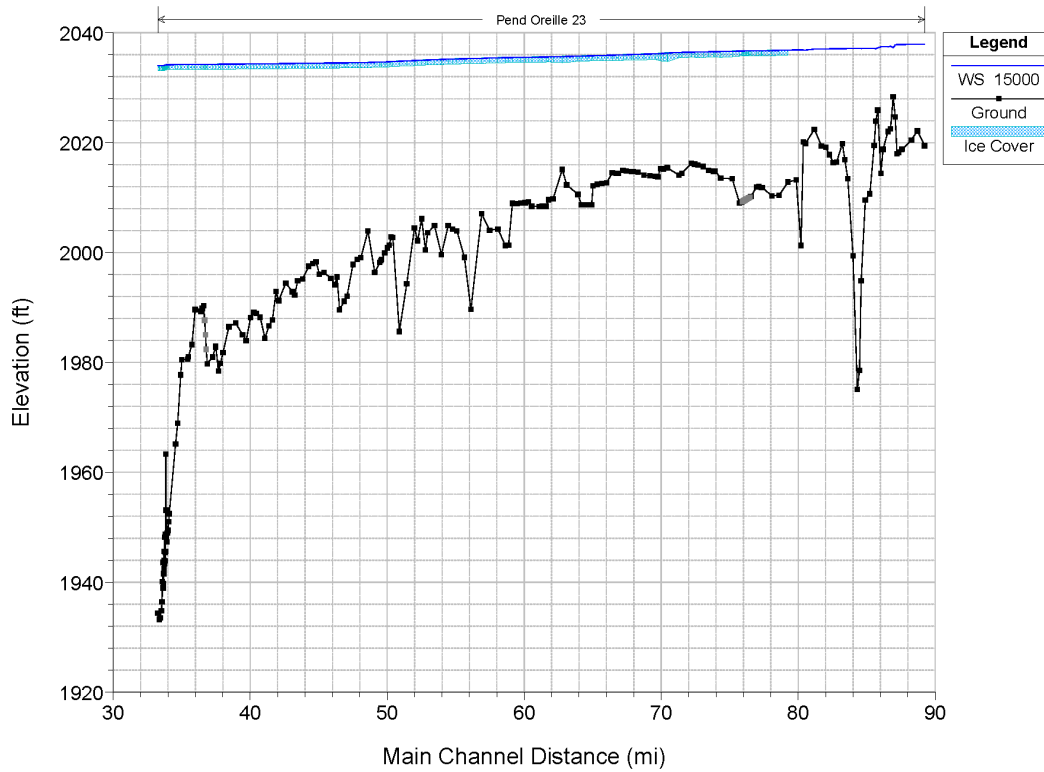


Figure 45. Ice jam during high winter flows of 40 kcfs with prebreakup ice cover shown for reference.

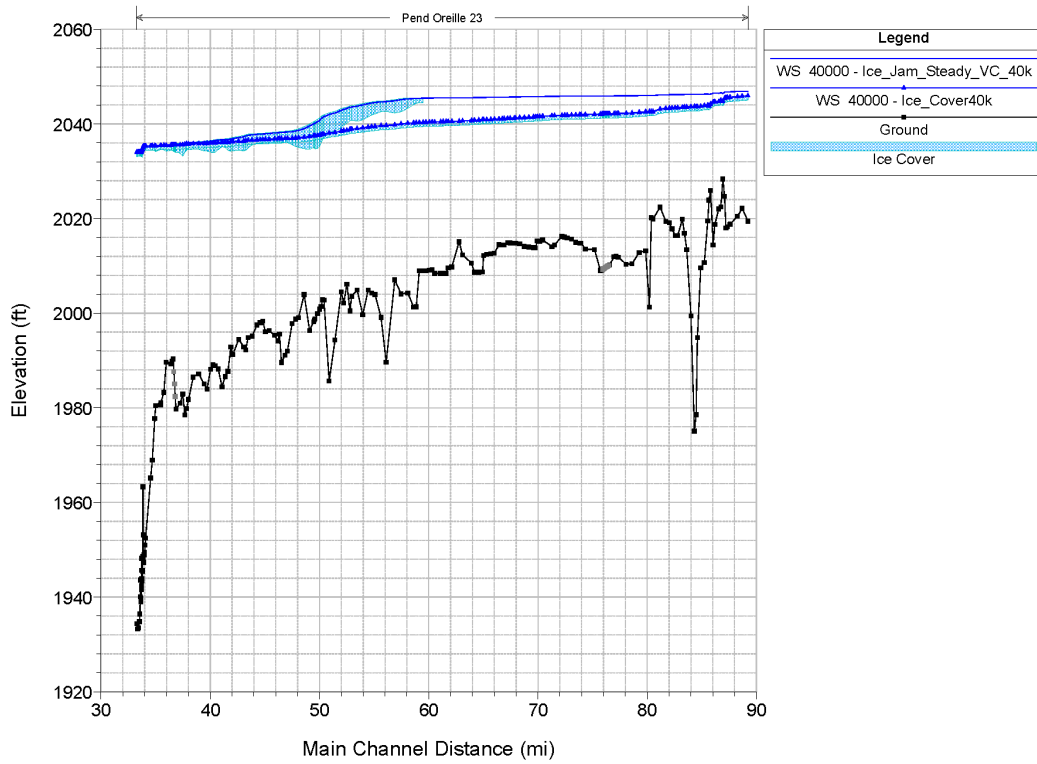


Table 15. Stage increases relative to open water for 40 kcfs. Stage increases are reported in feet.

Simulation	Ione (RS 36.6)	Bible Camp (RS 59.1)	Cusick (RS 68.5)	Below Islands (RS 78.4)	Newport (RS 87.1)
Open water (40 kcfs)	0.00	0.00	0.00	0.00	0.00
1 ft ice cover (40 kcfs)	0.13	1.54	1.77	2.16	2.82
1 ft ice cover ice jam (40 kcfs)	0.22	6.66	6.13	5.78	4.04
Open water (75 kcfs)	3.34	6.69	6.86	6.96	6.51

Figure 46. Ice jam during high winter flow of 40 kcfs compared with open-water flow of 75 kcfs

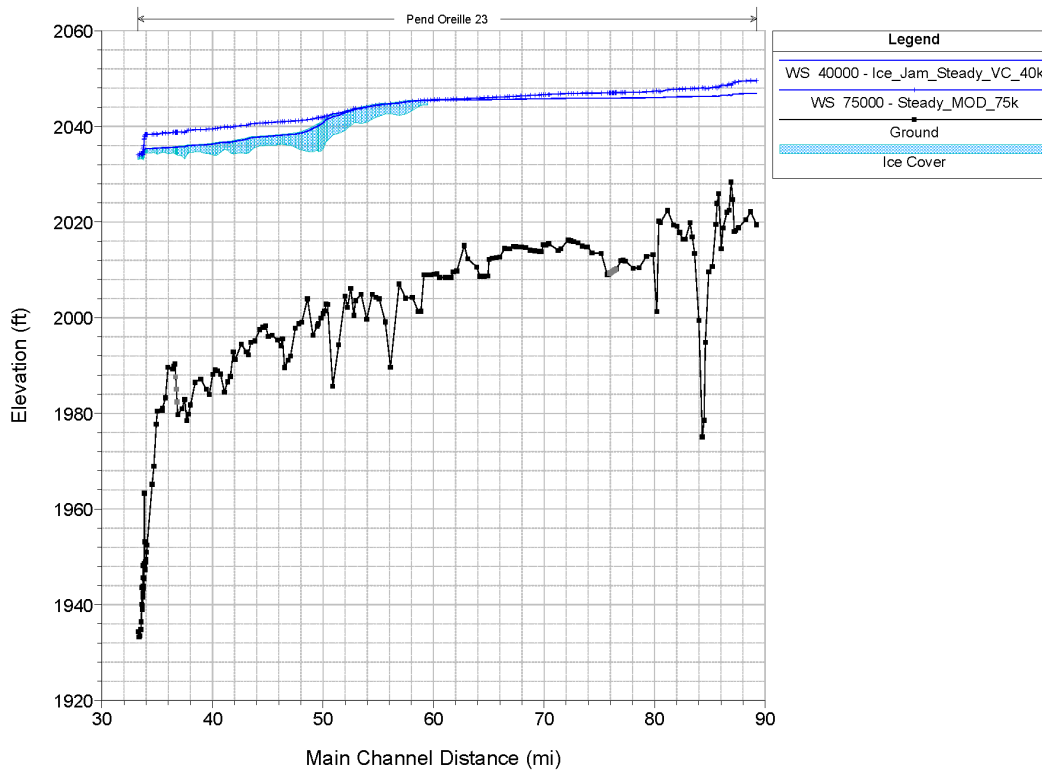
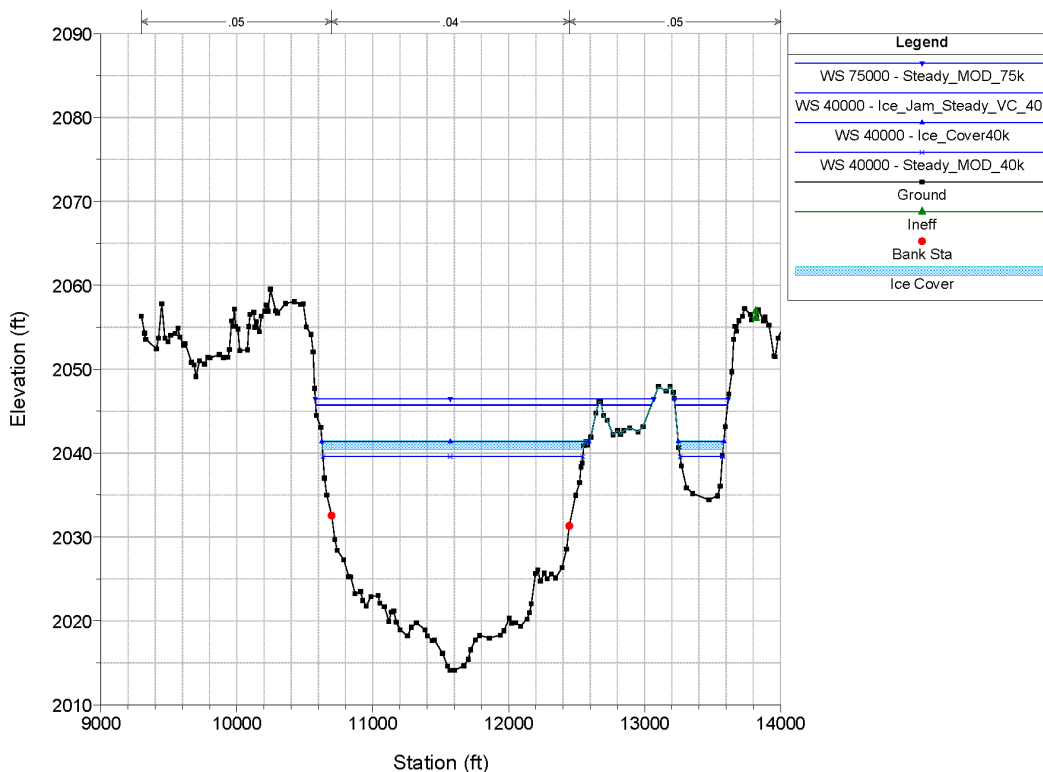


Figure 47. Stages at Cusick (RS 68.5). From *bottom*: 40 kcfs open water, 40 kcfs 1 ft ice cover, 40 kcfs ice jam, and 75 kcfs open water. No ice cover is present in the 40 kcfs ice jam case because the body of the jam is downstream of this cross section. All stages remain within the banks.



4.4 HEC-RAS water-temperature modeling

We modeled the water temperature of the Pend Oreille River between AFD and BCD using the HEC-RAS Water Quality Module. The goal was to assess the usefulness of water-temperature modeling for predicting the timing and location of ice formation downstream of AFD. The HEC-RAS Water Quality Module could potentially be an operational asset for determining the presence and location of ice covers downstream of the dam.

Admittedly, the HEC-RAS Water Quality Module has two main limitations when applied to the wintertime conditions in the Pend Oreille River. First, the Water Quality Module is strictly an open-water model and does not include the impact of ice formation or the presence of surface-ice covers. However, estimating water temperatures can indicate the time and location of initial ice-cover formation and provide a good estimate of the length of time the ice cover is in place. The second limitation is that the Water Quality Module assumes the flow is always well mixed vertically, so

the water temperature is uniform from the surface to the bed of the channel. This might not be the case throughout the reach that is strongly controlled by the backwater of BCD. In this reach, the water temperature may be stratified, especially at lower river flow rates. Exploration of this limitation is beyond the range of this study. However, the model accuracy results are very encouraging; so any stratification effects on the water-temperature calculations are likely to be relatively small.

We modeled water temperature for the winters of WYs 2012 through 2017 for the November through March. Water-temperature results were available at each HEC-RAS cross section between AFD and BCD at each time step. The input required for the Water Quality Module includes the upstream water temperature, shortwave radiation, cloudiness, atmospheric pressure, air temperature, relative humidity, and wind speed. This data is required to model the major heat fluxes between the water surface and the atmosphere. This range and quantity of data may be burdensome for real-time AFD operations. Therefore, we investigated alternatives to the complete set of required data inputs needed by HEC-RAS—chiefly by assuming that the long-term climatological averages for each hour of each day of the year could be used for some or all of the input parameters. The model accuracy was assessed by comparing the modeled water temperature with the observed water temperature at BCD, the downstream limit of the model.

4.4.1 Methods and data

The HEC-RAS water-temperature model requires hydraulic information from the unsteady flow simulations described in previous sections. The key input variables from the hydraulic model are water surface area, depth, and water velocity. Hourly flow data recorded at AFD was used as the upstream boundary condition of the hydraulics portion of the water-temperature model.

4.4.2 Water temperature

Seattle District and POPUD provided water-temperature measurement data collected at the AFD and BCD forebays. We used the temperature of the outflow at AFD as the upstream boundary condition of the water temperature model. The BCD water temperatures were not directly used in the model but were used to assess the model accuracy. Figure 48 shows histograms of the observed temperature distributions at AFD and BCD. There are distinct differences in the distribution of observed water temperatures

between the upstream and downstream boundaries used in the water-temperature model. There appears to be a shift in peak frequency of observed temperatures going from AFD to BCD as well as a more uniform distribution. The most frequent temperature range at AFD is 36°F–37°F while at BCD the peak number of observations is between 32°F and 35°F. This indicates that there is relatively warm water in Lake Pend Oreille, which is then cooled as it moves downstream, resulting in more frequent ice formation in the BCD forebay.

Figure 48. Observed water temperatures at AFD and BCD forebays for December, January, and February, WYs 2012–2017.

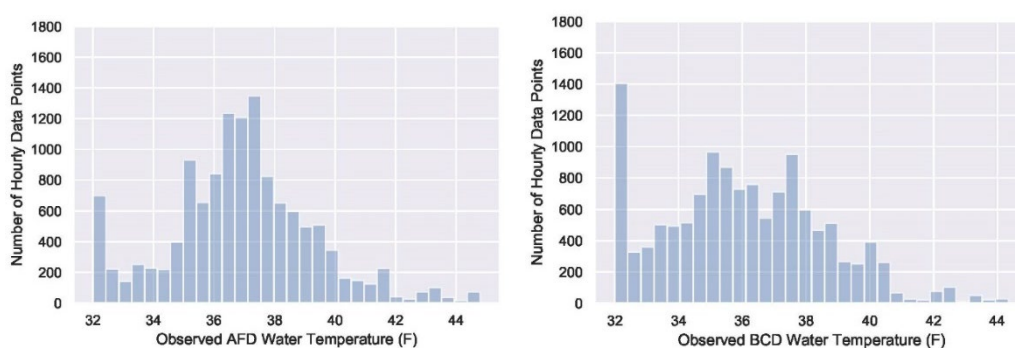
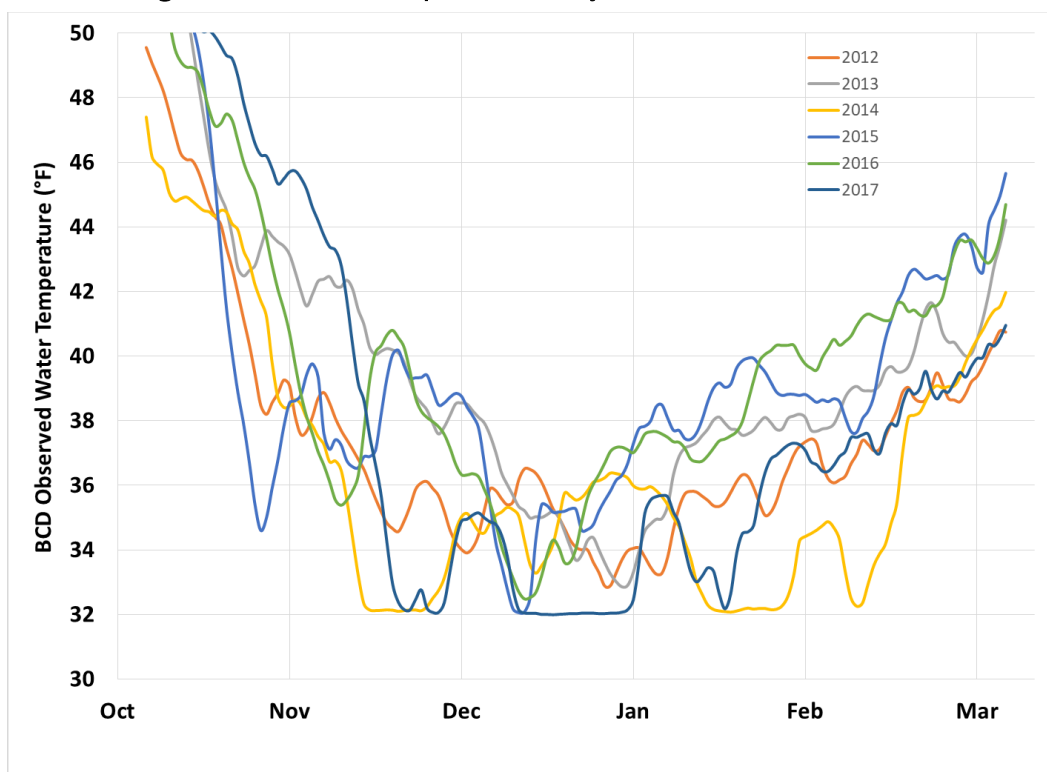


Figure 49. Observed temperature history at BCD for WYs 2012–2017.



The water-temperature time series at AFD has extensive missing data during the winters of WYs 2008, 2010, and 2011. The BCD time series has extensive missing data during the winters of WYs 2008, 2009, and 2010. We adjusted our simulations for these missing data and limited them to the winters of WYs 2012 through 2017, when both data sets were available and had a minimum of missing data (Figure 49).

4.4.3 Meteorological data

Table 16 lists the sources of the meteorological data required by the Water Quality Module.

Table 16. Input data sources for the water-temperature model.

Input Parameter	Source	Time Interval	POR Start	POR End
Water temperature—AFD	USACE	hour	8/11/2007	9/28/2017
Shortwave radiation	SNOTEL—site 1053	hour	10/22/2013	9/29/2017
Air temperature	Sandpoint Airport	hour	12/1/2007	9/30/2017
Relative humidity	Sandpoint Airport	hour	12/1/2007	9/30/2017
Wind speed	Sandpoint Airport	hour	12/1/2007	9/30/2017
Cloudiness	Spokane Airport	day	10/1/1980	8/10/1994
Atmospheric pressure	USGS 12398600	day	9/30/2007	8/11/2017

The cloudiness data period for the period used in the simulations did not coincide with the historical data available in the area. To allow for its use in this study, the time series was shifted to the current simulation window and therefore does not directly represent observations during the study period. The historical cloudiness data is from WYs 1980 through 1994. This was translated and used in the simulation window from WYs 2004 through 2017.

4.4.4 Results

We ran six separate simulations, each beginning on 1 November and ending on 31 March for WYs 2012–2017. The simulations differed in the number of input parameters that used climatological estimates rather than actual observations.

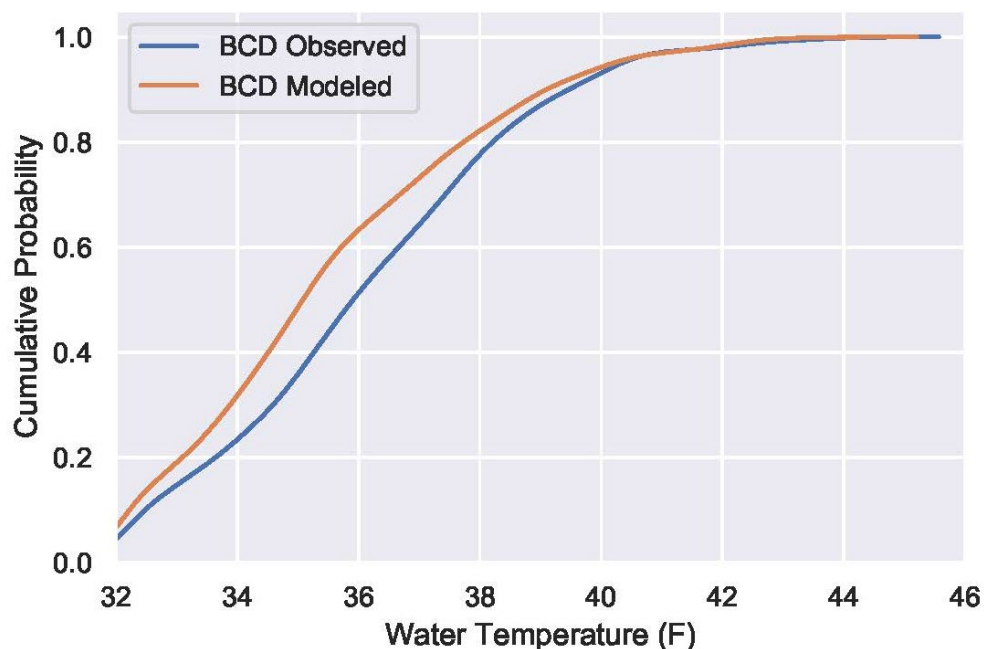
4.4.5 Model performance

During the winters of WYs 2012–2017, the mean measured water temperature at AFD was 36.9°F, and the mean air temperature (measured at

Sandpoint) was 29.3°F. As mentioned previously during winter, the river generally loses heat to the atmosphere, which results in decreasing water temperatures with increasing distance from AFD. The mean observed BCD temperature was 36.0°F, representing a 0.9°F observed average temperature loss between AFD and BCD. The mean water temperature at BCD computed with the model was 35.5°F, resulting in an average temperature loss of 1.4°F between AFD and BCD. On average, the modeled BCD water temperatures are slightly lower than the observed values. Figure 50 shows the bias towards lower modeled temperatures. The bias could be due to a number of issues, including underestimating positive heat fluxes (e.g., solar radiation or downwelling longwave radiation), assumed complete vertical mixing, measurement depth and location, measurement uncertainty, or presence of ice cover.

The model performance was measured by comparing the modeled and observed hourly water temperatures at BCD. The RMSE and the MAE during winters of WYs 2012–2017 were 0.91 and 0.73°F, respectively.

Figure 50. Nonexceedance probability of observed and modeled water temperatures at BCD forebay for December, January, and February, WYs 2012–2017.



4.4.6 Model sensitivity to input parameters

The sensitivity of the temperature model to input data was evaluated by replacing observed input data with time-averaged climatological values over a sequence of runs. The climatological values were computed on an

hourly increment over the six water years spanning 2012–2017 to develop an average hourly time series spanning December through February. Table 17 summarizes the input values used for each run.

Table 17. Input data in water-temperature-model simulations where X represents observed values and C represents climatological values.

Simulation	Water Temperature	Shortwave Radiation	Cloudiness	Atmospheric Pressure	Air Temp.	Relative Humidity	Wind Speed
1	X	X	X	X	X	X	X
2	X	X	C	C	C	C	C
3	X	C	C	C	C	C	C
4	C	C	C	C	C	C	C
5	X	C	C	C	X	C	C
6	C	C	C	C	X	C	C

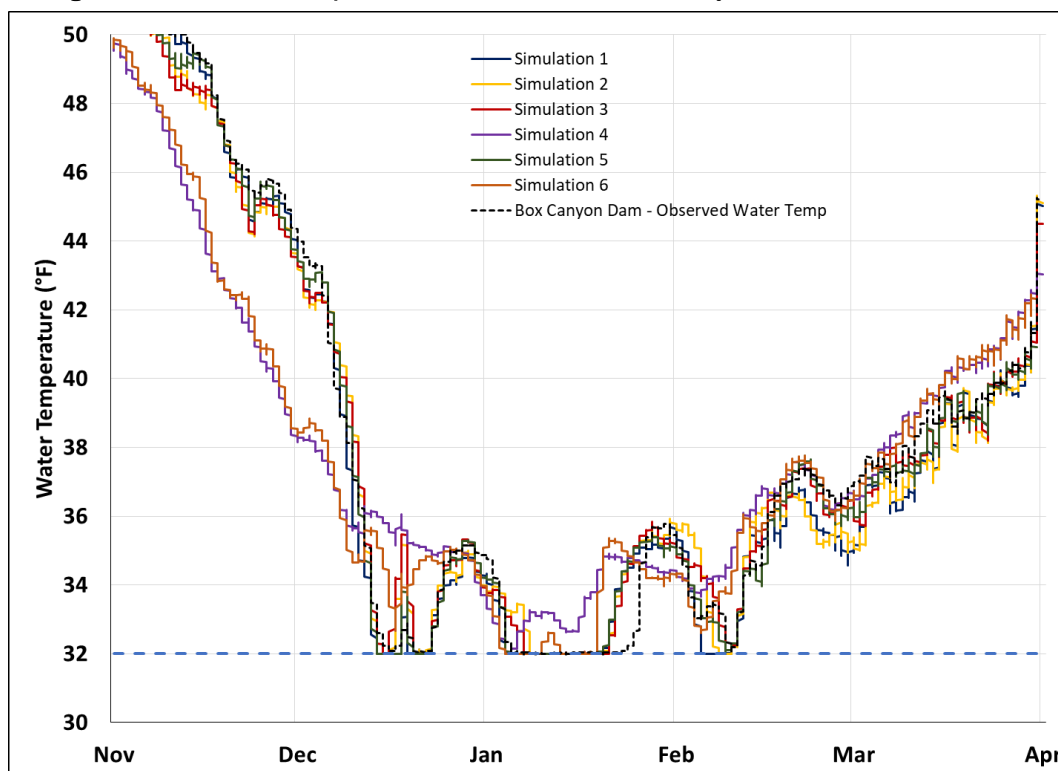
The sensitivity to input data is summarized in Table 18 using model error metrics. Figure 51 shows an example of the computed water-temperature time series in comparison to the observed water temperatures at BCD.

For Simulation 1, all input data were based on observations. The error metrics suggest that the model accuracy is under 1°F. For Simulation 2, all inputs were time averaged except water temperature and shortwave radiation, based on the assumption that these variable were major drivers of the temperature variability at BCD. As a result, model performance decreased slightly from Simulation 1's results. Interestingly, when shortwave radiation is time averaged in Simulation 3, leaving AFD water temperature as the only observed input, model performance increased slightly, suggesting a potential issue with the solar radiation input data or the way that the model handles heat flux. For Simulation 4, all input values were time averaged, essentially simulating the water temperature during a "generic" winter. Model performance was reduced significantly. Simulation 5 inputs are time averaged except for AFD water temperature and air temperature. It is interesting that Simulation 5 actually slightly outperformed Simulation 1, suggesting that AFD water temperature and air temperature are the most important variables in the model. Simulation 6 tests model performance using time-averaged inputs except air temperature. The model performance was relatively poor, suggesting that, while air temperature is an important input, water temperature is the dominant source of variability. This analysis shows that reasonable temperature estimation at BCD can be accomplished by using AFD discharge water temperature and air temperature and by using time-averaged values for all other inputs.

Table 18. Summary of errors of modeled hourly water temperatures at BCD, root-mean-square error (RMSE), mean absolute error (MAE), mean bias error (MBE), and Nash-Sutcliffe efficiency (NSE).

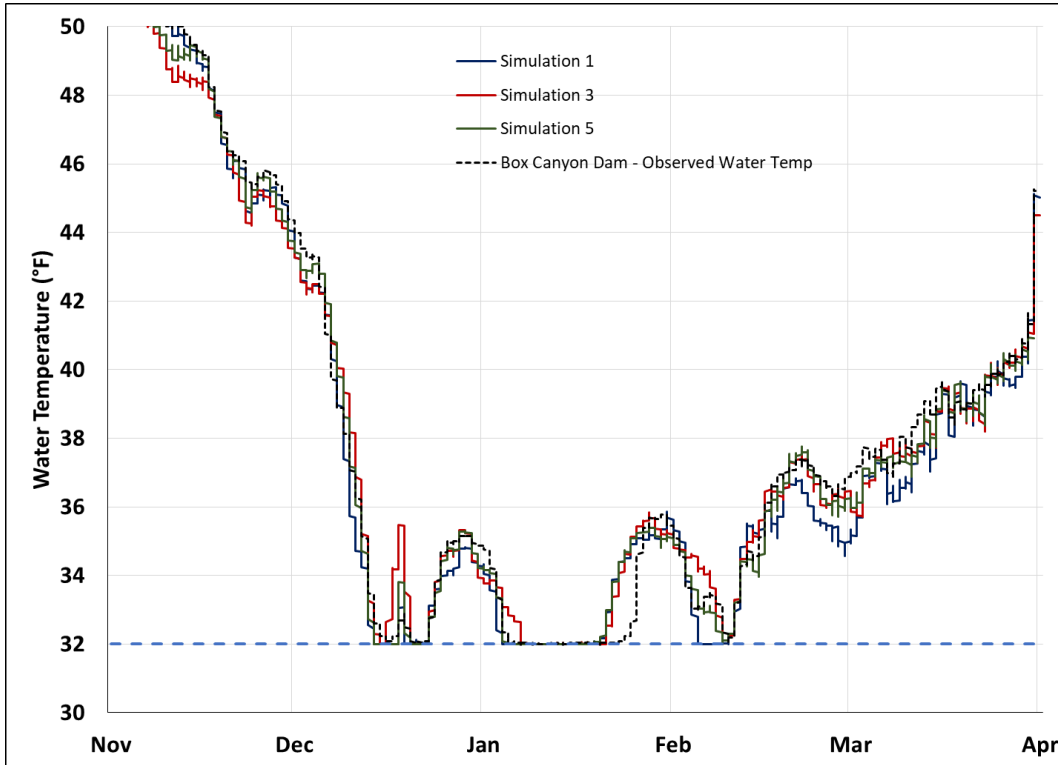
Simulation	RMSE	MAE	MBE	NSE
1	0.91	0.73	-0.48	0.96
2	1.24	0.98	-0.46	0.93
3	1.13	0.88	-0.43	0.94
4	2.37	1.98	-0.75	0.73
5	0.76	0.60	-0.40	0.97
6	2.03	1.66	-0.75	0.80

Figure 51. WY 2017 temperature-model results at Box Canyon Dam, Simulations 1–6.



Simulations 1, 3, and 5 have the most accurate water-temperature predictions, especially for timing of ice-forming conditions (Figure 52). The initial cool down of the BCD forebay in the simulations matches very well the late December moderation of temperatures. The timing of increased water temperature in late January does indicate some differences. This is likely explained by the lack of accounting for ice cover in the water-temperature model.

Figure 52. WY 2017 temperature-model results at Box Canyon Dam, Simulations 1, 3, and 5. Simulation 1 is based on all observed input data. Simulation 3 is based on observed AFD water temperature and average climatological data. Simulation 5 is based on observed AFD water temperature and air temperature and on average climatological data.

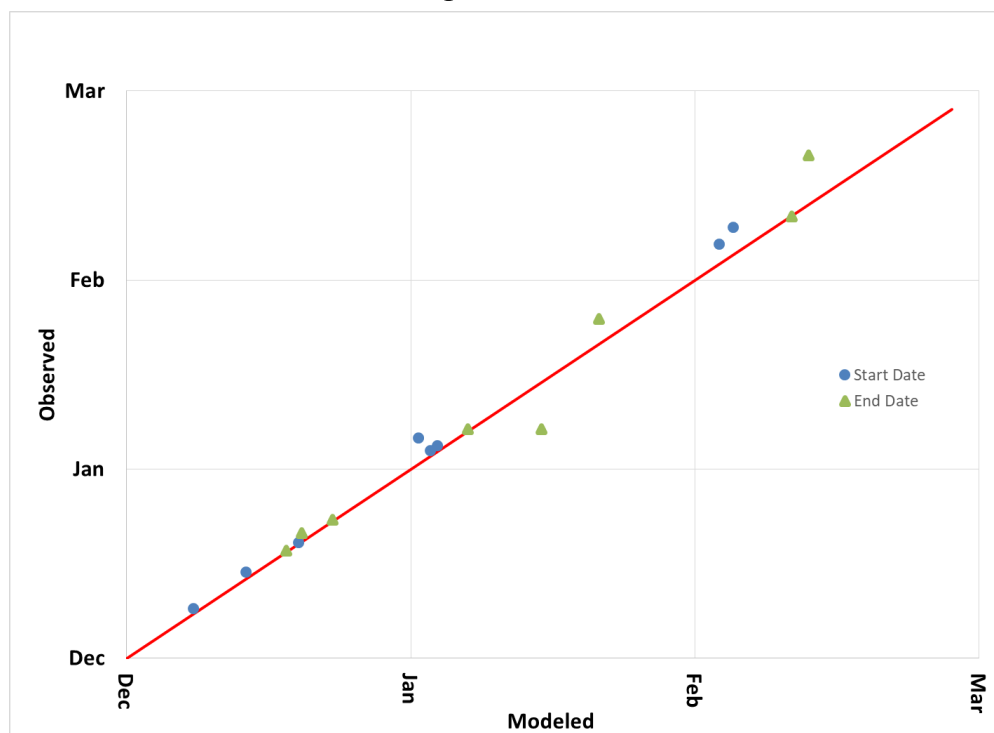


We compared the modeled and observed ice event duration. Using all observed inputs for the HEC-RAS Water Quality Module (Simulation 1) the accuracy of the ice event duration varies by event (Table 19). Again this can be explained by the lack of persistent ice cover being represented in the model. Overall the beginning and ending dates along with the event duration are reasonably represented by the Water Quality Module (Figure 53) even when using climatology for most of the necessary inputs.

Table 19. Comparison of modeled and observed ice events for BCD using observed values for all model inputs (Simulation 1).

WY	Modeled (Simulation 1)			Observed			Difference of Event Start Dates (Modeled – Observed) (Days)	Difference of Event End Dates (Modeled – Observed) (Days)
	Begin Date	End Date	Duration (Days)	Begin Date	End Date	Duration (Days)		
2012	1/20/12 16:00	1/22/12 3:00	1.5	-	-	-	-	-
2012	1/23/12 15:00	1/25/12 16:00	2.1	-	-	-	-	-
2014	12/8/13 7:00	12/20/13 3:00	11.9	12/9/13 2:00	12/21/13 12:00	12.5	0.8	1.4
2014	2/3/14 16:00	2/13/14 10:00	9.8	2/6/14 20:00	2/21/14 10:00	14.6	3.2	-0.2
2014	2/17/14 16:00	2/21/14 14:00	4.0					
2015	1/3/15 3:00	1/7/15 5:00	4.1	1/4/15 0:00	1/7/15 13:00	3.6	0.9	0.3
2016	1/1/16 21:00	1/15/16 7:00	13.5	1/6/16 1:00	1/7/16 14:00	1.6	4.2	-7.7
2017	12/14/16 0:00	12/18/16 11:00	4.5	12/15/16 2:00	12/18/16 14:00	3.5	1.1	0.1
2017	12/19/16 19:00	12/23/16 11:00	3.7	12/19/16 23:00	12/23/16 17:00	3.8	0.2	0.3
2017	1/3/17 22:00	1/21/17 13:00	17.7	1/4/17 20:00	1/25/17 15:00	20.8	0.9	4.1
2017	2/5/17 5:00	2/11/17 13:00	6.4	2/9/17 15:00	2/11/17 11:00	1.9	4.4	-0.1

Figure 53. Comparison of Simulation 1 results and observations for beginning and ending ice event dates.



4.4.7 Model results discussion

The ice-prediction potential of the Water Quality Module can be demonstrated using the model configuration from Simulation 1. This simulation

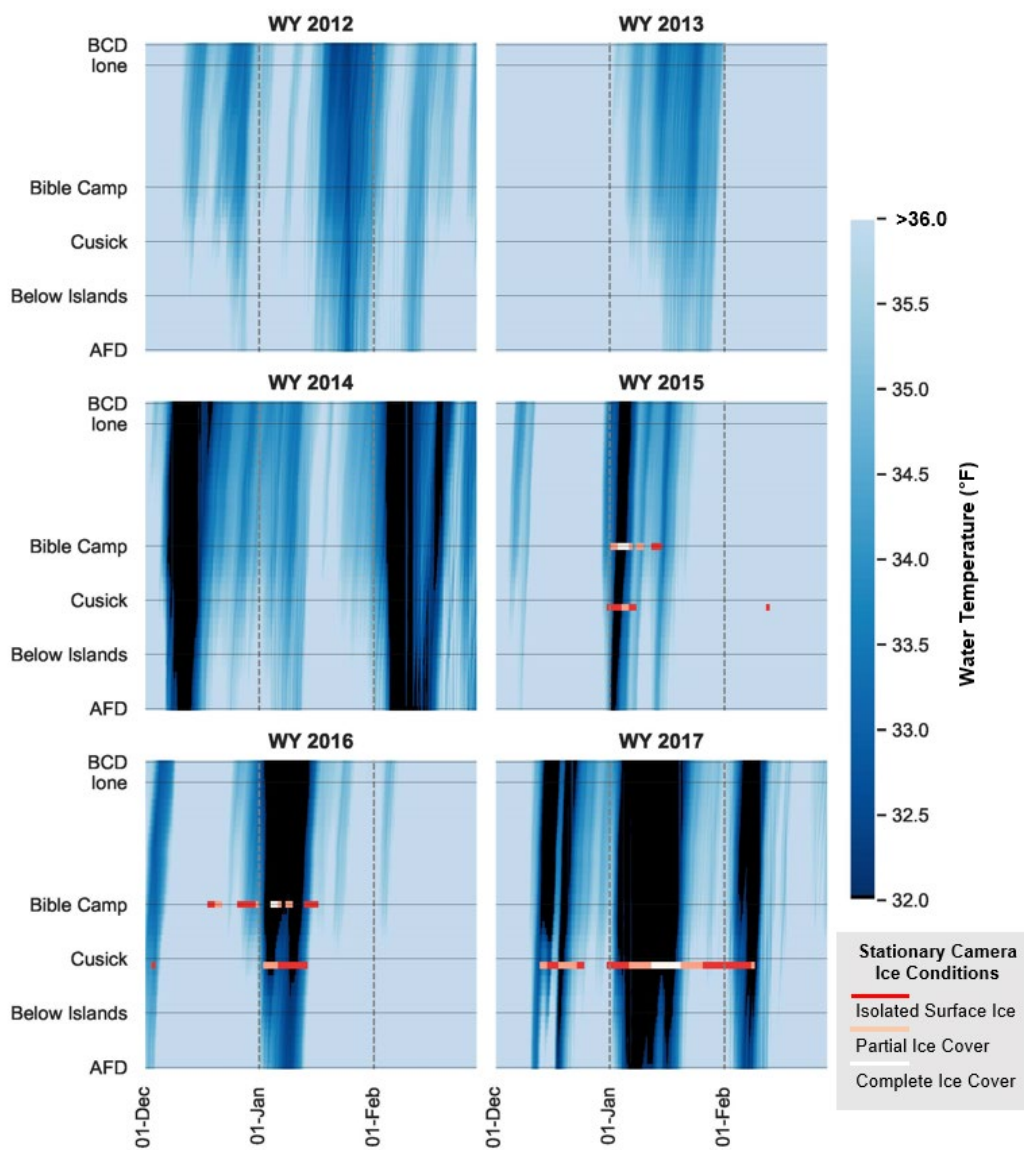
represents having perfect forecasts of all the necessary input variables and can be validated using the shoreline-ice-camera information for WYs 2012–2017 (Figure 54). Water temperatures during WYs 2012 and 2013 were relatively mild, rarely approaching freezing anywhere along the entire reach. During WYs 2014–2017, there were several discrete periods when predicted water temperatures reached 32.0°F and likely formed ice for much of the distance between AFD and BCD. Several of these events occurred when water temperatures immediately below AFD were above freezing, and heat loss cooled the water to 32.0°F as it traveled downstream to BCD (e.g., January 2016 and December 2016). In some cases, persistent low temperatures drove the AFD forebay water temperatures to the freezing point, which typically resulted in the entire reach being prone to ice growth (e.g., January 2015 and January 2017).

There are limitations to the heat transfer methods in the HEC-RAS Water Quality Module. This is demonstrated by an event in mid-February 2014 when air temperatures above freezing caused the model to predict that 32.0°F water at AFD would warm 1.5°F before reaching BCD. Temperature measurements at BCD show an almost negligible warming, however. The discrepancy is likely due to a combination of ice cover on the reach insulating the river from heat in the air and the ice melting and depressing the water temperature. The water-temperature calculations in the model do not consider the effects of ice cover on heat transfer, which can insulate flow, contribute heat from ice formation, or absorb heat from ice melting. In general, the water-temperature model will be more accurate during freeze-up events as compared to periods with existing ice cover.

The time series of ice conditions based on analysis of the shoreline-ice-camera photographs was overlaid on Figure 54. Color codes correspond to three levels of ice presence: isolated patches of surface ice, partial ice cover, and complete ice cover. The camera data were available at two locations downstream of AFD: Bible Camp (WYs 2015 and 2016) and Kalispel (WYs 2015–2017). The ice conditions observed by the shoreline ice cameras are highly correlated with the modeled water temperatures, with complete ice cover occurring only when modeled water temperatures were approximately 32.0°F. Ice breakup is captured by the cameras in January 2015 and 2017 when modeled water temperatures rise above freezing. The WY 2016 camera data for Bible Camp does not appear as well correlated with water temperature due to a malfunctioning camera that collected only intermittent images through that season.

Water temperatures estimated at or very near 32.0°F on the reach between AFD and BCD appear to be very strong indicators of ice growth based on the ground truth observations made with the shoreline ice cameras. As demonstrated with the sensitivity analysis, the water-temperature model is able to estimate hourly water temperatures at BCD with an error of around 0.76°F by using precalculated, time-averaged meteorological variables and real-time input of discharge water temperature at AFD and Sandpoint air temperature.

Figure 54. Modeled river temperatures for December, January, and February in WYs 2012–2017. Images are overlaid with ice conditions observed with shoreline ice cameras located at Kalispel (WYs 2015–2017) and Bible Camp (WYs 2015–2016).



5 Ice Formation in Lake Pend Oreille

There are very few recorded observations of ice conditions on Lake Pend Oreille. The primary source of information is the recorded images from shoreline ice cameras located at the Windbag Marina in Sandpoint, Idaho. Another source of information that can be used to infer ice conditions are water-temperature measurements made by the U.S. Naval Sea Warfare Center, Carderock Division, Acoustic Research Division (Naval Sea System Command 2018) and measurements made in a fishery study of the lake (Vidergar 2000). This section will first review the available data and then includes a general discussion of ice formation on Lake Pend Oreille.

5.1 Shoreline camera ice observations

Four stationary cameras are located on Lake Pend Oreille at Windbag Marina. Table 20 describes the data available from the cameras. Each shoreline ice camera faces in a different direction (Figures 55 and 56). Camera 1 faces north and captures an expanse of the lake near shore and shallows and shore structures. Camera 2 faces in an easterly direction across Lake Pend Oreille. It captures a narrow strip of shoreline in the foreground and the horizon of the lake. Camera 3 faces south along the northern shore towards the Highway 95 Bridge. It captures the lake near shore and shallows up to the bridge. Camera 4 faces in a westerly direction, capturing Windbag Marina.

Table 20. Shoreline ice cameras located at Sandpoint, Idaho, 48.2758, -116.5398.

Sandpoint Location	Resolution (pixels)	Start Date	Last image Date	Total Number of Images	Number of Images with Ice	R/L Bank	Miles from Albeni Falls
4	704 × 480	12/20/12	5/15/17	11,698	3661	Right	27 upstream
3		12/20/11	5/15/17	11,488	2685		
2		12/20/11	5/15/17	14,323	1758		
1		12/20/11	5/15/17	14,464	3106		

Figure 55. Direction of view for each shoreline ice camera located at Sandpoint.



Figure 56. Typical views from Sandpoint shoreline ice cameras.



Figure 57 shows an overview of the imagery collected by each of the Sandpoint cameras, and Table 21 summarizes this imagery. They show that ice was observed each winter except in WY 2014 when imagery was not available except at Camera 1 and 2012 when imagery was missing throughout most of the winter. Over all the available winters, Camera 4,

which faced the Windbag Marina, captured 274 days with ice, the most of any camera. This is probably not unexpected given the relative shallow depths in the marina and its protected location. Cameras 2 and 3, which face parallel to the shoreline and thus cover the near-shore shallow water of the lake, captured 214 days and 198 days with ice, respectively. This is about 75% of the days that ice was in the marina as seen by Camera 4. Camera 1, which looks directly out to the lake captured 111 days with ice, the fewest days with ice of any of the cameras. This is about 40% of the days that ice was in the marina as seen by Camera 4.

Figure 57. Overview of imagery data collected at Sandpoint.

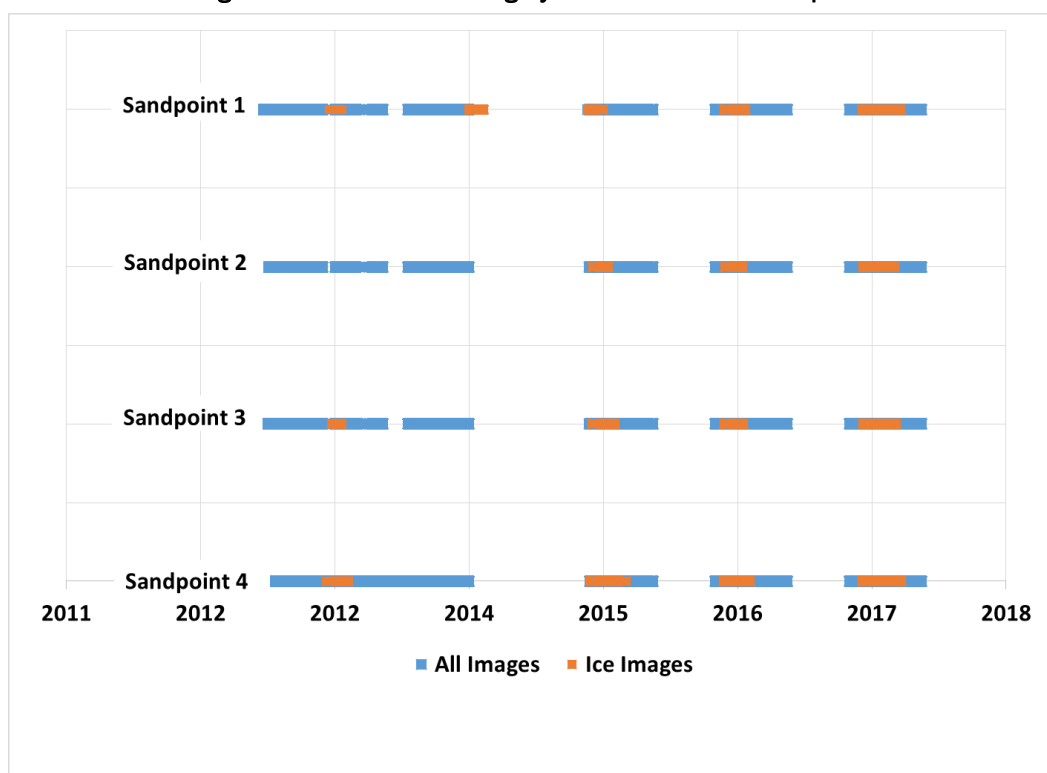


Table 21. Summary of days with ice for each Sandpoint shoreline ice camera.

Camera	2013	2014	2015	2016	2017	Total Days
Sandpoint 1	5	39	23	41	106	214
Sandpoint 2			20	19	72	111
Sandpoint 3	27		40	39	92	198
Sandpoint 4	39		60	68	107	274

The days during each winter season when ice was observed in the camera imagery is shown in Figure 58 for WY 2015, Figure 59 for WY 2016, and Figure 60 for WY 2017. The ice-coverage classification follows criteria

from the National Oceanic and Atmospheric Administration's (NOAA) *Observers Guide to Sea Ice* (Smith 2007). The ice coverage captured by Camera 4, the marina ice, starts the earliest each season and lasts the longest. This ice forms in the very shallow water of the marina and is protected by the marina breakwater. The ice observed in Camera 2, which looks out over the lake, starts the latest each winter season and has the shortest duration. This camera views only the northwestern corner of the lake, which is not representative of ice on the entire lake. The durations of the ice captured by Camera 1 and Camera 3, each looking along the shoreline, start roughly at the same time each winter. The ice captured by Camera 1 tends to last longer than the ice captured by Camera 3 except during WY 2015 when the ice captured by Camera 1 ended about 1 month before the ice captured by Camera 3.

Figure 58. Ice coverage recorded by Sandpoint shoreline ice cameras during WY 2015.

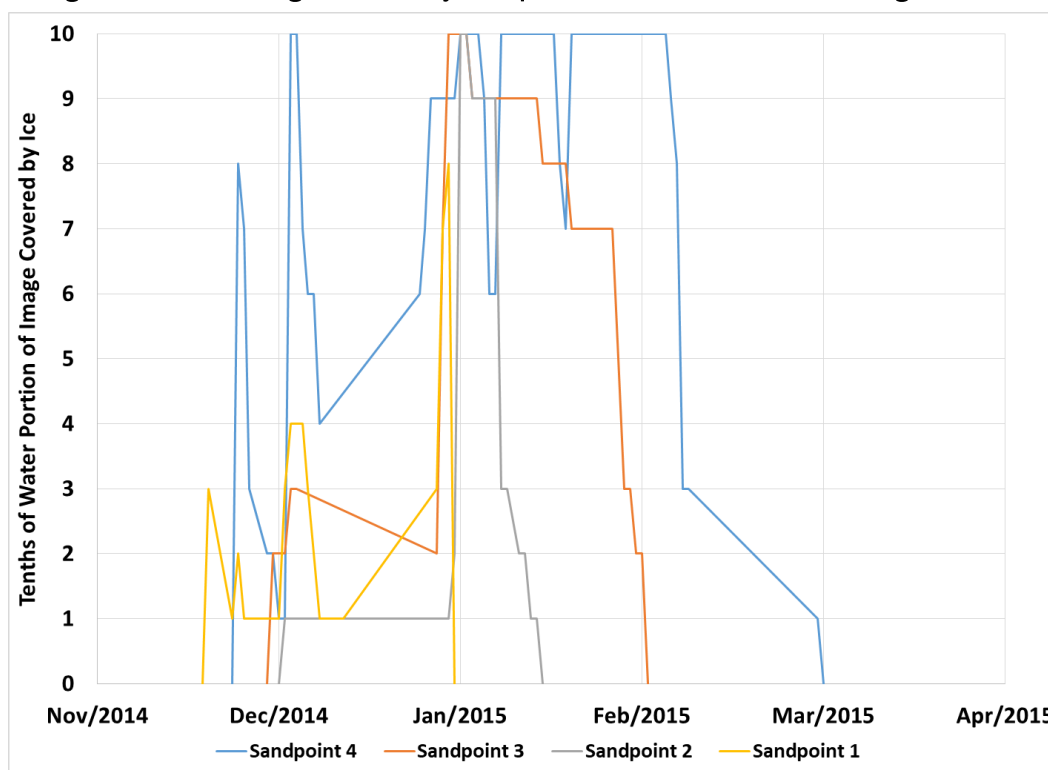


Figure 59. Ice coverage recorded by Sandpoint shoreline ice cameras during WY 2016.

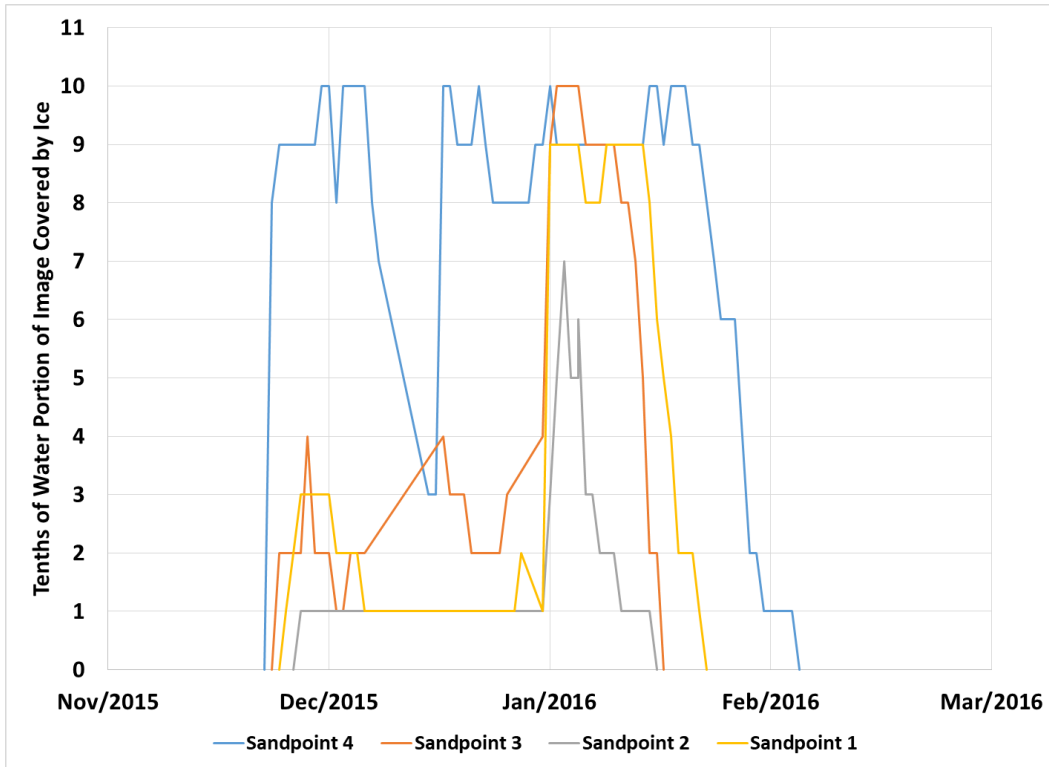
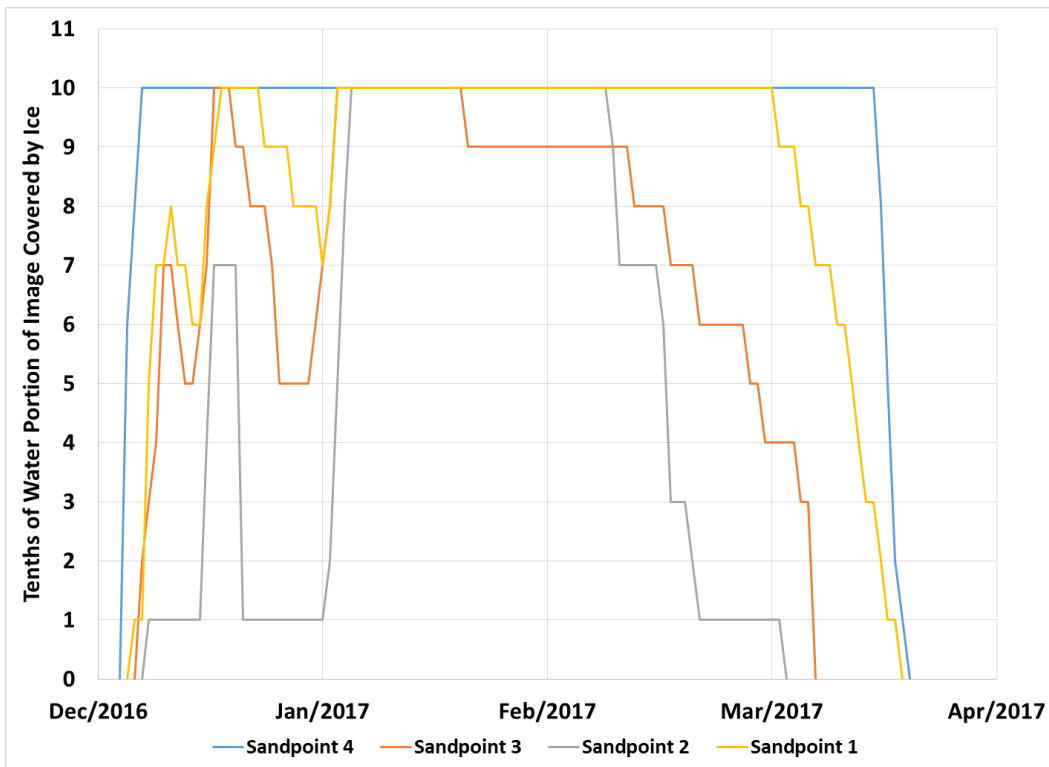


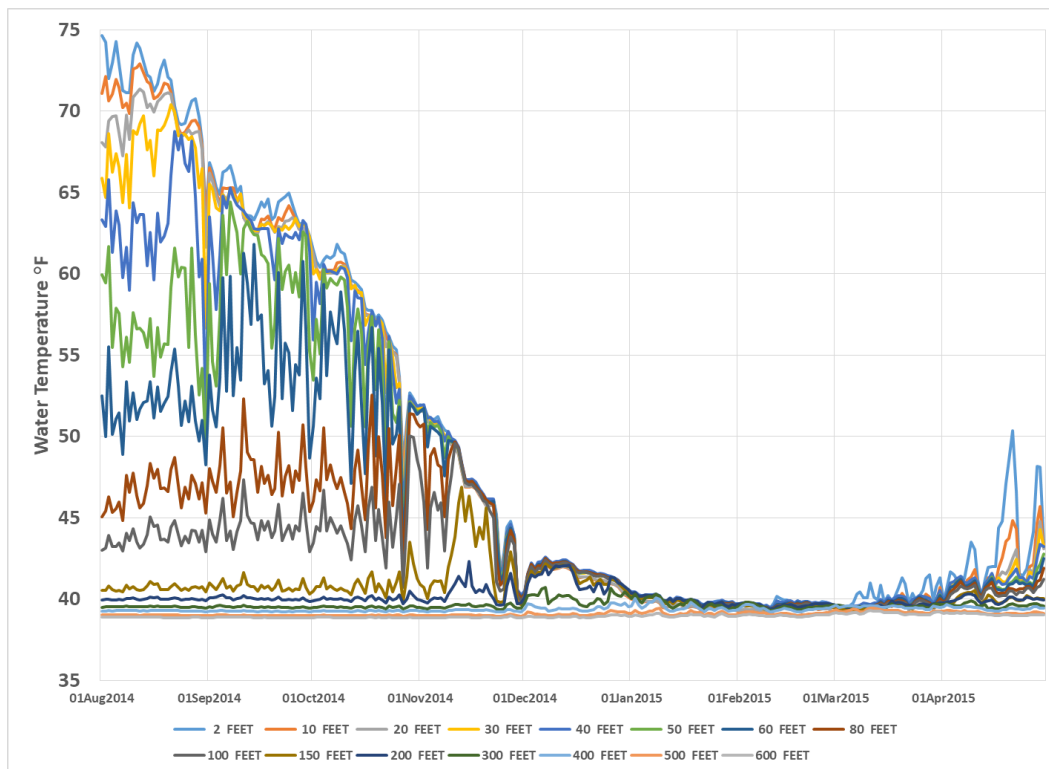
Figure 60. Ice coverage recorded by Sandpoint shoreline ice cameras during WY 2017.



5.2 Water-temperature observations

For ice to form at the surface of lakes and reservoirs, the water temperature at the surface must first cool down to 32°F. Therefore, water-temperature measurements made near the water surface that are at or very near 32°F can indicate the presence of surface-ice covers. The Navy has recorded water temperatures in Lake Pend Oreille for a number of years (Naval Sea System Command 2018). This water temperature is recorded in the deepest section of the lake where the depth is over 1000 ft. We reviewed data from 2012 through 2017. Water temperature was available on a near-hourly basis at depths of 2, 10, 20, 30, 40, 50, 60, 80, 100, 150, 200, 300, 400, 500, and 600 ft. Figure 61 provides an example of water temperature recorded at depths from 2 ft to 600 ft for the winter of 2014–2015. Note that the water temperature at depths of 200 ft or more remain consistently near 39.4°F, the temperature at which water is at its maximum density. More importantly, note that the water temperature at any depth did not drop below 39.4°F. This indicates that ice did not form in this area of the lake during this winter.

Figure 61. Recorded Lake Pend Oreille water temperature for winter 2014–2015.



5.3 Summary of Lake Pend Oreille ice conditions

Based on the shoreline-ice-camera imagery, water-temperature measurements, and discussions with locals, ice cover in Lake Pend Oreille seems to be limited to shallow areas at the north end of the lake, where the depth is less than 10 ft (referenced to 2048.2 ft above sea level) (Figure 62). This map can be compared to a satellite image of Lake Pend Oreille acquired on 14 January 2017 that displays ice in Lake Pend Oreille (Figure 63). There is a good match between the observed ice-covered area and the 10 ft contour.

Figure 62. Shallow areas of Lake Pend Oreille indicating likely ice-covered areas (highlighted in *white*).

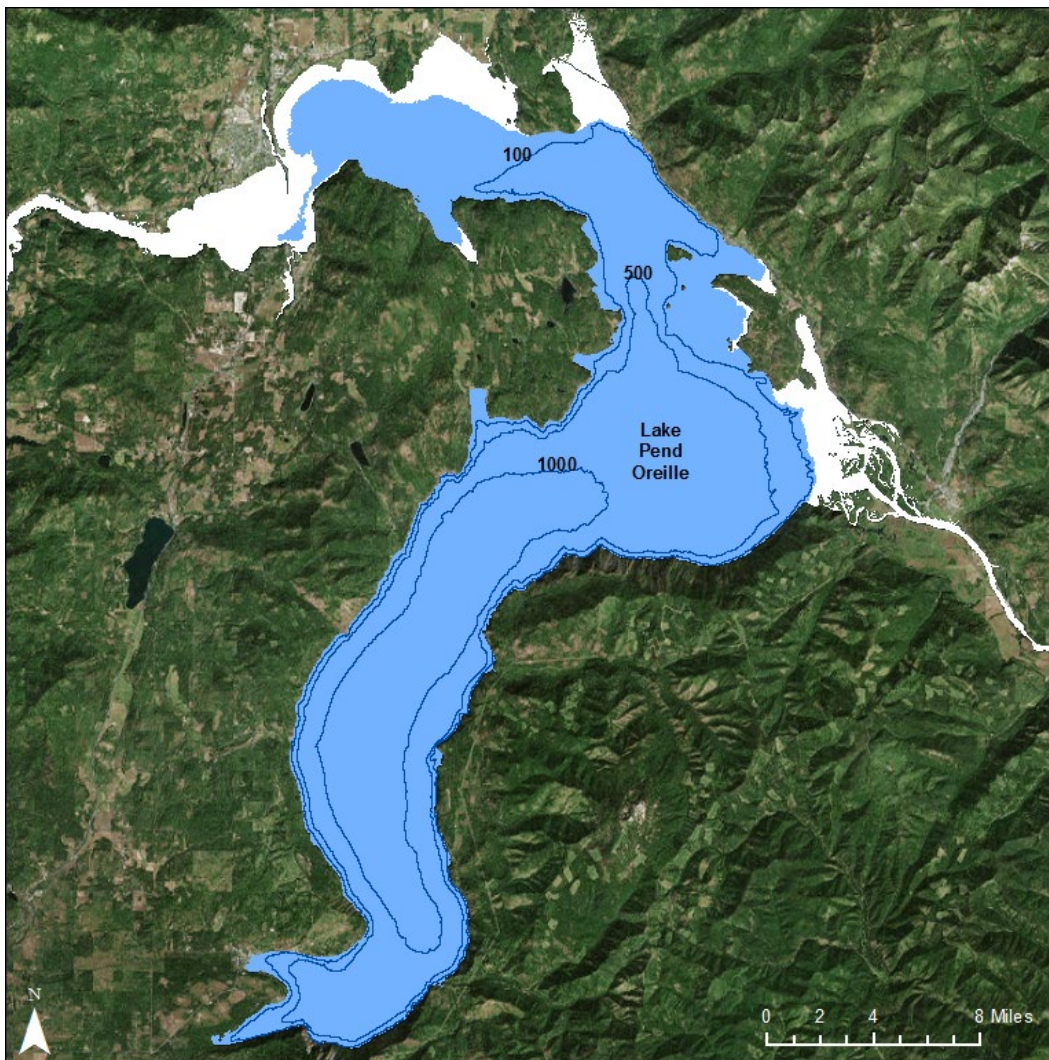
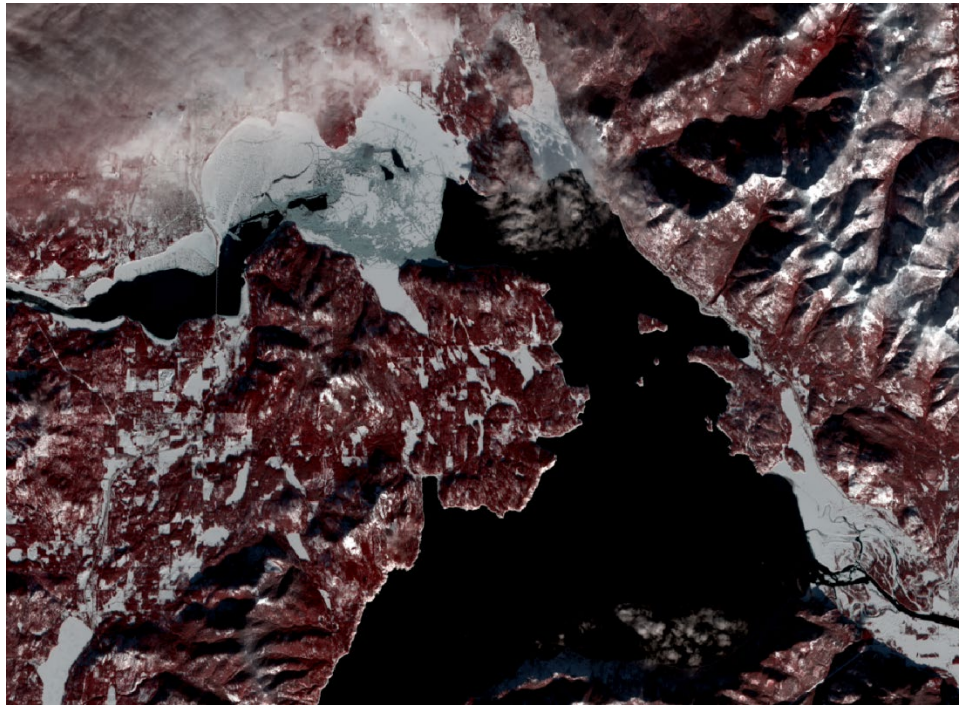


Figure 63. Landsat image of Lake Pend Oreille acquired on 14 January 2017 showing ice cover.



6 Ice Forces on Shoreline Structures

6.1 Wintertime conditions on Lake Pend Oreille

Two aspects of the wintertime conditions of Lake Pend Oreille are relevant with regard to uplift forces caused by ice on structures located along the shoreline. The first is that, in winter, the lake level of Lake Pend Oreille is lower than the summertime water level. The wintertime elevation of Lake Pend Oreille varies from year to year but is generally held at 2051.5 ft NGVD29 or 2055.5 ft NGVD29. The summertime water level is generally near the allowed maximum of 2062.5 ft NGVD29, which is 7 to 11 ft higher than the normal wintertime water level. Shoreline structures are designed exclusively for summertime operation. The wintertime drop in lake water levels tends to protect structures from ice action by reducing water buoyancy on the structure, which increases the effective pile weight, making the piles less susceptible to pullout. At some locations, the structure may be completely out of the water in winter; and in the case of floating docks, the docks may rest close to or on the bottom. The second aspect is the small range of water-level fluctuations that occurs in the winter. The lake-level records indicate that there are daily stage increases about 43% of the days during December through February, but the increases are small. The daily average increase in the lake level from one day to the next is 0.09 ft (about 1 in.), and the daily average decrease is 0.08 ft.

6.2 FWPO SOP criteria

6.2.1 Introduction

The Flexible Winter Power Operations for Lake Pend Oreille are concerned with reducing possible ice damage to docks and marinas located along the shoreline of Lake Pend Oreille. This section evaluates the effectiveness of the criteria included in the FWPO SOP (Exhibit 7-4 of the AFD WCM).

6.2.2 Potential ice damage on Lake Pend Oreille

There are several ways in which the lake ice could potentially damage docks and marinas. These include horizontal forces caused by thermal expansion of the ice cover or wind-induced ice motion and vertical forces caused by changes in the water level of the lake. Horizontal ice forces are severely limited on Lake Pend Oreille due to the relatively small extent of the ice cover in the lake. The most likely source of ice damage is vertical

forces exerted by the ice cover caused by changes in the lake level. These types of forces are generally termed *uplift forces*. Uplift forces are generated when an ice sheet frozen to a pile is deformed due to a rise in the water level. If the force does not cause the ice sheet to break or slip, the pile will be *jacked*, or pulled from the harbor bottom, when the uplift force exceeds the sum of the skin frictional resistance in the soil and the effective weight of the pile (Edit et al. 1988). Typically, damage from uplift occurs where there is periodic short-term (daily or shorter) water-level fluctuations of sufficient magnitude to enable an ice sheet of adequate thickness and strength that is firmly frozen to the pile to overcome the pullout resistance of the pile. Estimating the susceptibility of a given shore structure to uplift damage is difficult because of the many factors that can influence the occurrence of uplift damage. These factors include the layout geometry of docks and piles of a marina, the pullout resistance of the piles, the ice thickness and ice adhesion to the piles, and the rate and magnitude of the changes in the water surface elevation.

6.2.3 The layout geometry of docks and piles of a marina

The number and spacing of piles used in supporting docks significantly impact the potential uplift forces that the piles must resist. At one end of the spectrum is a single, solitary pile with no other piles nearby. This single pile must resist all the uplift force generated by the ice cover during changes in water level. There have been a number of investigations of uplift forces caused by ice on solitary piles (e.g., Christensen 1986; Kerr 1975; Terahima et al. 2006; Zabilansky 1998). At the other end of the spectrum are groups of piles, connected by horizontal beams, that are used to support dock structures. Groups of piles act in tandem to resist ice forces, and piles located in the interior of the group are protected from uplift forces. End piles may see an uplift much greater than interior piles. Still, compared to the uplift on a solitary pile under similar ice conditions, the uplift forces on end piles may be 25% or less of the load on the solitary pile, and interior piles may experience as little as 3% to 5% of the load (Kerr 1978). The connections between the piles can also be important in distributing the loads between piles and applying extra downward weight to the piles. Typically, single solitary piles are the most likely to suffer damage due to uplift.

6.2.4 Pullout resistance of the piles

The pullout resistance of piles is largely due to the soil-pile adhesion; the soil-pile friction, which is proportional to the normal stress of soil acting on the pile; and the effective pile weight (the weight of the pile and any connecting structure minus the buoyancy of the water). In granular soils, the soil-pile adhesion is normally small. The effective pullout resistance depends on the pile penetration depth, pile shape, soil types and layering within the penetration depth, and other factors. Methods are available for estimating the pullout resistance (U.S. Navy 1986).

6.2.5 Ice thickness and ice adhesion to the piles

The total uplift force that an ice cover can apply to a solitary pile is sensitive to the ice thickness. Estimated annual maximum ice thicknesses for Lake Pend Oreille are modest. The model results indicate that the average annual maximum ice thickness for the period 2003 through 2017 is approximately 7 in., with the greatest annual maximum of just over a foot in 2017. Generally, the adhesion force of the ice to metal or wooden piles is quite large and is usually large enough to transfer all the force that the ice can transmit to the pile. It is generally expected that the ice cover itself will fail before the adhesion of the ice to the pile will be overcome.

6.2.6 Rate and magnitude of changes in the water surface elevation

As reported by Edit et al (1988), uplift damage in the Great Lakes is associated with short-term (daily or shorter) water-level fluctuations. The ice sheet is likely to *creep* during longer-term fluctuations, which reduces the stress level the ice sheet can apply to a pile. Creep is the ability of the ice sheet to strain continuously under constant stress. This property of ice is not surprising considering that ice is floating in a pool of its own melt (liquid water) and so is always relatively close to its melting temperature. Lake Pend Oreille has no reported short-term fluctuations such as seiches. This is expected for such a small yet deep lake as seiches are usually associated with large, relatively shallow lakes. Fluctuations of the Lake Pend Oreille water surface generally arise due to differences in its inflow and outflow rate. The inflow is generally at its annual minimum during the winter when ice is present as snowmelt is not occurring and rainfall is unlikely. As a result, the daily fluctuations in the Lake Pend Oreille water level are quite small during the winter ice period as measured by the USGS gage at Hope, Idaho.

6.2.7 Simulating the interaction of the ice cover and piles

The FWPO SOP calls for the formation and maintenance of active and hinge cracks through active management of changes in the lake water surface elevation. *Active cracks* are cracks that extend completely through the ice cover from its top surface to the water below. Active cracks become nonactive by refreezing. There is no exact definition of *hinge cracks*, but their formation is often referred to in reference to uplift forces on piles and structures. Given that the goal of water management is to prevent damage to docks and marinas located along the shoreline of Lake Pend Oreille, our study focuses on hinge cracks.

Hinge cracks occur when the maximum stress level in an ice cover frozen to a pile or other structure is exceeded through bending. The analysis begins by assuming that the ice cover acts as a relatively thin, elastic plate. The assumption of elasticity is common with plates made of other material, such as steel. The elasticity assumption makes the analysis tractable to analytical solutions and also limits the analysis to relatively short-term loads—situations where creep is not an issue. The loads are a result of an increase in water level, which provides an upwards pressure on the ice sheet. The connection between the ice sheet and the pile or structure must be considered first. If a *fixed* connection is assumed, the maximum bending moment in the ice sheet occurs immediately next to the pile or structure. The first failure of the ice sheet therefore occurs at that location. This initial ice failure changes the ice sheet connection from fixed to *hinged*, and further analysis proceeds with the assumption of a hinge connection between the ice cover and the pile or structure. The maximum bending stress in the ice sheet then occurs some distance away from the structure, and a second fracture occurs at that location. This fracture is the *hinge crack*. It is interesting to note that, at the point when the hinge crack forms, the ice sheet is applying its maximum upward force on the pile or structure. The appearance of a hinge crack is generally thought to indicate that the ice cover has applied the maximum upwards stress that it is capable of.

There are two approaches to analyzing uplift forces, depending on the geometry of the situation. The first is the analysis of a single, solitary pile. In this case, the pile is assumed to be frozen into an axisymmetric ice sheet that extends away from the pile in all directions. The second is the analysis of vertical wall frozen into an ice sheet that extends away from the wall. The wall is assumed to extend in both directions for enough distance that

end effects of the wall are not considered. The vertical wall analysis applies to a group of interacting piles, such as found in a marina.

The single, solitary pile analysis is complex because the ice fails in a series of three steps that occur as the water level increases. The first step is fracture of the ice cover immediately at the pile. The second step is formation of 4 to 6 *radial cracks* that extend outward from the pile circumference. The radial cracks are usually spaced symmetrically around the pile. The final step is the formation of *circumferential cracks* at some distance from the pile. The circumferential cracks are the hinge cracks for single piles. Generally, the maximum uplift force occurs on the pile when the circumferential crack forms.

The analysis of a vertical wall frozen into an ice sheet indicates that the ice fails in a series of two steps that occur as the water level increases. The first step is fracture of the ice cover immediately at the edge of the wall. This fracture changes the ice connection to the wall from a fixed connection to a hinge connection. The second step is the formation of a hinge crack at a distance away from and parallel to the wall. The maximum uplift force occurs on the wall when the hinge crack forms. This is because the uplift force just moments before the ice fails (the hinge crack) will be the maximum for that ice sheet.

6.2.8 Forming hinge cracks through active management of the Lake Pend Oreille water level

This section evaluates the current FWPO SOP direction on active management of the Lake Pend Oreille water levels to produce hinge cracks. The direction calls for the water level of Lake Pend Oreille to be increased during likely ice periods with a rate of rise of 0.1 ft/day for 6 days to “maintain the active and hinge cracks.” The question that needs to be addressed is whether this rate of rise is sufficient to cause the ice sheet to crack or whether the ice sheet will be able to creep and relax the stresses created by the water-level rise. In addressing this concern, we will analyze the case of a vertical wall frozen into an ice sheet that extends away from the wall. This case is much more straightforward to analyze than the case of a single solitary pile, and it applies to most of the larger marinas on the lake that generally have groups of pile supporting their dock systems.

Christensen (1986) analyzed the case of ice frozen to a vertical wall reacting to a change in water level, assuming that the ice had strictly elastic

properties. However the assumption of elastic properties does not allow the impact of ice creep to be addressed. To address the question of creep, our study developed a new approach that assumed that the ice-cover response was governed by the sum of its elastic, delayed elastic, and viscous properties. The viscous properties allow the ice cover to strain continuously (change its length) under constant stress. The continuous strain can prevent the ice cover from reaching high stress levels because the ice creep causes a reduction in forces acting on the ice sheet.

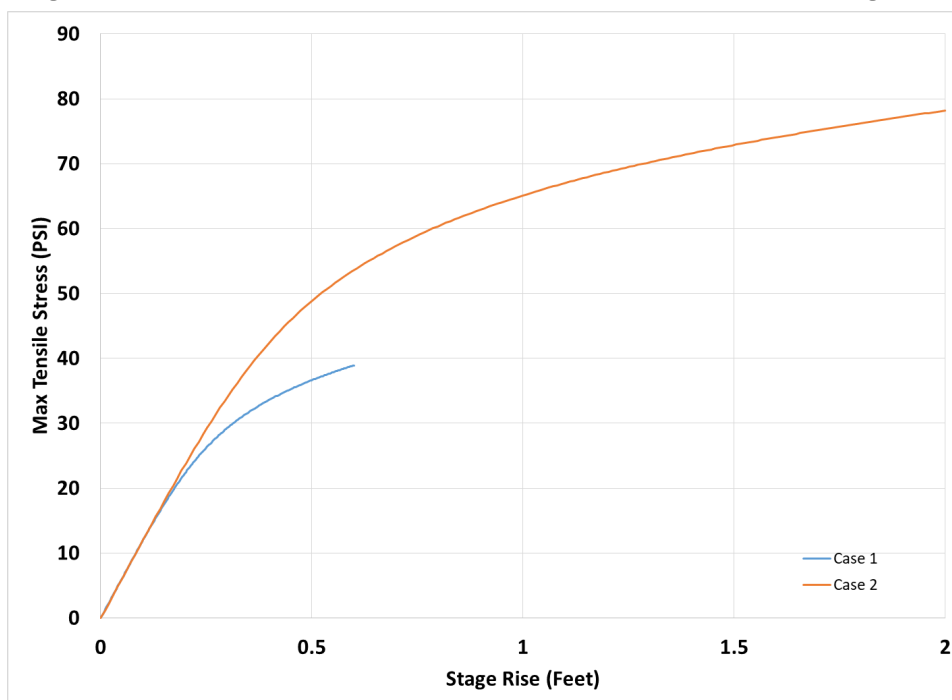
Our finite element model of the case of ice frozen to a vertical wall included the sum of its elastic, delayed elastic, and viscous properties. The ice-cover thickness was set at 1 ft. We analyzed two cases:

- Case 1. The lake elevation was increased 0.1 ft/day for 6 days for a total increase of 0.6 ft. This case corresponds to the directions in the FWPO SOP.
- Case 2. The lake elevation was increased 0.5 ft/day for 4 days for a total increase of 2.0 ft. This rate of change corresponds to the constraints on lake elevation change currently in the AFD WCM. The change of 2 ft in 4 days is larger than any observed change during the winter months.

The simulations for both Case 1 and 2 began with the ice sheet floating on the water in hydrostatic equilibrium and the ice cover fastened to the wall with a hinge connection. Then the water level was increased at the rates specified, and the ice cover was allowed to react to the change in stage. At every time step, we determined the maximum tensile stress in the ice cover. The simulations did not model ice fracture but used the maximum tensile stress as an indicator of fracture. When the maximum tensile stress was exceeded, it was assumed that the ice cover had fractured. The maximum tensile stress of freshwater ice has been measured to be about 600 kPa (roughly 90 psi) in the field (Chistyakov et al. 2016) and has been assumed in previous analysis (Christensen 1987). Using this maximum-tensile-strength value provides an upper envelope of force estimate on piles.

Figure 64 shows the maximum stress in the ice sheet for both Case 1 and Case 2. It is interesting to note that in neither case does the maximum tensile stress in the cover exceed the maximum tensile strength of freshwater ice. This strongly suggests that hinge cracks would not form in either case.

Figure 64. Maximum tensile stress in the ice cover as a function of the stage rise.



6.2.9 Uplift forces

It is interesting to compare the uplift forces that the ice cover can generate and the ability of the piles to resist the uplift forces. Our study estimated the uplift force per unit width along the vertical wall at each time step of the model. In the present analysis, we are assuming that the vertical wall represents a group of piles. Previous analysis has shown that the group of piles will act together if the spacing between the piles is less than one characteristic length of the ice cover. The characteristic length of the ice cover depends on the elastic rigidity of the cover and the ice thickness. The characteristic length of the ice is about 25.3 ft in the present simulations of Lake Pend Oreille. So we are assuming that the spacing between the piles ranges from 5 to 20 ft. The uplifting force acting on the piles is shown in Figure 65 for Case 1 and Figure 66 for Case 2. These show that the uplift force increases as the lake stage increases. In addition, the uplift force on each pile increases as the spacing between piles increases.

The resistance of individual piles to uplift forces can be estimated using the procedures described in Design Manual 7.02, *Foundations and Earth Structures* (U.S. Navy 1986). The pullout resistance for steel piles is shown in Figure 67 and for wooden piles in Figure 68. The ice-force analysis for

Lake Pend Oreille has primarily focused on vertical uplift forces. The ability for ice to jack piles depends on many variables, including the pile depth and construction quality. A separate analysis is needed to quantify risk for specific facilities and structures on the lake.

Figure 65. Uplift force on each pile for different pile spacings for Case 1.

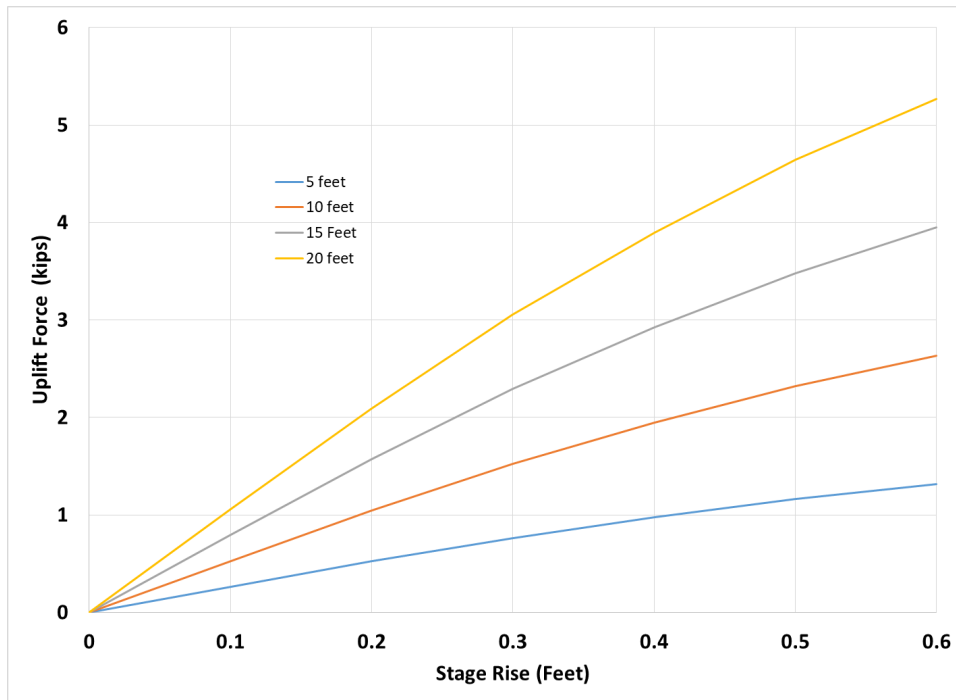


Figure 66. Uplift force on each pile for different pile spacings for Case 2.

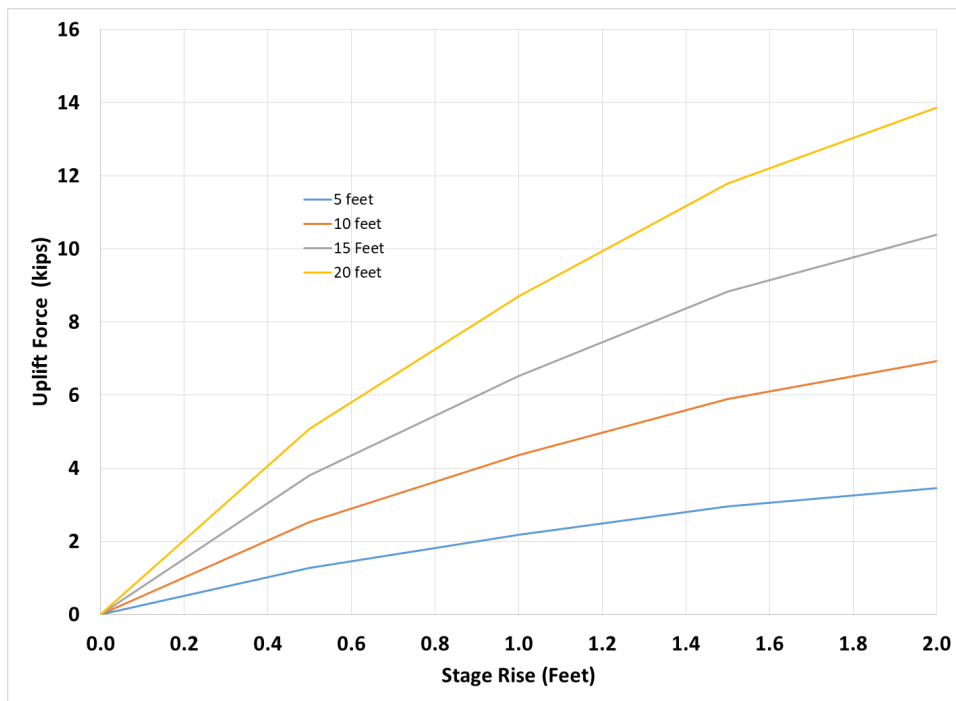


Figure 67. Steel pile resistance to pullout with various factors of safety (FOS).

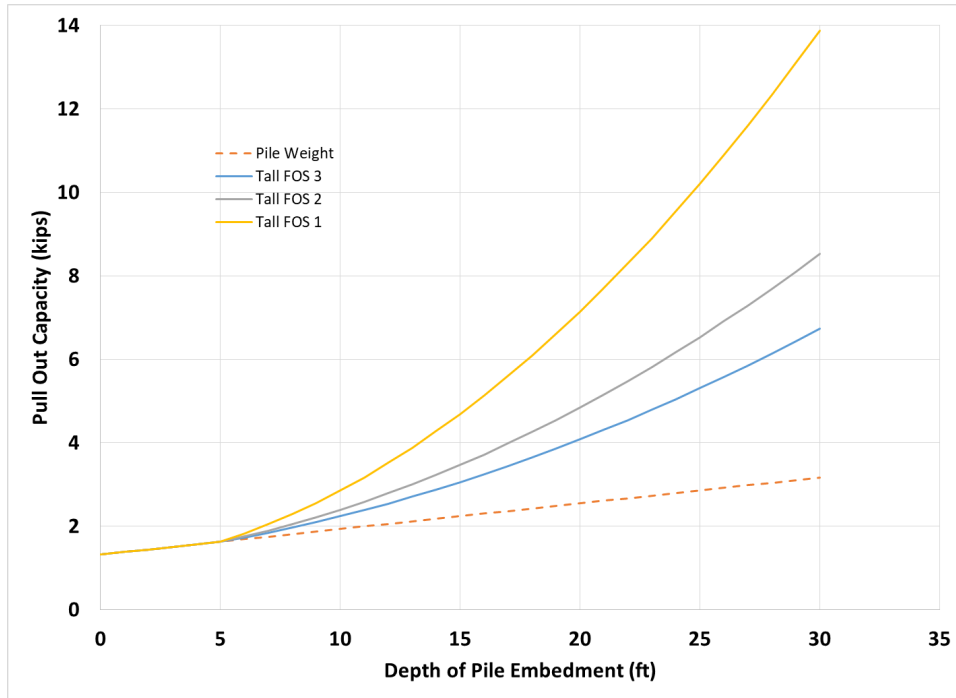
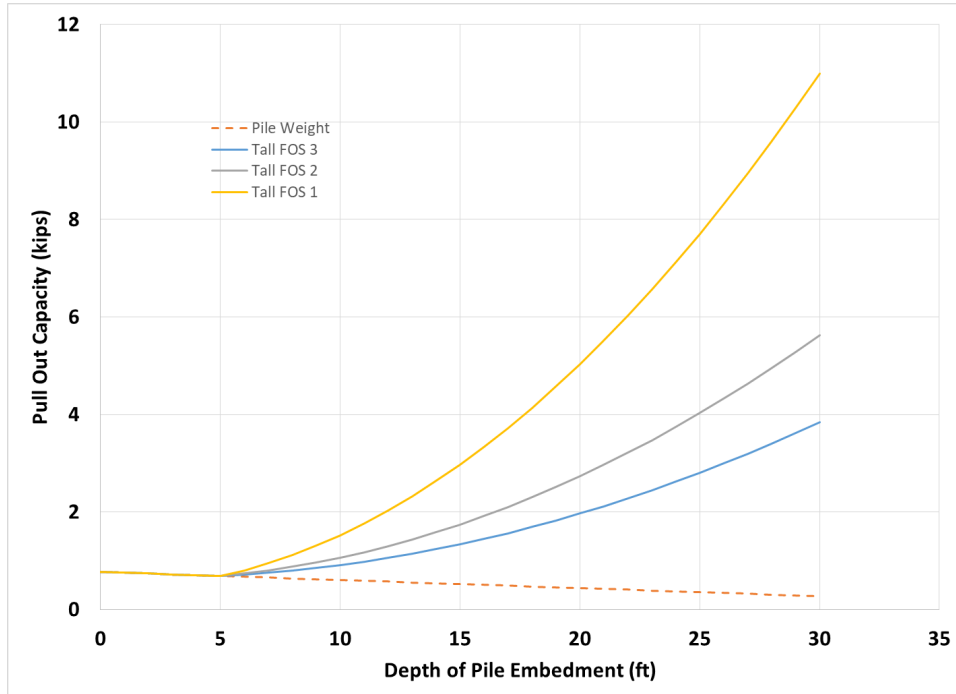


Figure 68. Wooden Pile Resistance to pullout.



As an illustration of how Figures 64–68 can be used to determine the impacts on piles with varying stage increases, we can step through an example of a marina facility with steel piles that are spaced 10 ft apart. If there was an operational situation that required increasing lake elevation by

0.5 ft (total), then using Figures 65, 66, and 67, both Case 1 and Case 2 would result in an uplift force of approximately 2.3 kips. Based on this uplift force estimate, Figure 67 can be used to determine the minimum pile foundation depth needed to resist the uplift force. In this example, an uplift force of 2.3 kips would require a foundation depth of at least 7 ft and preferably closer to 10 ft for a factor of safety.

Our analysis is not intended to determine which structures or piles on Lake Pend Oreille will be at risk of ice jacking but to demonstrate (1) the forces piles will experience with ice on the lake and (2) the insensitivity of uplift force between operational Case 1 and Case 2.

6.3 FWPO BMP criteria

6.3.1 Introduction

The FWPO BMP is concerned with reducing possible ice damage to over-water structures and facilities located along the banks of the Pend Oreille River downstream of AFD. This section evaluates the directions included in the FWPO BMP (Exhibit 7-3 in AFD WCM, USACE 2013).

6.3.2 Potential ice damage on Pend Oreille River

The ice-force descriptions and wall geometry presented in the previous section also apply to the river downstream of AFD. The difference in the force analysis for the FWPO BMP is the rate of change and total stage change conditions. Also, creation of a hinge crack is not necessarily the desired effect of the restricted ramping from the dam. The primary purpose of the FWPO BMP operations are to minimize risk of ice jam formation and damage to shoreline facilities. As discussed earlier, the risk of ice jams and the subsequent flooding is minimal for this reach even under relatively extreme ice conditions on the Pend Oreille River. Therefore, this section will address the FWPO BMP criteria based on uplift forces that may result from river stage changes.

6.3.3 River stage change and uplift force

We analyzed were four cases for uplift forces for the river:

Cases 1 and 1a. The releases from AFD are increased at the maximum hourly discharge rate without going over the maximum daily discharge for non-ice and wintertime operations, respectively.

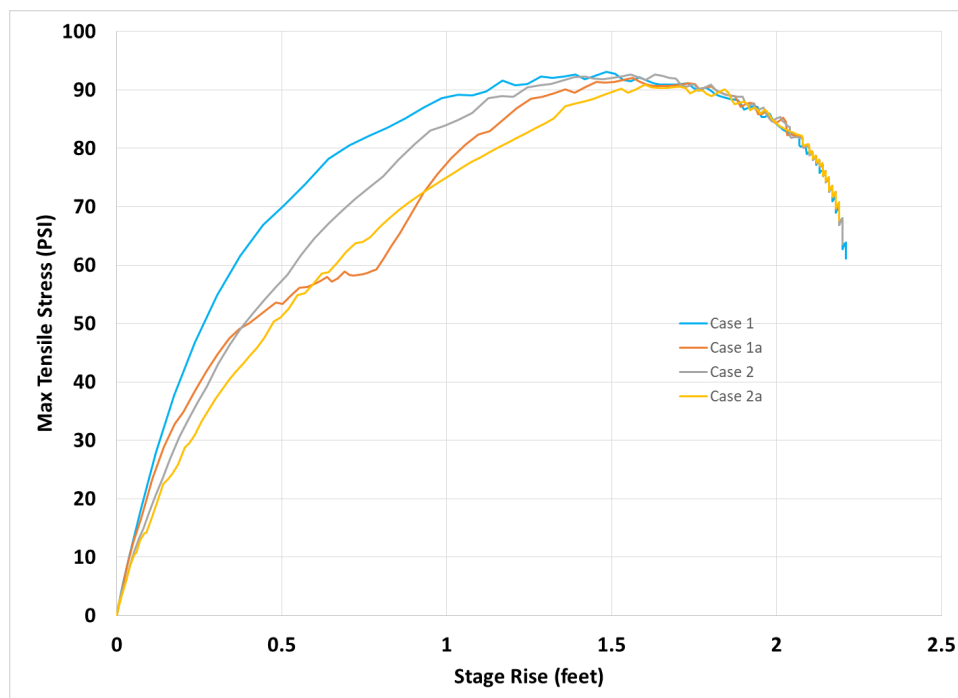
- Case 1 (non-ice condition). Release increase of 5 kcfs/hour for two hours, then constant ($\Delta Q = 5$ kcfs/hr).
- Case 1a (ice condition). Release increase of 2 kcfs/hour for 2.5 hours, then constant ($\Delta Q = 2$ kcfs/hr).

Cases 2 and 2a. The releases from AFD are increased by the daily maximum total change during non-ice and ice-cover periods. The daily discharge change is distributed evenly over the course of the 24 hours.

- Case 2 (non-ice condition). Release increase of 10 kcfs/24 hours over 24 hours ($\Delta Q = 0.41$ kcfs/hr).
- Case 2a (ice condition). Release increase of 5 kcfs/24 hours for 48 hours, then constant ($\Delta Q = 0.21$ kcfs/hr).

The maximum tensile stress for the river is larger than that computed for the lake (Figure 69). This is due to the larger stage change when compared to the lake cases. The maximum stress using the FWPO BMP ramping criteria is approximately equal to that of the open-water periods for both cases. This means that the pullout forces will be very similar whether water managers use the FWPO BMP criteria or normal ramping criteria for AFD.

Figure 69. Maximum tensile stress in the ice cover as a function of the stage rise for river cases.



There are some differences between cases due to the flow change rate, which may be useful to water managers. However, given the same total flow change (and stage change) that may be required for operations of AFD, the ice breakup potential will be the same using the FWPO BMP criteria or open-water limits.

7 Improvements to Aid Wintertime Operations

7.1 Forecasting ice formation

Forecasting ice-formation patterns on rivers and lakes using a single criterion like AFDD is challenging even when there is high confidence in air temperature forecasts. Based on the analysis performed in this study, water managers anticipating ice formation patterns and the impacts to AFD operations should use multiple criteria and tools. The general process that will provide information related to future ice conditions can start with using the moving 7-day AFDD value computed from forecasted daily average temperatures. This will provide an indication of whether ice is reasonably possible for Lake Pend Oreille or the river downstream of AFD. Once water managers are closely monitoring the air temperature conditions, it will be useful to perform HEC-RAS simulations with the Water Quality Module using forecasted air and water-temperature information. This will provide an initial location for where ice formation may start. As the cold weather event continues, using the HEC-RAS unsteady flow model will be helpful to compute tailwater stage deviations. The deviations can be used with Figure 37 and Figure 43 to estimate the spatial extents of the ice formation using observed information. The steady hydraulic model can then be used with anticipated releases. It is also important for AFD personnel to drive the river between AFD and BCD to confirm the model estimates.

7.2 Recommendations for improving existing camera performance

An important consideration to improve the performance of the shoreline-camera installations is camera position. If a camera view contains the horizon or distant terrain features, this reduces the number of pixels that contain information about the water surface, which increases river ice identification uncertainty. Oblique imagery is classified as imagery that is collected at angles between vertical and horizontal. Low-angle oblique imagery is collected at angles with a small departure from vertical and has minimal ground distortions, whereas high-angle oblique imagery is collected at angles with a small departure from horizontal and is characterized by large amounts of distortion in the horizontal plane. This distortion introduces uncertainty in the image interpretation. An optimal shoreline-camera position is one that minimizes the camera's angle of departure

from vertical while still providing enough background information to understand the scale of the features on the water surface.

7.2.1 Riley Camp

The performance of the Riley Creek camera installation can be improved by adjusting the camera's view perpendicular to the main channel with the top of the camera's view set on the opposite river bank.

7.2.2 Kalispel

The performance of the Kalispel camera installation is primarily limited by the surrounding vegetation that occasionally obscures the camera's view of the water surface. The surrounding vegetation should be trimmed when the cameras are serviced before each winter season.

7.2.3 Bible Camp

The performance of the cameras at Bible Camp is limited by the quality of the images. The cameras installed at this location are analog and rely on an image server to convert the data stream to a digital format before they are transmitted to the external servers. We recommend upgrading the camera hardware to support digital cameras.

7.2.4 Sandpoint

The performance of the cameras at Sandpoint is limited by the camera housings and the quality of the images. The installation is unsheltered and prone to debris on the camera lens, which reduces image clarity. In addition, the cameras installed at this location are analog and rely on an image server to convert the data stream to a digital format before they are transmitted to the external servers. We recommend upgrading the camera housings and switching to digital-format cameras.

7.3 Automating shoreline-ice-camera ice detection

Shoreline ice cameras have commonly been used for remotely monitoring ice conditions (Vuyovich et al. 2009). One of the limitations of this method is that collected images must be visually inspected to identify ice conditions. This can be a prohibitively time-consuming task. To address the challenges associated with manually reviewing and interpreting imagery collected from remote camera installations, machine learning algorithms

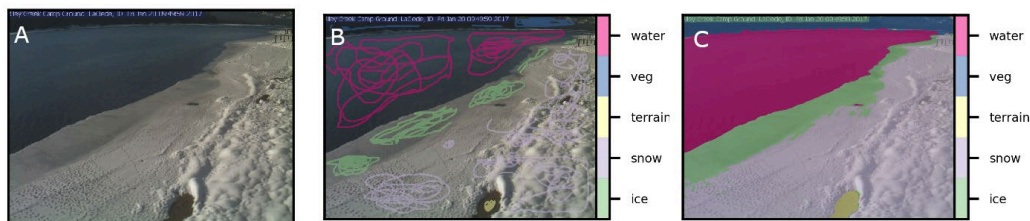
have been demonstrated to reliably interpret imagery for scientific and engineering applications (Kalke and Lowen 2018; Chaouch et al. 2014). Deep convolutional neural networks (DCNN) are a subclass of machine learning algorithms that have emerged as the standard for the computer-vision industry (Szegedy et al. 2015; Long et al. 2015; Andriluka et al. 2014).

We used a DCNN built in TensorFlow (TensorFlow Hub 2018) to automatically detect shoreline ice by using the imagery collected at the Riley Creek shoreline-ice-camera installation. The DCNN classifier was trained using a subset of all imagery collected at Riley Creek between 2015 through 2017. The training and testing data consisted of tiles that represent various land cover surfaces (e.g., ice, water, snow, and terrain). The DCNN classifier is used to reconstruct a daily time series of historical ice conditions that can be compared against results from the shoreline camera ice observations.

7.3.1 Ground truth data

The ground truth data required to train the DCNN consists of a library of tiles (96×96 pixels) organized by land cover type. Each land cover type is manually identified for training the DCNN by using a conditional random field (CRF) (Figure 70).

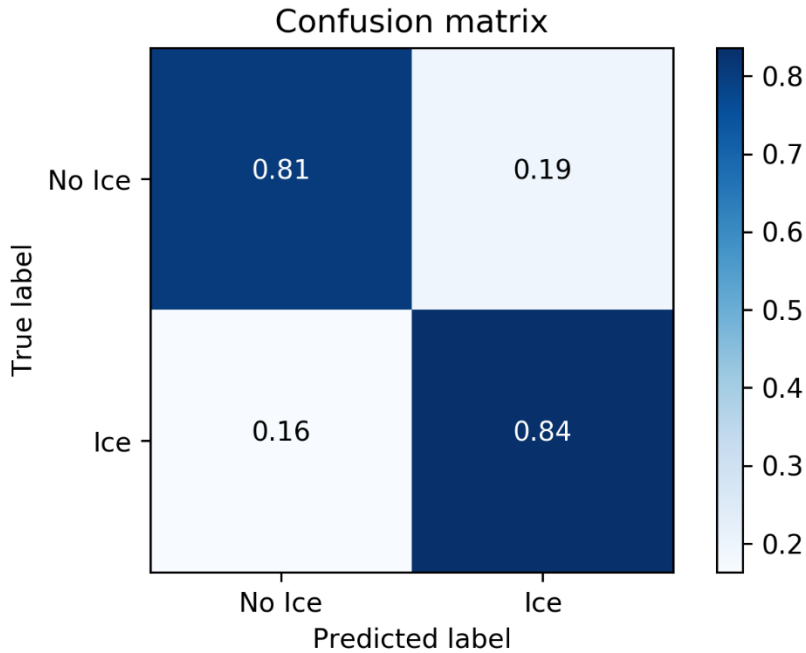
Figure 70. Example of manual annotations and CRF predictions. Panel *A* shows the input image. Panel *B* shows the weakly supervised user annotations. Panel *C* shows the results of the CRF-derived label image used to create training and testing tile libraries.



7.3.2 Model training and results

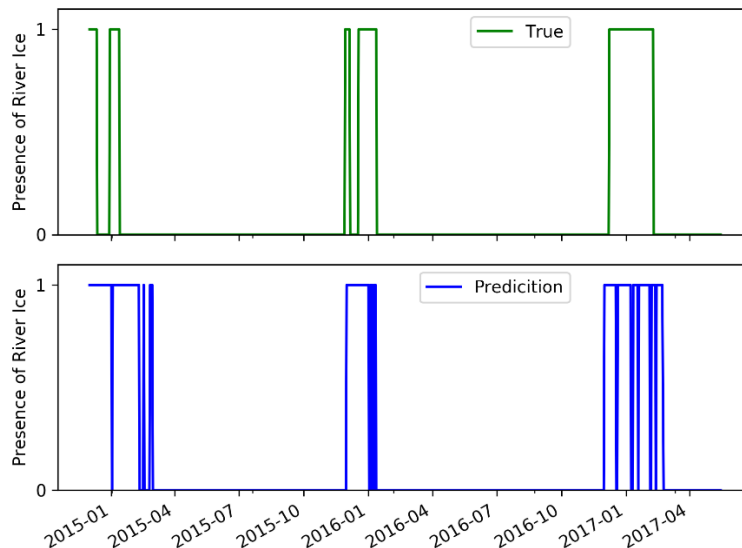
The retrained DCNN most commonly misclassified ice training tiles as water but achieved an overall accuracy of 82%. Water was most commonly misclassified as snow and ice. The trained DCNN tended to over predict the presence of river ice at Riley Creek in the winter months (Figure 71). The algorithm had classification accuracies for ice and no ice of 81% and 84%, respectively.

Figure 71. Confusion matrix showing the results of applying the trained DCNN to the testing tile library for Riley Creek. Values within the matrix show the percentage of the label library classified as the label indicated on the x-axis.



A daily time series of ice conditions at Riley Creek was developed for WYs 2015, 2016, and 2017 (Figure 72). The time series was constructed by applying the DCNN classifier to all of the images collected before 13:00.

Figure 72. Time series of river ice conditions at Riley Creek.



Finally, a time series was resampled to a daily time step by assigning the most frequent classification for each portion of the image. For example, if a computational window was classified as ice for more than half of the images collected throughout the day, the daily ice prediction was assigned as 1. There is an overestimate of predicted ice cover duration in WY 2015, while WYs 2016–2017 are very similar. This demonstrates that both the spatial and temporal ice classification estimates with the DCNN are useful for water management and planning study purposes.

7.3.3 Discussion

Automated ice classification using the DCNN method can be relatively highly accurate at the Riley Creek camera location. Training of individual models will be necessary for other shoreline-ice-camera locations given the site-specific camera angles and land surface types visible in the image. Using this method combined with an image database will help efficiently flag and sort images with potential ice cover for water managers to use. In addition, any historical analysis of ice images will be straightforward for future studies.

8 Summary

The current FWPO SOP direction on active management of the Lake Pend Oreille water levels to produce hinge cracks is not necessary for the following reasons:

1. The wintertime elevation of Lake Pend Oreille varies from year to year but is generally held at 2051.5 ft NGVD29 or 2055.5 ft NGVD29. The summertime water level is generally near the allowed maximum of 2062.5 ft NGVD29, which is 7 to 11 ft higher than the normal wintertime water level. Shoreline structures are exclusively designed for summertime operation. The wintertime drop in lake water levels tends to protect structures from ice action by reducing water buoyancy on the structure, which increases the effective pile weight, making the piles less susceptible to pullout. At some locations, the structure may be completely out of the water in winter, and in the case of floating docks, the docks may rest close to or on the bottom.
2. The risk of damaging uplift to piles and structures on Lake Pend Oreille is very low given the small range of water-level fluctuations observed during winter. The fluctuations were measured by the USGS Hope gage.
3. The rate of rise of the water level, 0.1 ft/day for 6 days, is likely not to be effective in causing active or hinge cracks to form because this slow rate of rise allows the ice sheet to creep and relax the stresses. This creep response offsets the stresses that the increase in water level induces in the ice sheet. In addition, the underlying assumption with the hinge crack operation is that any ice failure caused by continuous lake elevation change would persist during the cold weather event. This is likely not the case because any crack would fill with water and refreeze almost immediately, thus negating the effectiveness of the crack to decouple the force between the ice sheet and pile.

The current FWPO BMP direction for limiting releases from AFD during ice-cover periods is not necessary for the following reasons:

1. The potential risk for ice jams is low in the reach between AFD and BCD due to the relatively low flow velocities and downstream hydraulic control by BCD. The primary mechanism for any ice jam, if it were to occur, would be accumulation of surface ice since the formation of frazil ice would be

- very minimal. The section with the highest jam potential is near Blueslide, Washington, which limits the upstream surface area contributing to any ice jam.
2. The flood risk from a significant ice jam (if it were to form) is low. Using a relatively high winter flow of 40 kcfs, an ice jam would result in an open-water-equivalent stage of 75 kcfs, which is still below the flood stage used by water managers.
 3. The current FWPO BMP ramping criteria result in approximately the same stress on the ice cover as compared to AFD ramping limits for non-ice periods. Therefore, the potential for ice breakup due to release changes from AFD is relatively insensitive to rates of flow change and is mainly dependent on the total flow change.

The result of our analysis indicates that there is no evidence that the measure specified by the FWPO SOP and BMP will effectively eliminate risk due to ice formation on the lake or river. However, the recommendation to discontinue using the criteria is based on analysis performed using limited information. Extreme conditions may present ice and flow combinations that our analysis did not consider, which will require increased real-time monitoring and adaptation by water managers to ensure issues related to ice do not occur.

9 AFD Ice Monitoring

Our analysis has resulted in several recommendations for changes or modification to AFD wintertime operating criteria. The objective of this analysis was to assess the effectiveness of the current wintertime operating criteria of Albeni Falls and to provide tools to aid water managers. This analysis is, however, limited by the available field measurements of ice. Many of the recommendations are based solely on model results that could not be validated. Seattle District should evaluate all recommendation before implementation because operations of high-profile projects like AFD have many aspects (e.g., social, political, legal, etc.) that our analysis may not have considered.

9.1 Lake Pend Oreille

Our suggested ice-monitoring methods include regular measurements of ice depth and continued collection and archival of shoreline-ice-camera images. Details of these data collection methods for Lake Pend Oreille are listed below.

1. During cold weather events, document ice-formation conditions, including areas of persistent ice on the lake and ice thickness.
 - a. Make ice-thickness measurements weekly during cold weather events (7-day average air temperature less than 32°F).
 - b. Take ice-thickness measurements Windbag Marina in Sandpoint (Figure 73) during cold weather events. This will validate the ice-thickness model results.
 - c. Ice-cover extents should be estimated for the lake during cold weather (7-day average air temperature less than 32°F). This can be simple highlighting of areas using Google Earth, which can then be archived.
2. Continue archiving shoreline-ice-camera data and perform ice classification of images for both real-time and planning studies. Archive the classified images for quick future reference.

Figure 73. Recommended ice-thickness measurement location at Windbag Marina.



9.2 Albeni Falls Dam and Pend Oreille River

Our suggested ice monitoring includes continued collection and archival of shoreline-ice-camera images and use of the HEC-RAS model that has been calibrated for wintertime flows. Details of these data collection methods for Pend Oreille River downstream of AFD are listed below.

1. Calculate the stage deviation between the open-water HEC-RAS model and observed tailwater gage daily during cold weather. Compare these deviations to figures included in section 4 of this report to estimate locations of ice formation.
2. During cold weather events, document ice-formation conditions, including areas of persistent ice on the river and ice thickness.
 - a. During cold weather events (7-day average air temperature less than 32°F), document the spatial ice-formation mode from BCD to AFD. This will require either driving the river or having a network of observers. This information will validate the ice-growth mode assumed in this study. This can be simple highlighting of areas using Google Earth, which can then be archived. Current and future water management staff can then use these images to verify any claims of river-level fluctuations causing ice issues.

- b. Take ice-thickness measurements at Bible Camp and Kalispel camera locations during cold weather events (7-day average air temperature less than 32°F). Near-shore measurements are sufficient, but the ice should not be grounded against the channel bottom. This data will validate the ice-thickness model results and will be necessary for future studies evaluating site-specific ice-damage risks on the river.
3. Continue archiving shoreline-ice-camera data and perform ice classification of images for both real-time and planning studies. The classified images should also be archived for quick future reference.
4. Incorporate the HEC-RAS Water Quality Module into the CWMS modeling chain for real-time forecasting of potential ice conditions.

9.3 Future analysis

Because of the limited observational ice data, several focused studies could refine and validate the modeling results from our analysis:

- Create a method to estimate outflow temperature from AFD. This would be used as the upstream boundary condition for the HEC-RAS Water Quality Module. This model would be useful for both summer and winter operations when water temperature downstream of AFD is important.
- Conduct a field campaign to collect ice-thickness data for Lake Pend Oreille, the Pend Oreille River, and other nearby locations. This information will help to validate modeled ice thickness assumed in the current study.
- Perform a full Monte Carlo analysis using the wintertime HEC-RAS parameterization to fully quantify flood risk due to an ice jam. This would require a range of ice-thickness estimates, AFD discharges and BCD forebay elevations.

Our analysis had several objectives, which primarily focused on evaluating the existing winter operating criteria for AFD. Through our analysis, we found that the criteria specified in the FWPO SOP and BMP are not likely to be effective in reducing flood risk or reducing damages to shoreline structures. Our analysis does have limitations, mainly the available ice extents and thickness data.

Because of the variable ice conditions that can form on Lake Pend Oreille and the Pend Oreille River, we recommend targeted future analyses. This includes collection of additional ice data to verify the modeling assumptions we used because there were no ice thickness measurements available at the time of this study. In addition, the updated HEC-RAS for wintertime operations should be used in a Monte Carlo analysis to further explore both the uncertainty of model parameters and sensitivity to conditions outside of the historical range. One of the most important future tasks will be to develop methods of estimating AFD forebay temperatures, which will be used by the Water Quality Module. As the HEC-RAS ice modeling capability continues to improve, this could be a very useful tool for real-time water management.

References

- Andriluka, M., L. Pishchulin, P. Gehler, and B. Schiele. 2014. "2D Human Pose Estimation: New Benchmark and State of the Art Analysis." In *Proceedings of the IEEE Computer Society Conference on Computer Vision and Pattern Recognition*, 3686–3693. <https://doi.org/10.1109/CVPR.2014.471>.
- Beltaos, S. 2013. *River Ice Formation*. Edmonton, Alberta, Canada: Committee on River Ice Processes and the Environment, Canadian Geophysical Union Hydrology Section.
- Boese, R., G. Stevens, A. Hess, J. Jenkins, R. Barlow, A. Clary, J. Covert, J. Ekins, M. Galante, T. Hanson, L. Laumatia, M. LaScuola, R. Lindsay, S. Phillips, and L. Schmidt. 2015. *The Spokane Valley – Rathdrum Prairie (SVRP) Aquifer Atlas*. 2015 Edition. Spokane Valley, WA: Spokane Aquifer Joint Board. www.SVRPaquiferAtlas.org.
- Brunner, G. W. 2016. *HEC-RAS River Analysis System: Users Manual*. CPD-68. Davis, CA: U.S. Army Corps of Engineers, Institute for Water Resources, Hydrologic Engineering Center.
- Chaouch, N., M. Temimi, P. Romanov, R. Cabrera, G. Mckillop, and R. Khanbilvardi. 2014. "An Automated Algorithm for River Ice Monitoring over the Susquehanna River Using the MODIS Data." *Hydrological Processes* 28 (1): 62–73. <https://doi.org/10.1002/hyp.9548>.
- Chistyakov, P., E. Karulin, A. Marchenko, A. Sakharov, and B. Lishman. 2016. "The Tensile Strength of Saline and Freshwater Ice in Field Tests." In *Proceedings of the 23rd IAHR International Symposium on Ice*, 31 May–3 June, Ann Arbor, MI.
- Christensen, F. T. 1986. Interaction between Floating Ice Sheets and Vertical Structures Due to Water Level Fluctuations. PhD Thesis, Technical University of Denmark, Institute of Hydrodynamics and Hydraulic Engineering.
- Christensen, F. T. 1987. "Vertical Ice Forces on Long Straight Walls." *Cold Regions Science and Technology* 13:215–218.
- Easthouse, K. 2012. *Albeni Falls Dam: Flexible Winter Power Operations, Lake Pend Oreille Water Quality Monitoring Plan 2012*. Seattle, WA: U.S. Army Corps of Engineers, Seattle District.
- Edit, T. B., C. J. Roble, and C. A. Wortley. 1988. "Design Approach For Piles Subject To Ice Jacking." *ASCE Journal of Cold Regions Engineering* 2 (2): 65–85.
- Fields, R. L., P. F. Woods, and C. Berenbrock. 1996. *Bathymetric Map of Lake Pend Oreille and Pend Oreille River, Idaho*. Water Resources Investigations Report 96-4189. Denver, CO: U.S. Geological Survey.
- Flood Control Act of 1950, 17 May 1950, Pub. L. No. 81-516, Ch. 188, 64 Stat. 170.

- Kalke, H., and M. Lowen. 2018. "Support Vector Machine Learning Applied to Digital Images of River Ice Conditions." *Cold Regions Science and Technology* 155 (5): 225–236.
- Kerr, A. D. 1975. "Ice Forces on Structures Due to a Change of the Water Level." In *Proceedings of the 3rd International Symposium of Ice Problems*, 419–427.
- . 1978. "Forces an ice Cover Exerts on Rows or Clusters of Piles." In *Proceedings of IAHR Symposium on Ice, Part I*, Lulea, Sweden, 509–525.
- Long, J., E. Shelhamer, and T. Darrell. 2015. "Fully Convolutional Networks for Semantic Segmentation." In *Proceedings of the IEEE Computer Society Conference on Computer Vision and Pattern Recognition*, 7–12 June, Boston, MA, 3431–3440. <https://doi.org/10.1109/CVPR.2015.7298965>.
- Naval Sea System Command. 2018. "Acoustic Research Detachment - Bayview, Idaho." *Warfare Centers: NSWC Carderock Division*. <https://www.navsea.navy.mil/Home/Warfare-Centers/NSWC-Carderock/Who-We-Are/Bayview-Idaho/>.
- Smith, O. P. 2007. *Observers Guide to Sea Ice*. Seattle, WA: U.S. Department of Commerce, National Oceanic and Atmospheric Administration, NOAA Ocean Service.
- Spokane Daily Chronicle*. 1928. "Ice Jam Threatens to End Usk Bridge." 7 January 1928.
- Szegedy, C., V. Vanhoucke, S. Ioffe, J. Shlens, and Z. Wojna. 2015. *Rethinking the Inception Architecture for Computer Vision*. <http://arxiv.org/abs/1512.00567>.
- TensorFlow Hub. 2018. "A Library for Transfer Learning by Reusing Parts of TensorFlow Models." TensorFlow. <https://www.tensorflow.org/hub/>.
- Terahima, T., N. Nakazawa, S. Kioka, N. Usami, and H. Saeki. 2006. Vertical Ice Forces on Pile Structures under Water Level Changes. In *Proceedings of the 18th IAHR International Symposium on Ice*, 145–152.
- USGS (U.S. Geological Survey). 2018. "USGS Water Data for the Nation." U.S. Geological Survey. <http://waterdata.usgs.gov/nwis/>.
- USACE (U.S. Army Corps of Engineers). 1966. *Albeni Falls Project, Pend Oreille River, Idaho, O&M Manual*. U.S. Army Corps of Engineers.
- . 2002. *Engineering and Design: Ice Engineering*. EM 1110-2-1612. Washington, DC: U.S. Army Corps of Engineers.
- . 2013. *Albeni Falls Dam, Pend Oreille River, Idaho, Water Control Manual*. April 2002 r.2013. Seattle, WA: U.S. Army Corps of Engineer, Seattle District.
- . 2017. *Albeni Falls Dam and Lake Pend Oreille, Fall Public Meeting, Aug. 7, 2017*. PowerPoint Presentation. Seattle, WA: U.S. Army Corps of Engineer, Seattle District.
- . 2019. "Albeni Falls Dam." U.S. Army Corps of Engineers, Seattle District. <https://www.nws.usace.army.mil/Missions/Civil-Works/Locks-and-Dams/Albeni-Falls-Dam/>.

- U.S. Navy. 1986. *Foundations and Earth Structures*. Design Manual 7.02. Alexandria, VA: Naval Facilities Engineering Command,.
- Vidregar, D. T. 2000. Population Estimates, Food Habits and Estimates Of Consumption Of Selected Predatory Fishes In Lake Pend Oreille, Idaho. Master's thesis, University of Idaho.
- Vuyovich, C. M., S. F. Daly, J. J. Gagnon, P. Weyrick, and M. Zaitsoff. 2009. "Monitoring River Ice Conditions Using Web-Based Cameras." *Journal of Cold Regions Engineering* 23 (1): 1–17. [https://doi.org/10.1061/\(ASCE\)0887-381X\(2009\)23:1\(1\)](https://doi.org/10.1061/(ASCE)0887-381X(2009)23:1(1)).
- Zabilansky, L. J. 1998. Vertical Forces and Aspect Ratio of Pile Diameter vs. Ice Thickness. In *Proceedings, 14th International IAHR Symposium on Ice, Ice in Surface Waters, Vol. 2*, ed. H.T. Shen.

REPORT DOCUMENTATION PAGE*Form Approved*
OMB No. 0704-0188

Public reporting burden for this collection of information is estimated to average 1 hour per response, including the time for reviewing instructions, searching existing data sources, gathering and maintaining the data needed, and completing and reviewing this collection of information. Send comments regarding this burden estimate or any other aspect of this collection of information, including suggestions for reducing this burden to Department of Defense, Washington Headquarters Services, Directorate for Information Operations and Reports (0704-0188), 1215 Jefferson Davis Highway, Suite 1204, Arlington, VA 22202-4302. Respondents should be aware that notwithstanding any other provision of law, no person shall be subject to any penalty for failing to comply with a collection of information if it does not display a currently valid OMB control number. **PLEASE DO NOT RETURN YOUR FORM TO THE ABOVE ADDRESS.**

1. REPORT DATE (DD-MM-YYYY) October 2019	2. REPORT TYPE Technical Report/Final	3. DATES COVERED (From - To)
--	---	-------------------------------------

4. TITLE AND SUBTITLE Ice Management Operations at Albeni Falls Dam	5a. CONTRACT NUMBER
	5b. GRANT NUMBER
	5c. PROGRAM ELEMENT NUMBER

6. AUTHOR(S) Jeremy Giovando, Chandler Engel, Joseph Rocks, Steven F. Daly, Devin O'Connor, and Daniel Hamill	5d. PROJECT NUMBER
	5e. TASK NUMBER
	5f. WORK UNIT NUMBER

7. PERFORMING ORGANIZATION NAME(S) AND ADDRESS(ES) U.S. Army Engineer Research and Development Center (ERDC) Cold Regions Research and Engineering Laboratory (CRREL) 72 Lyme Road Hanover, NH 03755-1290	8. PERFORMING ORGANIZATION REPORT NUMBER ERDC/CRREL TR-19-21
--	--

9. SPONSORING / MONITORING AGENCY NAME(S) AND ADDRESS(ES) U.S. Army Corps of Engineers, Seattle District 4735 E Marginal Way S Bldg 1202 Seattle, WA 98134	10. SPONSOR/MONITOR'S ACRONYM(S) USACE
	11. SPONSOR/MONITOR'S REPORT NUMBER(S)

12. DISTRIBUTION / AVAILABILITY STATEMENT
Approved for public release; distribution is unlimited.

13. SUPPLEMENTARY NOTES
Funding Account Code G3149647, AMSCO Code 000200, "Albeni Falls Water Management"

14. ABSTRACT

Albeni Falls Dam is located on the Pend Oreille River in northern Idaho and is part of the federal reservoir system on the Columbia River, which provides flood risk reduction and hydropower generation. The Albeni Falls Dam Water Control Manual currently defines wintertime operations for Lake Pend Oreille and the Pend Oreille River. However, this analysis finds that the current wintertime operating criteria are likely ineffective in preventing damages to shoreline structures. Additionally, discharge ramping rates are not significant factors in determining the accumulation of ice on the Pend Oreille River.

This study recommends discontinuing the current wintertime operating criteria specified in the Albeni Falls Dam Water Control Manual and that water managers use hydraulic and water temperature models to assess and monitor the ice formation for both the lake and river. This will provide increased operational flexibility and rely on real-time assessment of ice and weather conditions.

15. SUBJECT TERMS
Albeni Falls Dam (Idaho); Flood damage prevention; Hydraulic structures--Ice prevention; Ice on rivers, lakes, etc.; Pend Oreille River

16. SECURITY CLASSIFICATION OF:			17. LIMITATION OF ABSTRACT	18. NUMBER OF PAGES	19a. NAME OF RESPONSIBLE PERSON
a. REPORT Unclassified	b. ABSTRACT Unclassified	c. THIS PAGE Unclassified			19b. TELEPHONE NUMBER (include area code)